January 2010

The Effect of Equal Channel Angular Extrusion (ECAE) and Boron Additions on the Mechanical Properties of a Biomedical Ti-Nb-Zr-Ta (TNZT) Alloy

Gian Colombo
Washington University in St. Louis

WASHINGTON UNIVERSITY IN ST. LOUIS

School of Engineering and Applied Science

Department of Mechanical, Aerospace, and Structural Engineering

Dissertation Examination Committee:
Shankar M.L. Sastry, Chair
David Bowden
Guy Genin
Thomas Harmon
Ken Jerina
Stavros Thomopoulos

THE EFFECT OF EQUAL CHANNEL ANGULAR EXTRUSION (ECAE) AND BORON ADDITIONS ON THE MECHANICAL PROPERTIES OF A BIOMEDICAL Ti-Nb-Zr-Ta (TNZT) ALLOY

by

Gian A. Colombo

A dissertation presented to the
Graduate School of Arts and Sciences
of Washington University in
partial fulfillment of the
requirements for the degree
of Doctor of Philosophy

May 2010

Saint Louis, Missouri

ABSTRACT OF THE DISSERTATION

THE EFFECT OF EQUAL CHANNEL ANGULAR EXTRUSION (ECAE) AND BORON ADDITIONS ON THE MECHANICAL PROPERTIES OF A BIOMEDICAL Ti-Nb-Zr-Ta (TNZT) ALLOY

Gian A. Colombo

Doctor of Philosophy in Mechanical Engineering

Washington University in St. Louis, 2010
Professor Shankar, M.L. Sastry, Chairperson

New metastable-β type titanium alloys based on the biocompatible elements Ti-Nb-Zr-Ta (TNZT) have been developed to address the shortcomings (e.g. incomplete biocompatibility, high modulus, etc.) of the traditionally used materials in joint replacement prostheses. Equal channel angular extrusion (ECAE) processing has the capability to improve the mechanical properties of these alloys to broaden their potential biomedical applications. The focus of this investigation is to evaluate and optimize the ECAE process to produce maximum property improvement, and explore the effectiveness of boron as a grain refining agent. Deformation mechanisms are identified for various processing conditions, and the strain distribution induced during extrusion is examined using finite element techniques. Multi-pass ECAE processed samples were examined using optical and transmission electron microscopy, and subjected to tensile, fatigue, and wear testing. It was found that ECAE has a beneficial impact on all of the properties tested. The modulus value was increased by approximately 25%, but it is still well below the value of other prosthesis materials.

Acknowledgements

I would like to thank all the individuals and groups involved in the development and execution of the body of this work, including Dr. Sastry, Pat Harkins, Jim Linders, Vadim Protasov, Brett Pond, Gene Bulfin, and Nicole Stennes.

Contents

List of Tables

List of Figures

Chapter 1

Introduction

The natural synovial joints (hip, knee, or shoulder) are capable of performing well under a wide variety of conditions. Unfortunately, these joints are also susceptible to degenerative and inflammatory diseases that can result in pain and stiffness. [1] In fact, approximately 90% of the population over the age of 40 suffers from some degree of degenerative joint disease. [2] The typical cause of degeneration is degradation in the joint's mechanical properties resulting from excessive loading conditions, or a failure of the normal biological repair processes. Because the natural joints can no longer function, they can be replaced by artificial biomaterials in a procedure known as total joint replacement (TJR) arthroplasty. [1][2] The increased life expectancy of the US population has produced a greater demand on the service lifetimes of TJR materials. It is projected that by the year 2030, there will be approximately 272,000 total hip replacements performed annually. In addition, of the 152,000 total hip replacements performed in the year 2000, approximately 12.8% involved revisions of previous implants. [3] This percentage of revision surgeries is undesirable since the procedure is more difficult, and has an overall lower success rate compared to the initial replacement surgery.

Failure of the joint replacement is rarely due to the structural failure of one of the components. The most common cause requiring revision surgery is the aseptic loosening of the implant. Loosening can be caused by either mechanical or biological factors. The mechanical factors include relative micro-motion between the implant and the host bone and stress-shielding, which is attributed to the high stiffness values of implant materials relative to human bone. This results in the implant absorbing a significant proportion of applied loads causing bone resorption and thinning. The biological factors include an adverse response to wear particles and toxicity of the implant materials themselves to body tissues. [4] There are many different metal alloys that are used in implant materials today including commercially pure titanium (CPTi), Ti-6Al-4V, stainless steels, Co-Cr-Mo alloys, and others. The use of these materials dates back to the middle of the 20^{th} century, but they all share the common shortcoming that they were originally designed for use in areas other than biomedical applications. [5] As such, they suffer from lack of both biocompatibility, and a modulus value (>100GPa) that is much higher than the modulus of human bone (10-40GPa). [1] In response to this, new metastable β-type titanium alloys with a lower modulus value, improved notch fatigue and toughness properties, increased biocompatibility, and better wear resistance have been developed. [5][6] However, some of the most promising alloys of this class of materials suffer from inferior tensile and fatigue properties that limit their use in implant applications. [7] In order to take advantage of the desirable characteristics of the β-type alloys, a technique must be

found that is capable of improving their weaker mechanical properties in order to make them viable candidates for biomedical applications.

Grain refinement has long been utilized as a method of strengthening metals and alloys. Normally this can be accomplished through the use of traditional metalworking techniques, rolling, forging, and extrusion, sometimes followed by a post-processing heat treatment. The major drawback to these techniques is that the potential for grain refinement is limited by the reduction is cross-sectional area that occurs during processing. While large values of strain are capable of being applied, the finished product will be in the form of very thin foils or wires that have limited applications. ECAE processing is a method of inducing severe plastic deformation (SPD) in a material without reducing the cross-sectional area of the workpiece. [8] The procedure has been shown to be capable of producing significant grain refinement in bulk samples down to sub-micron levels that can greatly improve the tensile and fatigue strength of a material while maintaining reasonable levels of ductility. [9] More importantly for biomedical implants, the grain refinement produced does not affect the low elastic modulus value. The application of ECAE to the class of metastable β titanium alloys has the potential to improve their performance in the critical areas where they are currently lacking.

Chapter 2

Background

2.1 Titanium alloys in biomedical applications

The use of titanium and its alloys for surgical implants dates back to the 1940s. [5] The excellent tissue compatibility and better corrosion resistance than stainless steel popularized the use of commercially pure titanium (CPTi) in implants, but the material was hindered by limited strength and very poor wear resistance. Interest in the use of Ti-6Al-4V for prostheses grew in the late 1970s grew because of its high strength and excellent corrosion resistance. In the 1980s however, retrieval studies began to indicate biocompatibility issues with the elements aluminum and vanadium present in the implants. Biocompatibility studies indicated that vanadium is toxic to cells and aluminum, while not toxic, undergoes rapid corrosion and ion exchange in the body environment which leads to oxygen depletion and high concentrations of the element in the surrounding tissues. [5][10][11] This lead to the development of alloys that were adaptations of those in common use at the time, such as Ti-6Al-7Nb which replaced the toxic vanadium with more compatible niobium and successfully duplicated the mechanical properties of Ti-6Al-4V. The alloy still used aluminum however, and retained its high modulus value, which lead to the problems of bone thinning and loosening commonly associated with stress-shielding. [5]

2.1.1 Biocompatibility requirements for joint replacement materials

The Consensus Conference of the European Society for Biomaterials (1986) defined biomaterials as nonviable (non-living) materials used in a medical device, intended to interact with biologic systems; they possess a combination of characteristics including chemical, mechanical, physical, and biologic properties that render them suitable for safe, effective, and reliable use within a physiologic environment, an environment that is both extremely hostile and yet sensitive to unforgiving irritating foreign bodies. [4] In addition, the materials must be able to perform their functions within the body environment for a long period of time (over 20 years) without deterioration.

In implant applications, one of the most critical mechanical properties is the elastic modulus of the material. Bone is a living anisotropic and viscoelastic material that adapts to the loads placed on it according to Wolff's Law which simply states that if the loading on the bone increases, the bone will remodel itself over time to thicker and stronger to resist that loading. The converse is also true. If the loading decreases, the bone will become thinner and weaker since it is less metabolically costly to maintain and there is no stimulus to maintain a high level of bone mass. [12] This is why a low stiffness value that approaches that of natural bone is critical in order to provide good load transfer between the implant and surrounding bone to stimulate new growth. The high stiffness of current implant materials causes stress-shielding which decreases the stresses experienced by the neighboring tissues causing resorption and thinning. [4]

Metal ions from metal implants are closely approximated by metal entry into the body through an open wound and its subsequent corrosion by interaction with the surrounding tissues through reduction-oxidation (redox) reactions. The kinetics and the products of these reactions are the determining factors that define the biocompatibility of an element. Metals with low corrosion resistance, or fast corrosion kinetics, in the body include silver, gold, aluminum, molybdenum, and iron. These metals, while not inherently toxic to cells, corrode so rapidly that the rate of oxygen migration through neighboring tissues cannot keep up with consumption and are therefore starved of oxygen. The body's response to this is to form an inert fibrous capsule around the implant to prevent damage to surrounding tissues. Commonly used alloying elements that exhibit toxicity to cells in the human body are vanadium, nickel, copper, and cobalt.

Metals that show inertness in body fluids are highly desirable for implant applications. The high biocompatibility and inertness of titanium is due to the characteristics of its oxide layer. The TiO_2 layer is an excellent insulator, and therefore does not readily transmit electrons to body tissues and fluids. Also, because the oxide layer forms by oxygen diffusing inward towards the metal interface instead of metal ions diffusing outward and combining with oxygen there is limited accumulation of ions into the surrounding tissue. Testing using pure metal plates with fibroblast cells placed on them in solution showed that titanium, niobium, tantalum, zirconium, and platinum are essentially inert due to their nonconductive oxide layers and do not cause any

deleterious effects upon cell growth and development. Therefore, these materials have the capacity to be used as alloying elements for improved biomedical titanium alloys. A map describing the biocompatibility of some of the various elements discussed above is shown in figure 2.1 below. [10][11] The map displays the tissue reaction as the abscissa, and polarization resistance as the ordinate. The polarization resistance of a material is defined by the ratio of a small potential applied to a freely corroding sensor, to the measured current response. This quantity is inversely related to the uniform corrosion rate; the higher the polarization resistance, the lower the corrosion rate.

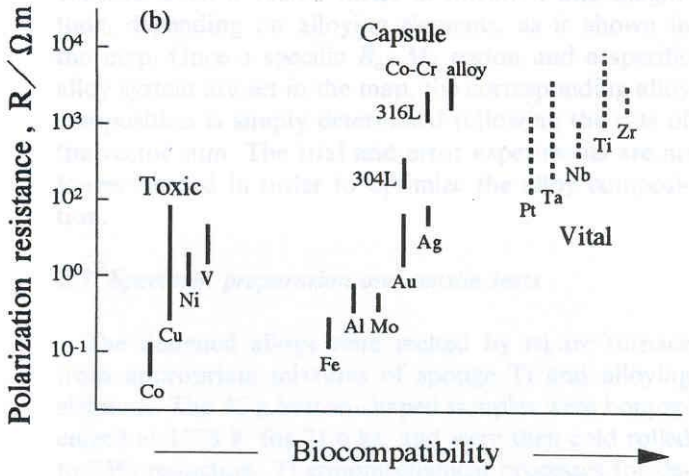

Figure 2.1 The relationship between polarization/corrosion resistance and biocompatibility of various metals [6]

2.2 Alloy design methods and current technology

The two main methods of controlling the properties of metals and alloys are thermomechanical treatments, and chemical methods or new compositions.

Thermomechanical treatments cover the traditional metalworking procedures along with pre- or post-processing heat treatments. The modulus can be sensitive to changes in the microstructure of a material if multiple phases are present, each with their own individual modulus contributing to the overall bulk value for the material. The volume fraction, orientation, and aspect ratio of the precipitate particles can be controlled through the use of these treatments. The modulus is not affected by the grain size of the material or the size of the precipitates. However, the strength properties are affected by these features which may allow for the modification or improvement of tensile properties while leaving the modulus undisturbed. [4]

Chemical methods and new material compositions focus on the effect of specific alloying elements and the properties of resulting individual phases. Recently, new types of orthopedic or "biomedical" titanium alloys have been developed. These are the metastable β-type titanium alloys. A titanium alloy may be classified as either α (hexagonal close-packed structure), near α, α + β, metastable or stable β (body-centered cubic structure) depending upon its room temperature microstructure. Alloying elements play a key role in determining the overall structure of the alloy. The simple elements, such as Al, O, N, C, etc., generally act as α stabilizers thus allowing the normally low temperature α structure to be maintained at higher temperatures. Transition metal elements, such as Mo, V, Nb, Ta, etc., generally act as β stabilizers thus allowing the high temperature β phase to be retained at low temperatures. [1][4] Metastable β alloys contain a sufficiently high amount of the

proper alloying elements to retain 100% of the high-temperature β phase upon quenching from above the α-β transition temperature. At ambient temperature however, these alloys exist in the two phase α-β region which results in the material being "metastable" with the potential to precipitate second phase α with the application of an aging heat treatment. [1] The alloying elements in these new materials are normally chosen to yield enhanced biocompatibility using the elements discussed above, and a low value elastic modulus compared to the alloys that are currently in use. Many of the compositions in this class of materials have been formulated through trial-and-error studies with some guiding empirical rules that may or may not represent the optimum choices. [4]

Trial and error studies have been performed using only titanium and varying quantities of tantalum as the alloying element. For alloys composed of 10wt% to 70wt% tantalum, it was found that the elastic modulus value first decreased, showed an increase from 30wt% - 50wt%, and then decreased again. These results were explained based on the resulting phases present. As more and more tantalum was added, different phases developed in the material possessing different modulus values. Variations in the modulus of a specific phase with different amounts of tantalum contained in it are explained by the different atomic sizes of the solute and solvent. The size discrepancy leads to lattice distortion which changes the average distance between atoms which results in a change in the modulus. The study also found that

the phases with the greatest potential for modulus reduction were the α´´ and β phases. A plot showing the modulus variation is shown in figure 2.2 below. [13]

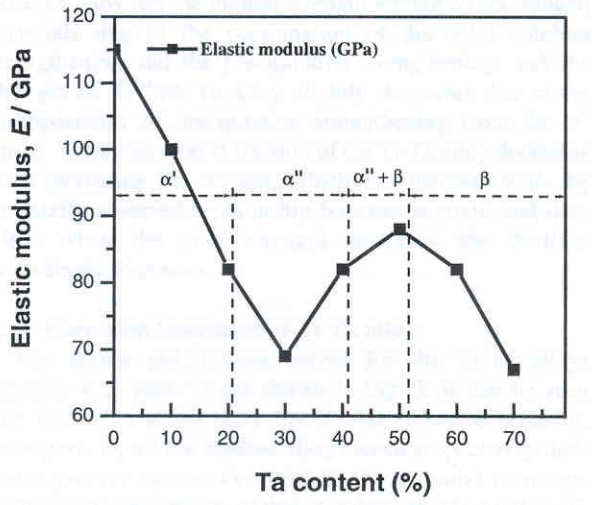

Figure 2.2 Elastic modulus of titanium alloys with varying tantalum content [13]

Trial-and-error studies using multiple elements based upon the biocompatibility results reported earlier resulted in the development of many different Ti, Nb, Zr, Ta alloys. The alloys ranged in compositions of 2.5wt% - 13wt% Zr, 20wt% - 40wt% Nb, 4.5wt%- 25wt% Ta, and the balance being Ti. This methodology resulted in three alloys of particular interest, with the most promising being an alloy composed of Ti, 35wt%-Nb, 7wt%-Zr, and 5wt%-Ta. [14] The map shown below in figure 2.3 is based on data taken from the trial and error study showing elastic modulus values for titanium alloys with niobium, tantalum, and zirconium content.

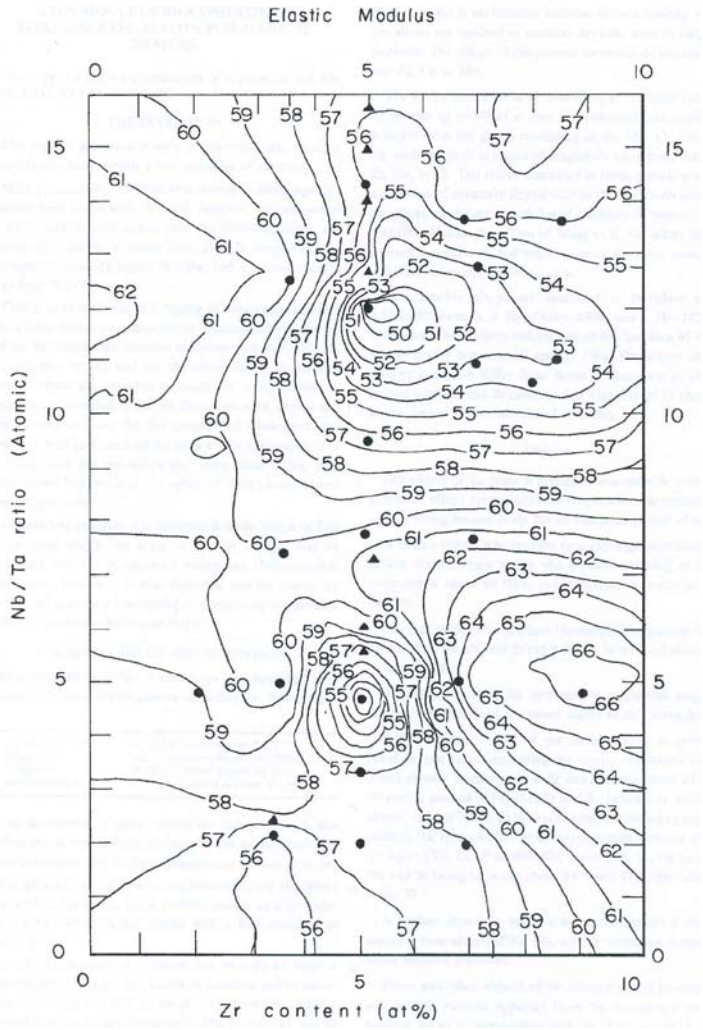

Figure 2.3 Modulus map for titanium alloys of varying Nb, Ta, and Zr content [14]

Researchers in Japan have attempted to develop a method for theoretical alloy design to eliminate the time and resource consuming trial-and-error method. The method is based on the calculation of electronic structures for titanium when it is alloyed with various elements. The two calculated parameters used to rank the alloys are the bond order (B_o) which is essentially a measure of the covalent bond strength between titanium and the alloying element, and the metal d-orbital energy level (M_d) which

correlates the electronegativity and the radius. It was found that the elastic modulus values of the β phase decrease with an increase in the bond order and d-orbital energy parameters. Phase stability maps (figure 2.4) that have been developed using these two parameters indicate that the high bond order and d-orbital energy regions that yield low modulus values coincide with β phase stability. The map has the locations of various alloys along with their modulus values printed in parentheses.

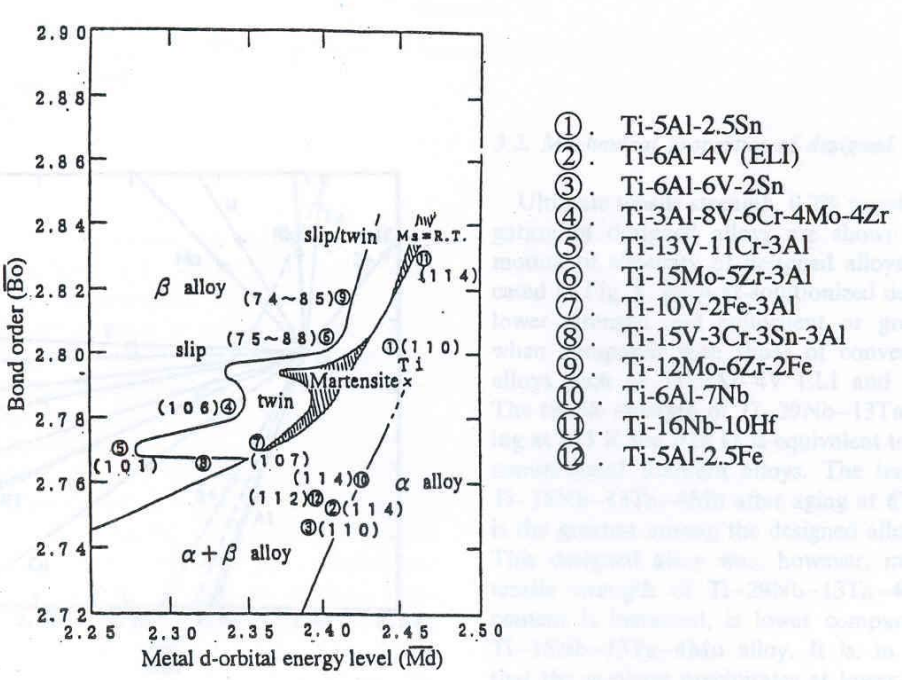

Figure 2.4 Theoretical phase stability map organized by bond order and d-orbital parameters [6]

This fact is rather fortunate since it implies that the biocompatible β-stabilizing elements discussed earlier can be used to develop a high-performance material for joint replacement applications. As the alloy composition varies, the alloy position will

move on the phase map. Figure 2.5 shows how alloying elements will affect the position of a titanium alloy through the use of vectors. Use of this method removes a significant amount of trial and error from the process of alloy design. [6]

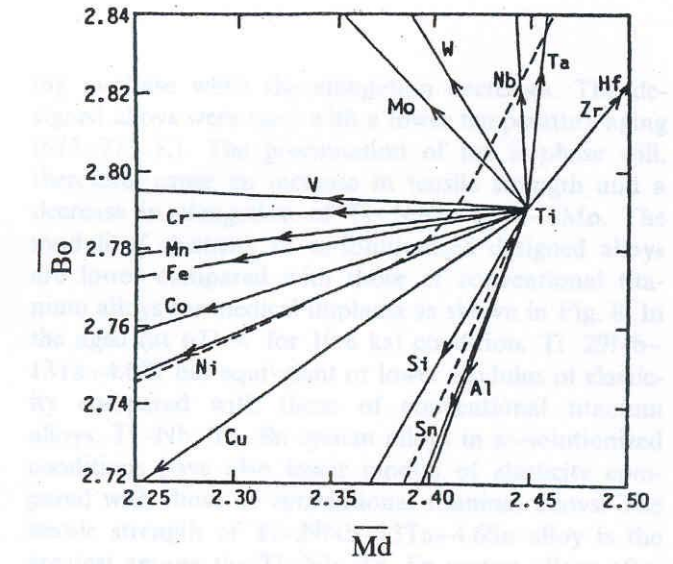

Figure 2.5 Vector map indicating the effect of alloying elements on the position of titanium alloys in the phase stability map [6]

The Ti, 35wt%-Nb, 7wt%-Zr, and 5wt%-Ta (TNZT) alloy, currently has the lowest modulus value of this class of materials (55GPa in the solution-treated condition). [1] Its alloying elements have been tested and found to be chemically and physiologically inert when placed in the human body. [10][11][15]

In order to confirm the claimed advantages in bone biocompatibility and healing with TNZT alloys, researchers Niinomi et al implanted rods of a Ti, 29wt%-Nb, 13wt%Ta,

and 4.6%Zr alloy into the legs of Japanese white rabbits and compared the results to equivalent implants made of Ti-6Al-4V and 316 stainless steel. The slight difference in alloy composition gives this particular TNZT alloy a slightly higher modulus value of 65GPa compared to the 55GPa obtained by the previously mentioned composition. Each specimen was surrounded by newly formed bone, but the extent of direct contact with the metal implant was greatest in the TNZT alloy, thus confirming the biocompatibility of the alloying elements with bone. The same group also created experimental fractures in the legs of the rabbits using an oscillating saw and subsequently implanted metal rods made of the either the TNZT alloy, Ti-6Al-4V, or 316 stainless steel in order to stabilize and fix the fracture. Bone healing, remodeling, and atrophy were observed using x-rays every 2 weeks up to 22 weeks. The rabbits implanted with the TNZT alloy showed a small fracture callus that gradually decreased from 6 weeks to 10 weeks, after which there were no traces of fracture. Rabbits with the Ti-6Al-4V implant showed similar features to those with the TNZT implant, but the entire process proceeded at a slower rate. The stainless steel implants exhibited the worst performance with a large fracture callus persisting until the end of the 22 week observation period along with the presence of bone atrophy and thinning. The end result is that the TNZT alloy was able to improve load transmission which resulted in an overall faster healing time. [16]

While the biocompatibility and modulus values of TNZT alloys are both excellent, the tensile and fatigue properties limit the joint replacement applications for human use

(σ_{yield}=530MPa, σ_{UTS}=590MPa, $\sigma_{fatigue}$=275MPa – Ti-35Nb-7Zr-5Ta). [1] The property values of a variety of joint replacement materials are shown below in table 2.1 and figure 2.6.

Table 2.1 Mechanical properties of biomedical titanium alloys [7]

Mechanical properties of titanium alloys for biomedical applications

Alloy	Tensile strength (UTS) (Mpa)	Yield strength (σ_y)	Elongation (%)	RA (%)	Modulus (GPa)	Type of alloy
1. Pure Ti grade 1	240	170	24	30	102.7	α
2. Pure Ti grade2	345	275	20	30	102.7	α
3. Pure Ti grade 3	450	380	18	30	103.4	α
4. Pure Ti grade 4	550	485	15	25	104.1	α
5. Ti–6Al–4V ELI (mill Annealed)	860–965	795–875	10–15	25–47	101–110	$\alpha+\beta$
6. Ti–6Al–4V (annealed)	895–930	825–869	6–10	20–25	110–114	$\alpha+\beta$
7. Ti–6Al–7Nb	900–1050	880–950	8.1–15	25–45	114	$\alpha+\beta$
8. Ti–5Al–2.5Fe	1020	895	15	35	112	$\alpha+\beta$
9. Ti–5Al–1.5B	925–1080	820–930	15–17.0	36–45	110	$\alpha+\beta$
10. Ti–15Sn–4Nb–2Ta–0.2Pd						
(Annealed)	860	790	21	64	89	
(Aged)	1109	1020	10	39	103	
11. Ti–15Zr–4Nb–4Ta–0.2Pd						$\alpha+\beta$
(Annealed)	715	693	28	67	94	
(Aged)	919	806	18	72	99	
12. Ti–13Nb–13Zr (aged)	973–1037	836–908	10–16	27–53	79–84	β
13. TMZF (Ti–12Mo–6Zr–2Fe) (annealed)	1060–1100	100–1060	18–22	64–73	74–85	β
14. Ti–15Mo (annealed)	874	544	21	82	78	β
15. Tiadyne 1610 (aged)	851	736	10		81	β
16. Ti–15Mo–5Zr–3Al						β
(ST)	852	838	25	48	80	
(aged)	1060–1100	1000–1060	18–22	64–73		
17. 21RX (annealed) (Ti–15Mo–2.8Nb–0.2Si)	979–999	945–987	16–18	60	83	β
18. Ti–35.3Nb–5.1Ta–7.1Zr	596.7	547.1	19.0	68.0	55.0	β
19. Ti–29Nb–13Ta–4.6Zr (aged)	911	864	13.2		80	β

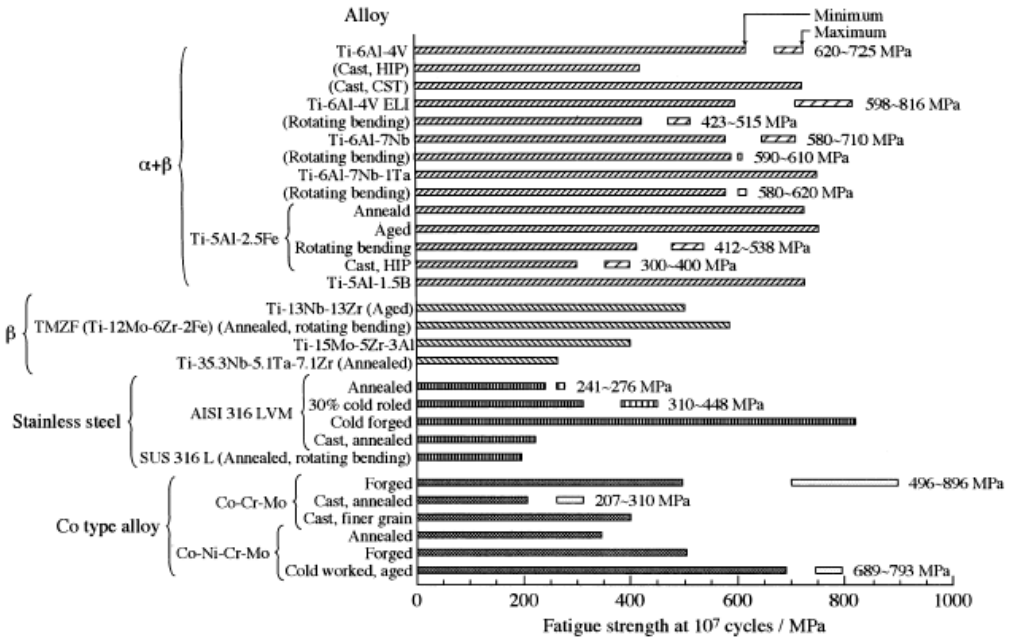

Figure 2.6 Fatigue strength values for various joint replacement alloys [7]

Inspection of the table shows that the TNZT alloy has the lowest modulus value (55GPa) of the alloys listed, however it can also be seen that it has some of the lowest values for tensile, yield, and fatigue strengths when compared to the others. Many studies have been done on attempts to improve the properties of TNZT and other metastable β type alloys. The most common approaches are to either increase the oxygen content of the alloys, or subject them to an aging heat treatment. Both methods result in the retention or precipitation of a second phase (α or ω) that is successful in improving the tensile and fatigue properties, but this increase comes at the expense of the elastic modulus which is increased by the presence of the stiffer second phase particles. [2][3][15]

2.3 The effect of boron addition in titanium alloys

Metastable β alloys are single phase materials, a characteristic that gives them their low modulus value. Unfortunately, single phase materials are susceptible to rapid grain growth at elevated temperatures since there are no obstacles to slow dislocation motion or grain boundary migration. The high temperatures required by ECAE processing and post-extrusion heat treatments, coupled with the tendency for grain coarsening, could effectively limit the maximum amount of grain refinement possible and restrict the potential property improvements. The addition of boron to titanium alloys has been used in the past to restrict grain growth through the formation of a second phase intermetallic compound TiB. [17] Both solid solution atoms and second phase particles are capable of restricting the motion of dislocations and grain boundaries which will impede the recovery, recrystallization, and grain growth processes. [18] The choice to use boron to induce the second phase particles can be explained by the titanium-boron phase diagram shown in figure 2.7.

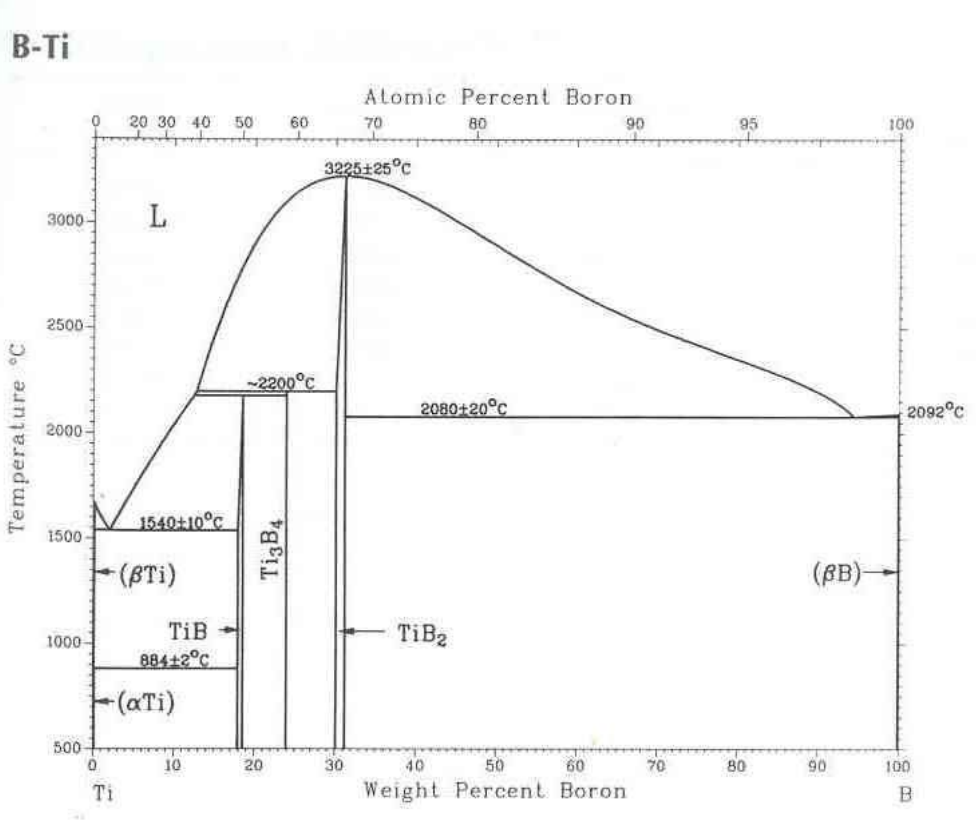

Figure 2.7 Ti-B phase diagram [19]

Examination of the phase diagram shows that boron has very limited solid solubility in titanium at any temperature up to melting. Instead the material will consist of α- or β-phase titanium, depending on the temperature, plus second phase TiB (titanium boride) particles. The preservation of the TiB particles at very high temperatures is advantageous because the particles will not disappear and go into solution when the material is heated. Since grain growth is most prevalent at higher temperatures, this means that the material can retain the pinning effect of the particles when it is most needed. Boron has been investigated for use in coatings on various metal implant alloys, and has been determined to be acceptable for use in biomedical applications in

the human body. [20] Boron's capacity to help achieve grain refinement and its biocompatibility make it an excellent candidate to help improve the properties of TNZT and other biomedical titanium alloys.

2.4 Severe plastic deformation by equal channel angular extrusion

Severe Plastic Deformation (SPD) is an effective method of altering the microstructures and improving the properties of different materials. Equal channel angular extrusion (ECAE) is a processing method during which large amounts of plastic strain are induced in a material through simple shear deformation. [8] This is done by forcing the material through a die consisting of two channels of equal cross-sectional area that intersect at some angle Φ. There is also an additional angle Ψ which defines the arc of curvature at the outer point of the two intersecting channels. Figure 2.8 shows a schematic of the ECAE process and the deformation of a cubic element as it passes through the shear zone.

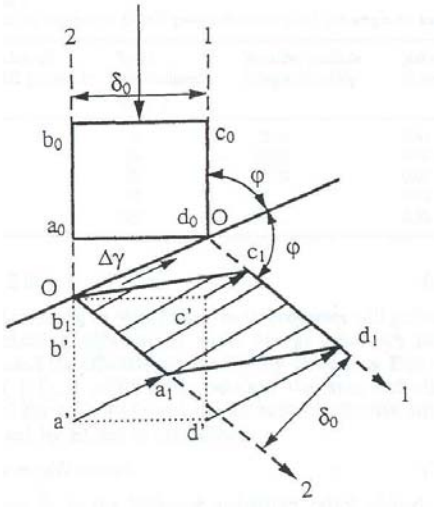

Figure 2.8 Schematic of the ECAE process [21]

Analysis has shown that the pressures required to extrude the billet are dependent upon the material properties and the amount of strain induced per pass. [8][22] The principal advantage of the ECAE process is that the deformed billet has essentially the same dimensions as the original undeformed billet. This eliminates the cross section reduction required by traditional methods which limits the usability of the finished piece, and also allows the billet to be subjected to multiple passes through the die. The strain induced during multiple passes is additive thus resulting in the ability to produce a theoretically unlimited amount of strain in single sample. The amount of strain introduced in the sample is highly dependent upon the channel angle Φ, and somewhat less dependent on the corner angle Ψ. The strain produced by a channel angle of 90° is approximately equal to 1 regardless of the corner angle used. [23]

When subjecting the material to multiple passes, the billet can also be rotated from its original orientation in between passes which enables the material to be subjected to different processing routes. These different processing routes allow for the production of various textures and structures in the material. ECAE produces homogeneous structure and properties throughout the deformed sample except for small sections at the leading and trailing edges of the billet. This homogeneity is one of the leading motives for the use of ECAE to produce severe plastic deformation that can result in ultra-fine grain sizes in a material. [8][24]

ECAE processing has the capacity to produce grain sizes in the sub-micron and sometimes nano-scale range. There are three mechanisms of grain refinement that can operate in ECAE processing. The first method is through grain fragmentation, in which the coarse grained microstructure is directly broken down into a fine grained structure with intense plastic strain induced by multiple passes through a die. It is based on the formation of subgrain boundaries (low-angle boundaries) produced by the induced shearing action during the first pass through the extrusion die. When subjected to subsequent passes the misorientation of the subgrain boundaries increases and the low-angle boundaries eventually become high-angle grain boundaries for the refined structure. Low-angle boundaries convert into high-angle boundaries by the absorption of moving dislocations into the low angle boundaries. [25][26][27] The second is dynamic recrystallization (DRX) which operates on the principle of realignment of induced dislocations into new grain boundaries during extrusion. The

third is static recrystallization (SRX) during which a new set of fine, equiaxed strain free grains are nucleated and grown during a post-extrusion heat treatment. The driving force for this to occur is a reduction of the strain energy induced during extrusion. [28][17] The particular method of grain refinement depends mainly on the ECAE processing conditions that are used. Grain fragmentation tends to occur in highly ductile materials that can be extruded at room temperature and tolerate multiple extrusion passes without fracture. DRX requires higher temperatures and specific strain rates in order to allow for dislocation migration, and time for full realignment into new grain boundaries. SRX can be used after extrusion at either high or low temperatures. It is normally employed to produce an equiaxed structure from the highly deformed structure left after only a few extrusion passes.

2.4.1 The structure of deformed materials and grain fragmentation

In order to more fully understand the grain refinement mechanisms in ECAE processing, it is necessary to begin with a discussion of the structure of deformed materials. Plastic deformation in metallic materials occurs by the motion of dislocations on specific crystallographic planes. The crystal lattice type, along with the ability of a material to allow dislocation cross-slip, determines the structures at higher levels of strain. Polycrystalline materials at high strain levels must have a deformation mechanism to accommodate changes in the overall grain shape in order to preserve coherency at the grain boundaries. In general, metals with a cubic crystal structure and higher stacking fault energies (easy cross-slip, or wavy slip) are capable

of accommodating grain shape changes by deforming in a complex manner on a multitude of slip-systems. Metals with a hexagonal structure and lower stacking fault energies (difficult cross-slip, or planar slip) only possess a limited number of operational slip systems, and therefore must accommodate grain shape changes through the use of alternate deformation mechanisms such as mechanical twinning. [29]

The grain fragmentation mechanism of grain refinement mentioned earlier results from the substructure formed during deformation. Early studies using electron microscopy showed that regions inside the grains of deformed high purity aluminum are broken up into units of slightly misoriented "crystal domains" that are now usually referred to as "cells". These cell interiors are relatively free from dislocations, but the walls are regions of high dislocation density. The arrangements in these walls are very complex, and are often associated with small loops. The misorientation across the cell walls was small during the early stages of formation, but as deformation continued the cell walls became more delineated and the misorientation increased. Studies performed on α-brass have led to the conclusion that this cell structure results from the ability of screw dislocations to cross-slip out of their original slip planes and to arrange themselves in localized regions that form the walls of the relatively strain-free cells. Therefore, it is much more likely that cells structures will occur in cubic materials with high stacking fault energy with many different possible slip systems, and easy cross-slip. [29] This reinforces the previous observation that grain

fragmentation is normally a feature of highly ductile materials that can be extruded at room temperature. Materials with a hexagonal crystal structure and low stacking fault energies will not have a tendency to form the cell structure, and are unlikely to even possess the ductility levels required for extrusion at room temperature. These materials must be extruded at higher temperatures where static and dynamic recovery and recrystallization processes counteract the cell structure formation.

2.4.2 Static recovery and recrystallization

During any type of deformation including ECAE processing, strain energy is stored within the material in the form of an increased number of dislocations, point defects, and stacking faults. It is this "energy of disorder" that provides that driving force for static recovery and recrystallization to occur. The term *static*, implies that the processes are occurring after the deformation has taken place, unlike *dynamic* recovery and recrystallization which occur during deformation processing. This energy can be released upon the application of heat in an annealing process at high temperature. Recovery can be defined as all of the various annealing phenomena that occur prior to the appearance of new strain-free grains, and recrystallization is defined as the nucleation and growth of strain-free grains up to the stage at which their boundaries impinge upon each other. The structural changes that occur during the recovery phase are relatively complex, but essentially they are associated with the annihilation of vacancies and the rearrangements of dislocations into low energy configurations to produce structures that are intermediate between the cold-worked

and recrystallized state. The rearrangement processes (e.g. dislocation climb, etc) tend to be much more difficult in materials with a low stacking fault energy versus the high stacking fault energy materials which allows for easier overall dislocation motion and rearrangement. [29]

A considerable amount of experimental evidence has been collated and condensed into six basic “laws of recrystallization”. These are given below.

1. A minimum amount of deformation is needed to initiate recrystallization.
2. The smaller the amount of deformation, the higher the temperature required to cause recrystallization.
3. Increasing the annealing time decreases the temperature necessary to cause recrystallization.
4. The recrystallized grain size depends chiefly on the degree of deformation and to a lesser extent on the annealing temperature, being smaller the larger degree of deformation and the lower the annealing temperature.
5. The larger the original grain size, the greater is the amount of cold deformation that is needed to give equivalent recrystallization temperature and time.
6. The amount of cold work required to give equivalent hardening increases with increasing temperature of working.

Recovery can have an impact on the recrystallization process since both procedures depend upon a fixed amount of strain energy that has been stored in a material at the beginning of the annealing process. A material that undergoes recovery easily (high stacking fault energy) will therefore utilize a greater percentage of the stored strain energy which will delay the onset and the completion of recrystallization, while materials in which recovery processes are difficult (low stacking fault energy) retain a greater portion of the stored strain energy for rapid recrystallization to occur. [29] Many various models for the nucleation of recrystallized grains have been proposed, but an in-depth discussion of each is beyond the scope of this work.

As previously mentioned, the large amounts of strain induced during the ECAE process can be used for grain refinement by static recrystallization. The technique can be used after extrusion at either high or low temperatures. Depending upon the processing route used and the number of passes, the grain structure may or may not be equiaxed. Achieving a uniform equiaxed structure normally requires multiple extrusion passes through the die which may or may not be desirable. If only a single pass or limited number of passes can be used, the deformed or elongated grain structure can be converted to a finer equiaxed structure by annealing the sample and inducing recrystallization. The procedure can also be used in applications where there is incomplete dynamic recrystallization that has left behind deformed and untransformed regions in the material. A significant drawback of static recrystallization is a relative lack of process control since recrystallization rarely

proceeds uniformly throughout the entire workpiece and thus will not reach completion (boundary impingement) at the same time. This makes it extremely difficult to determine annealing treatments that will allow for the total completion of static recrystallization and at the same time stop the process before some appreciable grain growth can occur. Therefore, this method of grain refinement may not yield the minimum achievable grain size.

2.4.3 Dynamic recovery and recrystallization

There are several reasons why metals and alloys are hot worked at temperatures greater than ~$0.5T_m$. The two most important to ECAE processing are that materials generally possess lower flow stresses at higher temperatures, and metals at high temperatures are generally capable of undergoing much larger deformation strains without fracture. The high temperature conditions make hot working in some respects resemble a creep phenomenon, but the strain rates and flow stresses are much higher in hot working which can alter the microstructure much more significantly than is usually seen in creeping materials.

A schematic of the structural changes that can occur during a typical hot working process is shown in figure 2.9.

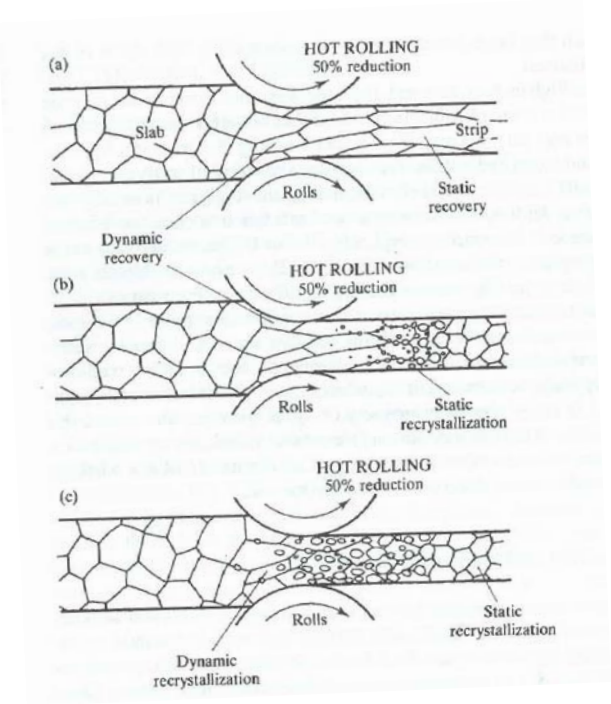

Figure 2.9 Common microstructural changes during hot working [17]

As indicated in the figure, dynamic recovery and or dynamic recrystallization can occur during hot working. Whether only dynamic recovery or both dynamic recovery and recrystallization occur depends on the stresses and strain rates involved. In general, the higher both stresses and strain rates are, the greater the tendency for recrystallization to occur. Some materials are not capable of dynamic recrystallization and only undergo dynamic recovery. These materials tend to be high stacking fault energy materials that exhibit rapid recovery rates, and therefore are not capable of developing dislocation densities and configurations that are sufficient to nucleate and drive recrystallization. In contrast, low stacking fault energy materials will experience dynamic recrystallization under most hot working conditions.

Dynamic recovery can be viewed essentially as creep occurring at high strain rates. The true stress-strain curve of a material undergoing only dynamic recovery is shown in figure 2.10.

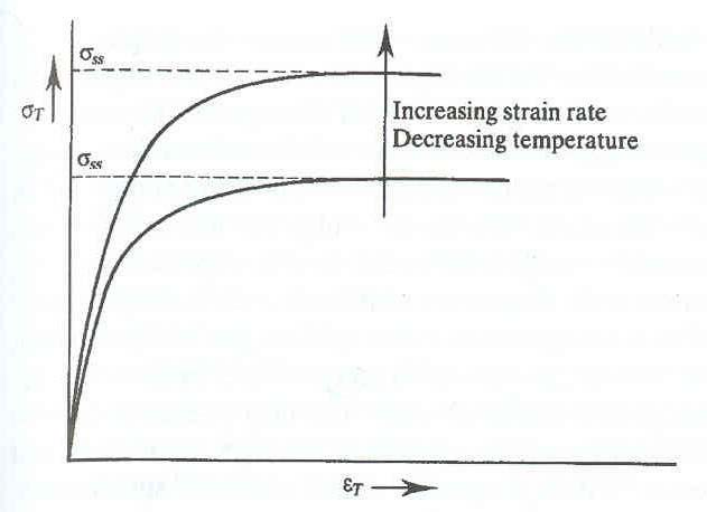

Figure 2.10 Characteristic stress-strain curve for a material undergoing dynamic recovery [17]

As can be seen in the figure, the flow stress rises to a steady-state value which will increase with either a higher strain rate or lower temperature. For dynamic recovery to occur it is generally necessary for dislocations to be able to leave their original slip-plane in order that mutual annihilations with dislocations of opposite sign can take place, or that they may take up positions which are energetically more favorable. This is normally achieved with screw dislocations by cross slip, and in edge dislocations by climb. [29] The microstructure after deformation appears similar to a material that has

undergone creep deformation. The grains become elongated in the primary strain direction and contract in the other directions. [17][29]

In dynamic recrystallization, the new set of strain-free grains is nucleated during high-temperature deformation. A schematic of the true stress-true strain behavior of a material undergoing dynamic recrystallization is shown in figure 2.11.

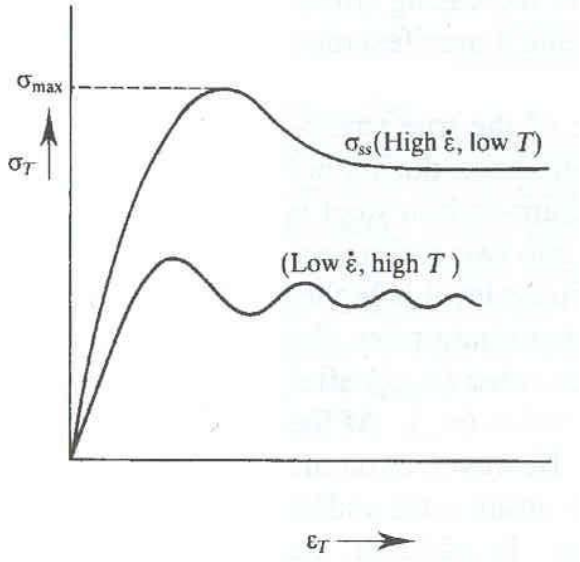

Figure 2.11 Characteristic stress-strain curves of a material undergoing dynamic recrystallization [17]

Material response can be divided into two categories depending upon the strain rates and temperatures applied. At higher strain rates or low temperatures, the flow stress increases following yielding and attains a maximum value after which the stress decreases and reaches a steady-state value. In addition, the overall flow stress levels are higher. At lower strain rates or higher temperatures, the stress-strain curves

develop an oscillatory nature which eventually dampens out to a steady value at higher levels of strain. Also, the overall flow stress values are lower.

This contrasting behavior reflects the different structures developed in materials under the different conditions. The high strain rate/low temperature condition possesses recrystallized and cold-worked grains throughout the material, or in other words, recrystallization occurs continuously throughout the material volume; prior to one recrystallization event being completed in one grain, another is initiated in another grain. This structure is heterogeneous, in that grains that have just recrystallized have a low dislocation density compared to non-recrystallized grains that possess a well-developed substructure with a high dislocation density. This implies that a critical substructure must be developed before recrystallization can commence in a single grain. Because of the high strain rates, there is not much time required for an individual grain to achieve this critical structure. Under low strain rate/high temperature conditions, it takes a longer time and a greater amount of strain to accumulate the critical dislocation density needed to trigger recrystallization. As a consequence, recrystallization "waves" pass through the material. At any specific time during deformation, the grains all possess approximately the same substructure which progressively becomes finer and develops a higher dislocation density until the recrystallization wave is initiated. [17]

Dynamic recrystallization has been used to refine the grain size in materials that must be ECAE processed at high temperatures. This is no menial task however, since the ECAE processing conditions (most notably temperature and strain rate) must be applied correctly such that recrystallization can be induced. In addition, similarly to static recrystallization it is difficult to induce recrystallization uniformly throughout the entire sample billet. The tendency is to have regions that have dynamically recrystallized adjacent to highly deformed regions that have yet to undergo transformation. Additional ECAE passes can help produce a more regular microstructure by giving the untransformed regions another chance to recrystallize. If this can be accomplished, it becomes much easier to control the grain size compared to the use of static recrystallization which normally results in larger final grain sizes.

2.4.4 ECAE variables

Channel angle and corner angle

The die channel angle governs the amount of strain accumulated in the billet during one ECAE pass. Iwahashi et al. derived a result for the strain induced during processing which incorporates the corner angle Ψ along with the channel angle Φ. This result was used to generate the plot shown in figure 2.12. The channel angle is the dominating parameter and for $\Phi = 90°$ the strain is approximately equal to 1 for a range of corner angles. [30] Studies performed by Nakashima et al. on the influence of the channel angle with respect to the development of small grain sizes have shown that in order to achieve an ultra-fine equiaxed microstructure with high angle grain

boundaries (HAB) the corner angle should be close to 90°. Tests were performed on dies with channel angles varying from 90° to 157.5° and the samples were subjected to a sufficient amount of passes to induce the same amount of total strain. When the structures were examined it was found that dies using progressively smaller channel angles were more successful at producing a fine equiaxed microstructure with high angle boundaries. Large angle dies showed some subgrain formation, but did not exhibit the conversion of subgrain boundaries to grain boundaries. Thus the conclusion was formed that better grain refinement is achieved through the application of a few passes at high levels of strain rather than many passes at low levels of strain. [23]

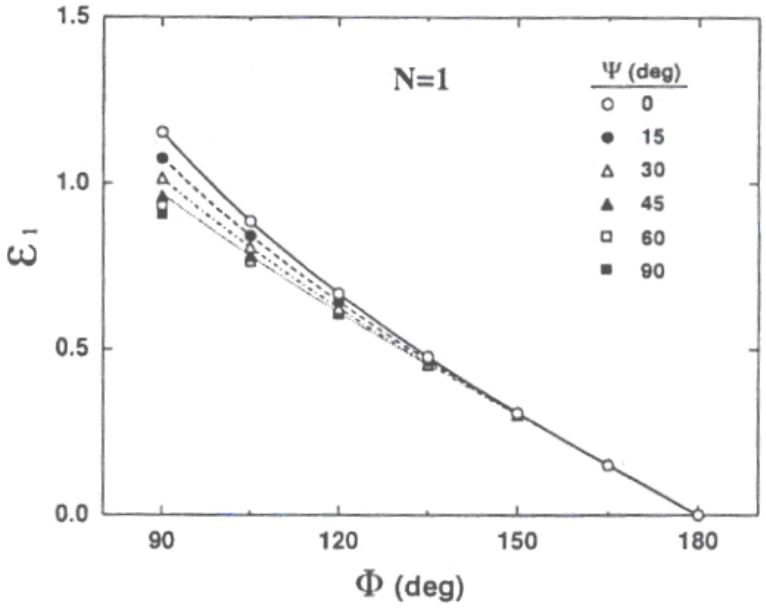

Figure 2.12 Strain vs. 90° channel angle for different corner angles [30]

There are two general types of dies commonly used in ECAE processing, the streamline and sharp-angle die. Both types are shown in figure 2.13.

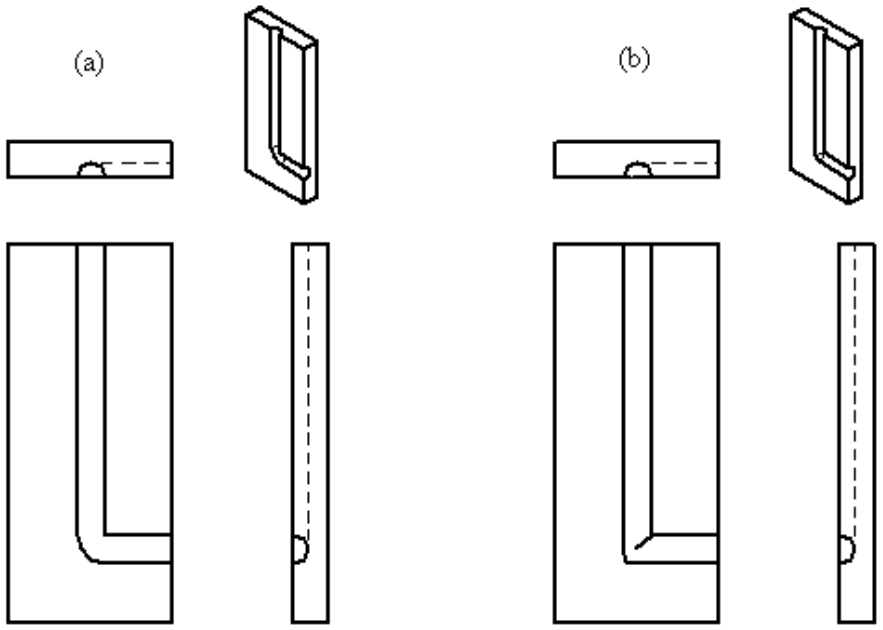

Figure 2.13 (a) Streamline die (b) Sharp-angle die [31]

Streamline dies (shown on the left) possess perfectly rounded corner angles ($\Psi = 90°$), while sharp-angle dies (shown on the right) have much smaller corner angles ($\Psi \approx 20°$). The corner angle can have a significant effect on the uniformity of the strain distribution produced during an extrusion pass. Studies performed by Bowen et al. concluded that the strain distribution in the billet is most homogeneous when the shear deformation zone is kept as narrow as possible. Streamline dies generally have slightly lower press force requirements and allow the billet to completely fill the die at the channel intersection, but the large corner angle spreads the deformation zone out

into what has been called a “fan-shape”. [32] The spreading of the deformation zone leads to a tendency for the material along the bottom portion of the die to be bent rather than sheared inducing significantly less strain and contributing to heterogeneity in the strain distribution. [32] Sharp-angle dies allow the material to completely fill the outer corner of the die, but the much smaller corner angle restricts spreading of the deformation zone and induces a much more uniform overall strain distribution. The corner angle effect becomes even more pronounced when the channel angle of the dies is increased to larger values beyond 90°. [32] FEM simulations performed by Pond reinforce the idea that the streamline dies produce strain distributions with a lower degree of uniformity than sharp-angle dies, and that this characteristic is independent of the diameter of the sample billet. This is easily seen by inspection of a simulation result performed on a 0.6” diameter billet shown below. [31]

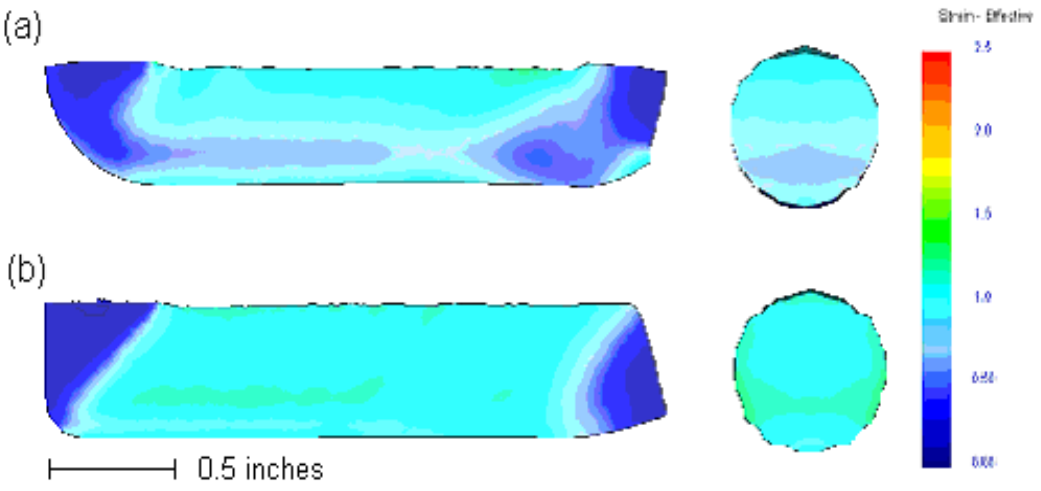

Figure 2.14 Strain distributions in samples extruded in 0.6” (a) SL and (b) SA dies..[31]

Processing routes

Various processing routes which control and alter the sample's orientation between passes during multi-pass processing have been developed and studied for their effect on microstructure and texture. Multiple processing routes for ECAE have been developed. These routes are represented by various capital letters and subscripts depending on the source being used. The convention for route representation in this work is summarized in table 2.2 below.

Table 2.2 ECAE processing routes [33]

Route	Number of pressings						
	2	3	4	5	6	7	8
A	0°	0°	0°	0°	0°	0°	0°
B_A	90° ↖	90° ↘	90° ↖	90° ↘	90° ↖	90° ↘	90° ↖
B_C	90° ↖	90° ↖	90° ↖	90° ↖	90° ↖	90° ↖	90° ↖
C	180°	180°	180°	180°	180°	180°	180°
B_A-A	90° ↖	0°	90° ↘	0°	90° ↖	0°	90° ↘
B_C-A	90° ↖	0°	90° ↖	0°	90° ↖	0°	90° ↖

Table 2.3 Shearing characteristics for six processing routes [33]

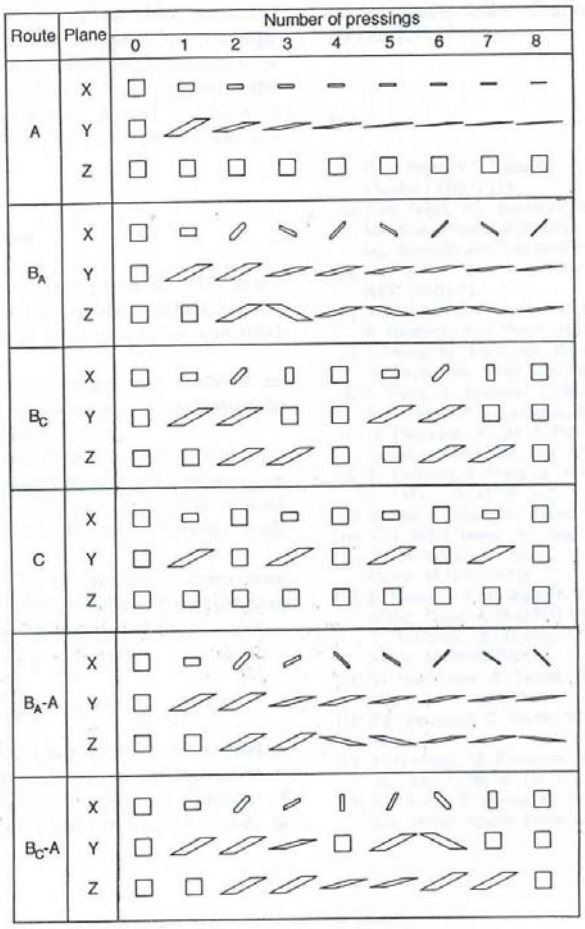

These processing routes were studied based upon the shearing effect they induce upon a cubic element passing through a 90° die. The effect is summarized in table 2.3 shown above. It can be seen that the different processing routes have the capacity to introduce different textures and also optimize grain refinement through examination of the distorted element. Routes B_C, C, and B_C-A all restore the cubic element to its original shape after four, two, and eight passes respectively. These processing routes are the most likely to produce grain refinement with an equiaxed microstructure.

Routes A, B_A, and B_A-A all continue to deform the billet with increasing passes through the die, and will likely have a tendency to induce strong rolling or extrusion textures. [33] The efficiency of the route for the production of a refined equiaxed microstructure has been studied in aluminum and titanium alloys. When the channel angle is equal to 90°, the most efficient route for grain refinement has been found to be route B_C. It can be seen why route B_C has emerged as a kind of optimum route because it deforms the billet in the X,Y, and Z planes unlike route C which does not affect the Z plane, and it restores the billet to its original shape before route B_C-A. The effect of the texture produced during extrusion, the angle of interaction between shear planes on subsequent passes, the channel angle, and the crystal structure of the material also affect the efficiency of grain refinement, but that is beyond the scope of this work. [24][27][30][34][35]

Temperature

Temperature is one of the most investigated ECAE variables because it can have a large impact on ECAE processing. Extruding at high temperatures is beneficial for materials with limited ductility, since the intense shear strain generated may cause cracking in the samples. Studies on aluminum alloys have shown that an increase in the processing temperature results in an increase in the subgrain size produced, and thus the final grain size. [22] It has also been shown that the grains become more equiaxed, and the number of low angle grain boundaries increases. [25][26] Low angle boundaries evolve into high angle boundaries by the absorption of moving dislocations

into the boundaries during deformation. At elevated temperatures, dislocation annihilation by cross slip is facilitated, and therefore dislocations have a greater chance of being annihilated within the grain interiors. Consequently, the frequency of dislocation absorption into low angle boundaries is lessened and boundary disorientation decreases. [25][26] Temperature also has a large effect on the operating mechanism that will control microstructural deformation and evolution. During deformation at low temperature, the grains are elongated into HAB fragments which are oriented along the shear direction. The internal stresses cause high internal energies that can be used to convert the fragments into equiaxed grains using a subsequent heat treatment. [36]

Strain rate

Studies conducted on aluminum alloys have shown that pressing speed does not have a significant effect on the resulting grain size over a range of 10^{-2} to 10 mm s^{-1}. Pressing speed does have an effect on the nature of the microstructure when deformation occurs at high temperatures since recovery and dynamic recrystallization occur more easily at slower strain rates. Therefore, the resulting microstructure is more equilibrated and contains fewer extrinsic dislocations when the material is processed at slower speeds. Hardness, strength, and failure elongations of the samples were relatively unaffected by the pressing speeds, except for a small increase in the yield strengths in the higher speed samples. The same study also contains findings that suggest samples with small cross sections may be more influenced by frictional

effects between the sample and the die walls. These frictional effects become significant at the surface of the sample since they can lead to the development of significantly lower strains than predicted and also cause the strain field to develop non-homogeneities. [37]

2.5 The effect of ECAE processing on mechanical properties

2.5.1 Fatigue

As with most types of fracture, fatigue fracture involves crack nucleation, growth, and coalescence eventually leading to final rupture. The fatigue process has been broken up into three stages. Stage I being crack nucleation, stage II being crack propagation, and stage III being final fracture of the component. The crack nucleation process is initiated by inhomogeneous plastic flow usually occurring at the microscopic level. Cracks in metals can originate at either internal or external surfaces, with the latter being the more common locations. The inhomogeneous plastic flow mentioned just mentioned can, under the action of cyclical stress or strain, produce surface features that bear a resemblance to a crack or flaw. The schematic shown in figure 2.15 illustrates where surface “intrusions” and “extrusions” arise from local heterogeneous plastic flow sometimes called persistent slip bands.

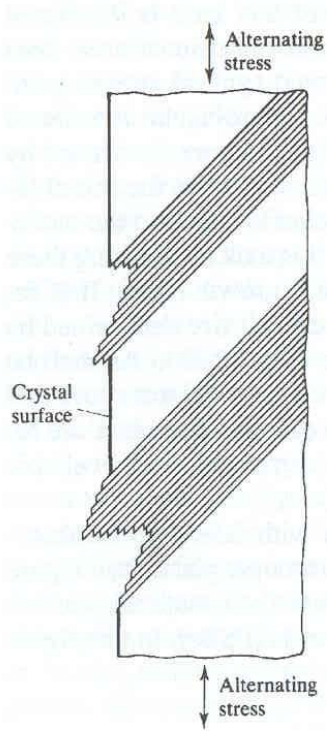

Figure 2.15 Schematic illustrating the formation of intrusions and extrusions on a material surface [17]

Continued cycling enhances these features and eventually at some point, a surface crack can be considered to be nucleated. Crack initiation can come about through other causes of strain heterogeneity. For example, cracks have been observed to nucleate at grain boundaries where localized flow is not accommodated. Second phase particles are also known crack initiation sites due to stress concentrations resulting from the different flow behavior between the particles and the matrix. [17]

Improving the fatigue properties of a material means either arresting crack initiation or crack propagation. The response of a material's fatigue characteristics to grain refinement normally depend on the initial fine-grained microstructure, the dominating

slip mode, fatigue mode (low-cycle or high-cycle), and any cyclic hardening or softening that may occur. [18] The characteristics of ECAE processing are such that many different microstructures can be produced including either an equiaxed structure, or a fragmented and elongated structure oriented in the shear direction. The dominating slip mode in this context refers mainly to the material having either wavy-slip (easy cross-slip) or planar-slip (difficult cross-slip). Wavy-slip materials, such as copper or aluminum, generally have high stacking fault energies and an FCC structure that yields higher dislocation mobility. The planar slip materials, such as titanium, generally have lower stacking fault energies and HCP or BCC structures. Dislocation mobility is usually lower in these types of materials. Low-cycle fatigue (LCF) and high-cycle fatigue (HCF) are separated from each other according to the applied strain amplitudes. Short fatigue lives are associated with higher cyclic strain values, termed strain-controlled or constant strain fatigue. The higher strain values means that the plastic strain component of the material is dominant, and therefore the overall fatigue life is determined by the ductility and crack propagation rate. Long fatigue lives are characterized by lower strain values induced by constant stress, or stress-controlled fatigue. In this mode, the elastic strain amplitude becomes dominant, and the overall fatigue life is determined by the fracture strength and rate of crack initiation. [38] Therefore, improving both LCF and HCF is a difficult task since improvements in the ductility and strength are normally competitive processes. The often claimed high strengths and reasonable ductility of ECAE processed materials would seem to have the potential to produce enhancements in both LCF and HCF regimes. [18]

The effects of grain refinement are strongest in the stress-controlled/high-cycle regimes where stage I (crack initiation) dominates. Improvements due to grain refinement in this fatigue regime are due to the increased number of grain boundaries which act as obstacles to dislocation motion. In coarse-grained materials, the relatively unobstructed dislocation motion leads to slip interactions and intersections that create intrusions which are the precursor to the formation of fatigue cracks. Wavy-slip materials usually do not show the same level of improvement as planar-slip materials. During cyclic loading, wavy-slip materials tend to form dislocation cell structures within the grains that act as obstacles and minimize the role of the grain boundaries and grain size. The planar-slip materials do not form these cell structures which results in the grain boundaries playing the dominant role in limiting crack nucleation, and the fatigue strength following a Hall-Petch type relationship. [38][39] ECAE processing may still be beneficial to both types of materials. The dislocation cell size formed in wavy-slip materials is on the order of 0.5μm. If the grain structure can be refined below this size threshold, the grain boundaries will take over and become the dominant resistance mechanism. [38] Planar-slip materials will of course benefit from any magnitude of ECAE induced grain refinement.

The material response in the strain-controlled/low-cycle regime is also dependent on the slip mode. The wavy-slip materials exhibit shorter LCF lives upon grain refinement, while planar-slip materials seem to be capable of at least maintaining the

same life as a coarse-grained counterpart. Two reasons for the shortening of LCF life have been proposed – cyclic softening and strain localization. [18] The ECAE produced grain structure is strengthened by a dense dislocation network. This substructure has a tendency to recover during fatigue due to the back and forth motion of dislocations, which can cause dislocation annihilation. The wavy-slip materials with their ease of cross-slip are more susceptible to this cyclic softening/recovery process than planar-slip materials with their characteristically lower dislocation mobility. [38] Therefore, in order to improve or at least maintain the LCF life in fine-grained materials, softening and strain localization must be controlled. Since softening is essentially a recovery process, any traditional technique of restricting dislocation motion through the bulk can be used such as solid solution-strengthening or precipitation hardening. [38] Susceptibility to slip band formation is greatly reduced in annealed materials that exhibit higher ductility and harden upon cycling instead of softening. Application of post-extrusion heat treatments to ECAE produced equiaxed microstructures could produce a partly recovered structure that would increase ductility, and lessen the localization of plastic flow. [18]

Fatigue studies performed on the metastable β-type biomedical titanium alloys including TNZT, TNZT with greater oxygen content, and 21SRx (TIMET ®) have shown that the grain boundaries serve as the one of the material's primary obstacles to crack nucleation and propagation. It was observed that fatigue failure originated at the specimen surface and progresses transgranularly through the matrix. Crack initiation

with intersecting planar slip bands that resulted in the formation of surface intrusions as shown in figure 2.16. [40]

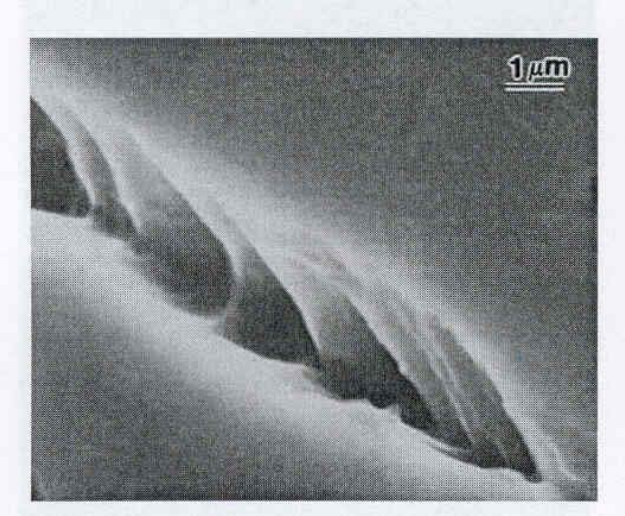

Figure 2.16 SEM micrograph of surface intrusions in TNZT alloy [40]

Further investigation revealed that the slip bands were not constrained within one grain, but propagated through several grains without obstruction or redirection. The cause of this was attributed to the grain boundaries in the sample being mostly low angle boundaries (<15º) that allowed for slip to proceed from one grain to another without significant resistance. This effectively increased the grain size of the material and lowered the fatigue resistance of the material allowing larger amounts of damage to accumulate and cause crack nucleation and reduced life. [40] The application of the ECAE process, and its capacity to produce materials with small grain sizes and a high proportion of high-angle boundaries should be a major benefit to this class of materials.

Fatigue in fine-grained ECAE processed material is a relatively complicated process depending upon many things including but not limited to: the initial microstructure, fatigue response under constant stress amplitude, cyclic hardening/softening and its dependence on the plastic strain amplitude, and the morphology of fatigue damage. To gain a better understanding of the contributing factors, Vinogradov et al, experimented with the ECAE processing of copper, AA5056 (Al-Mg alloy), and CPTi. Copper served as a popular model of typical FCC wavy-slip materials, the Al-Mg alloy has the same FCC and wavy-slip characteristics as copper but allowed for the evaluation of solid solution contributions, and titanium served as the planar-slip HCP material. Depending upon the processing conditions applied to the samples, the structures produce were either equiaxed, or elongated in the material flow direction. The grain sizes were varied between 0.1-5μm and the structures all had high dislocation densities and internal stresses. [18]

In the stress-controlled/high-cycle fatigue regime, titanium being a planar-slip material responded dramatically well to ECAE induced grain refinement by increasing the fatigue limit by a factor of two. The other two materials as expected showed limited moderate improvement in the high-cycle regime. See the S-N curve in figure 2.17.

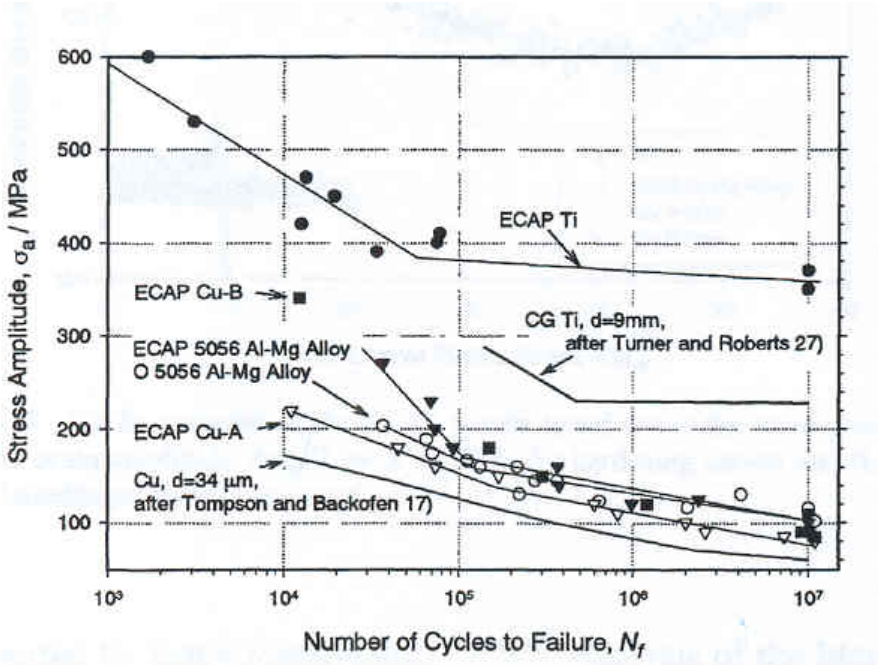

Figure 2.17 S-N diagrams of ECAE processed materials [18]

Limited data also indicated that the elongated grain structure lasted slightly longer under constant stress amplitudes, which could only be connected to the higher tensile strengths of the materials in that condition. Under strain controlled fatigue, the wavy-slip copper and Al-Mg materials suffered shorter fatigue lives, while the planar-slip titanium was able to maintain its fatigue performance as shown in the Coffin-Manson plot in figure 2.18.

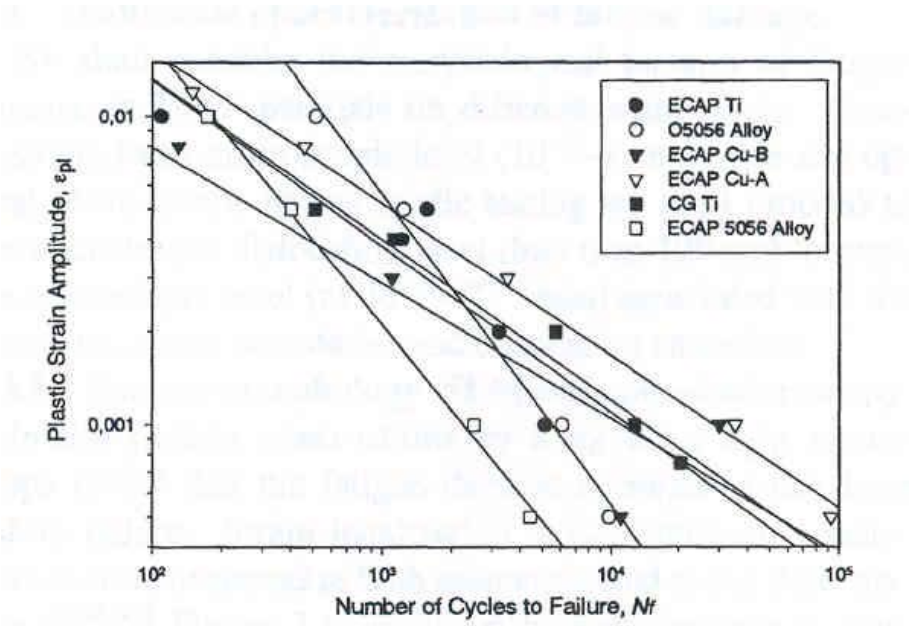

Figure 2.18 Coffin-Manson plot of materials before and after ECAE processing [18]

The elongated structures did slightly worse in the strain-controlled regime, most likely due to the reduced ductility values compared to the equiaxed specimens. The copper and aluminum being wavy-slip materials are more prone to softening due to enhanced recovery processes that can be activated during cyclic straining. These recovery processes are not uniform throughout the materials however, and thus can lead to inhomogeneous material characteristics that can produce flow localizations. The Al-Mg alloy performed better than the copper due to the presence of a solid solution which acted to slow down the recovery processes. Enhanced recovery and the presence of an elongated microstructure contribute to an increased susceptibility to flow localizations that lead to crack nucleation and lower fatigue life. Recommendations at the end of the study for the wavy-slip materials were to restore some ductility to the structure to prevent the flow localizations seen in the strain

controlled-regime by some quick annealing treatments which would allow for a more uniform partial recovery process to take place, but prevent massive grain growth. [18]

2.5.2 Friction and wear

The study of friction, wear, and lubrication in materials is known as tribology. A basic understanding of friction and wear begins with the realization that the surfaces of normal engineering materials are found to be uneven with some type of topography in the form or peaks and valleys. When two of these surfaces are brought together, contact will initially occur and only a few points. As the normal load is increased, the surfaces will move closer together and a larger number of higher areas, or asperities, will come into contact. These asperities are the only points at which the surfaces touch, and are therefore responsible for supporting the normal load and generating any frictional forces that act between them. [41]

Friction is a well explored concept and has been defined as the resistance encountered by one body in moving over another. The ratio of the frictional force (F), or the resistance encountered, to the normal load (W) defines the well known coefficient of friction which is normally represented by the symbol μ.

$$\mu = \frac{F}{W}$$

The friction coefficient can vary over a very wide range, but for most common materials sliding in air the values are between approximately 0.1 and 1. Experimental

observations have led to the development of three laws of friction sometimes called Amontons laws. These are listed below.

1. The friction force is proportional to the normal load

2. The friction force is independent of the apparent area of contact

3. The friction force is independent of the sliding velocity

The three laws apply to most common situations encountered in engineering practice, but there are some situations where the laws are not completely followed. For example, polymers often do not obey the first or second law, and the third law is somewhat confounded by the common observation that the force needed to initiate sliding is usually greater than the force needed to maintain it; the coefficient of static friction is greater than the coefficient of dynamic friction. However, once sliding is established, the coefficient of dynamic friction is found to be nearly independent of velocity over quite a wide range for many material pairs. [41]

Most current theories of sliding friction originate from the work of Bowden and Tabor. Their model assumes that the frictional force arises from two sources: 1) an adhesion force developed at the real areas of contact between the surfaces (asperity junctions), and a deformation force needed to plough the asperities of the harder surface through the softer. The adhesion term arises from the attractive forces that operate at the asperity contacts. The concept of an adhesive force has been confirmed by experiments conducted on clean metal surfaces places in contact under vacuum conditions. Strong adhesive forces have been observed under these conditions, for

example clean iron lightly pressed into copper reveals traces of copper that have adhered to the iron surface. [41]

Friction behavior in metals is highly dependent on the presence, thickness, strength, and stability of an oxide layer. This is due to the fact that the oxide layer prevents the development of strong adhesive bonds at the asperities, and it is a low shear stress layer meaning that if bonds do develop the application of a shear stress would quickly fracture one of the asperities and the bond would be broken. The effect of loading and temperature are also tied to interactions with the oxide layer. At extremely high levels of normal loading, the oxide layer may be penetrated or completely scraped away thus exposing surfaces with the capacity to form much stronger adhesive bonds. High temperatures tend to increase the oxidation rate in metals which would have a tendency to counteract the high loading because the freshly exposed material would be rapidly oxidized. Temperature can also affect friction response by causing changes in the mechanical properties or phase transformations in the material. [41]

Titanium alloys may have superior biocompatibility and corrosion resistance compared to other alloys, but they generally exhibit poor fretting and wear resistance. Previous studies have attributed this behavior to either poor integrity of the TiO_2 oxide layer or plastic deformation behavior of the surface and subsurface layers. [42] Studies done on the metastable β titanium alloys indicate that the dynamic friction behavior is controlled by their surface deformation behavior and transfer characteristics. The

amount of damage and transfer depend on the properties of the tribological layer that forms between the mating surfaces. [42] Attempts have been made to improve the wear resistance of other TNZT type alloys by increasing the niobium content or applying an oxidizing heat treatment. The effect was an increase in the presence of Nb_2O_5 in the oxide layer of the material which was beneficial since Nb_2O_5 has good lubricating properties and is more durable than the titanium oxides that form. [43]

The effect of ECAE induced grain refinement on the wear resistance of materials has not been greatly explored. The essential theory is that the adhesion component can be affected by mechanical properties including the ductility and hardness which are modified by grain refinement. Since the adhesion component plays a key role in the sliding wear performance of the material, any reduction should improve the wear resistance. A study was performed using CPTi as the investigated material which indicated an improvement, or a drop in the adhesion component of the friction coefficient. Unfortunately, no specific reason or mechanism explaining the drop was discussed. [44] Assuming a similar result can be obtained in TNZT, ECAE processing may also provide a method to improve the alloy performance in this critical area.

2.5.3 Tensile properties

It has long been known that cold working a material or reducing its grain size results in an increase in the yield stress. The grain size dependence of yield stress of a material is defined according to the Hall-Petch relation given below.

$$\sigma_y = \sigma_o + k_y d^{-1/2}$$

In this relation, σ_y is the yield strength, σ_o is the friction stress that opposes dislocation motion, k_y is the dislocation locking term, and d is the grain size. The strength increase is due to the increase in grain boundary area which acts as an obstacle to the motion of dislocations. However, this grain size dependence is contingent upon the number of deformation modes that are capable of operating in the material depending on the environment it is exposed to. For example, at higher temperatures where creep deformation mechanisms can be activated, it is found that the flow stress decreases with a grain size decrease. [45]

The large strains and grain refinement produced by ECAE processing can greatly increase the tensile strength levels of materials. Samples that can be extruded at room temperature normally achieve greater levels of strengthening over their coarse-grained counterparts than those that must be extruded at higher temperatures due to dynamic recovery processes that can be activated at such temperatures. Materials with sufficient ductility to undergo low temperature deformation are hardened not only by the increased grain boundary area, but also by the ability to maintain a greater dislocation density compared to materials that undergo recovery which will reduce the dislocation density. Increased dislocation density is an advantage because the stress-strain fields that surround these defects interact with one another. These interactions

can be either attractive or repulsive, but the net result is that dislocation motion is restricted thus increasing the strength [17]

2.6 Finite element analysis with DEFORM^{TM} 3D

DEFORM-3D is a finite element method based software package that is specifically designed to simulate very large deformation problems such as metal forming. The code is broken into three parts: pre-processing, FEM solver, and post-processing. Pre-processing consists of user-defined parameters including the simulation type, geometry of objects, material properties, tool movements, lubrication, temperature, environment, and boundary conditions. Ordinarily, the geometry of the tool, die, and workpiece is provided by CAD models which are imported into DEFORM's workspace where tetragonal mesh elements are generated to break the workpiece up into discrete domains. Computer analysis of metal flow is based on the idea that the material will follow the path of least resistance. The FEM solver uses material data from compression tests at various temperatures and strain rates and calculates the force required to deform each element based on the parameters defined in pre-processing. The behavior of the entire workpiece is calculated based upon the assembled behavior of each individual element. The boundary conditions for interior elements are defined by the results for the elements surrounding it. Therefore, many equations are solved simultaneously in matrix form to find a solution at a specific time step. After the completion of one step, or calculation, the shape of the workpiece is

updated, contact with other objects is checked and modified, and the calculation is repeated. [31][45]

Workpiece shape is updated after each step by calculating the velocity at each node point and then moving the nodes in the calculated direction for a very short time interval. This is accomplished by using the assumption that the material flows into a shape which follows the path of least resistance. This is defined in another way by the minimum work rate principle, which states that the velocity distribution that predicts the lowest work rate is the best approximation of the actual velocity distribution. Initially, a guess for the velocity of each node is applied and the force and energy required to deform each element is calculated. All individual element behaviors are assembled to determine global behavior, and the velocity of each node corresponding to the minimum energy is calculated. [31][45]

Solution accuracy is dependent upon the generated mesh size and time step specification. Since the solutions vary continuously across the entire workpiece, smaller elements and time steps will yield more accurate solutions. The matrices used for calculation increase in size along with the number of elements. A mesh size that is overly fine will result in an exceeding large number of elements and in calculations that require long CPU times to solve. The solution tends to converge relatively rapidly with reasonable mesh sizes, and therefore, a satisfactory solution can be found in a practical time period. In post-processing, the problem solution is displayed in an easy

to understand graphical formulation. The post-processing section of DEFORM allows the user to perform all of the normal analyses that are found in a commercial code. Variables such as displacement, strain, stress, strain rate, velocity, temperature, density, grain size, phase volume fraction, etc, can all be calculated and plotted on a 3D image of the workpiece. Variables can also be plotted along a line, surface, or cross-section of the piece. [31][45]

It should be noted that the following simplifying assumptions are made for all simulations. 1) The dies are perfectly rigid, meaning that the total deflection during processing is small enough to be neglected 2) There is no die separation 3) The entire system is held at a constant temperature 4) The die and sample geometries are free from physical defects 5) The workpiece is assumed to be rigid-plastic, meaning that elastic deformation is small enough to be neglected. In reality, none of these assumptions is completely accurate. The dies are elastic, not rigid and there may a slight amount of die separation that occurs during processing. Experimental conditions are carefully controlled in an attempt to create true isothermal conditions, but some amount of localized adiabatic heating in the sample will occur which can cause a slight change in deformation due to the temperature dependence of material properties. Neither the samples nor the dies are free from physical defects, and there will always be a small elastic component of the overall deformation of the workpiece. However, rigorous studies comparing the DEFORM simulation results produced with these assumptions, with direct experiment have been performed and found to have

good correlation. [31][45][46] Therefore, these assumptions do not decrease the overall accuracy of the solution by a noticeable amount.

2.7 General strength requirements for a hip implant

There are many different joint replacement devices to replace the most commonly stricken locations in the human body; e.g. hip, knee, and shoulder. Examination of the standards governing these devices however does not reveal specific strength requirements for each individual component. Instead the strength requirements refer to standards for individual materials that have been used in implant applications in the past. These standards then list minimum values for the mechanical properties of the bulk material that will be used to construct a medical device. [47] A specific strength requirement for joint replacement devices is actually very difficult to generate because of the high degree of variability of both the patient population and prosthesis design. Stress levels seen in hip prostheses are affected by the ball diameter of the implant, its neck length, neck shaft angle, stem length, stem taper, modulus of the material it is composed of, fixation type (cemented or uncemented), patient weight, age and activity level, general skeletal geometry, and relative muscle strength. [48][49][50][51] An attempt will be made here to come up with some general strength requirements for a hip implant through a review of finite-element and experimental studies. These strength requirements will then be used as benchmarks to compare to the properties of TNZT in the ECAE processed condition.

Through the use of instrumented joint replacements, loading on the hip joint area has been determined for a wide variety of activities. Normal walking, stair climbing, and ramp negotiation have been found to produce forces approximately four times the body weight of the patient. Running increases the loading to five times, and stumbling or tripping can increase the load up to eight times the body weight. [52][53] Studies have taken these numbers and used them to perform finite-element analysis to determine the stresses in a variety of prosthesis designs. The most common load value is based on walking and stair climbing, which when calculated for the weight of an average person results in a force of approximately 3000N. A majority of these studies used materials with very high stiffness on the order of 150-200GPa such as stainless steels or Co-Cr alloys. In these cases, the stress levels are in the range of 300-400MPa which would be outside the operable fatigue strength range of the TNZT alloy at 275MPa. [49][50][51] However, a study by Yettram and Wright indicates that the stress levels in the femoral component of the prosthesis decrease by quite a significant amount when the modulus of the material is decreased down to the levels of TNZT. [48] Calculating with the modulus value of 55GPa, the stress level is approximately 200MPa which is below the fatigue strength of TNZT, but the device would have a relatively low factor of safety at around 1.4 and may encounter issues if exposed to higher stresses during running or stumbling or if it is installed in a heavier patient.

The results from Yettram and Wright demonstrate that hip implants can be fabricated from TNZT, but the stress levels are relatively close to the limits of the material. This

would limit the use of the implant to smaller and lighter patients that likely maintain a low activity level. Increasing the fatigue strength of the alloy to 400MPa or higher could widen its application to heavier and more athletics patients.

Chapter 3

Research Objectives

The goal of this study was to develop an improved titanium alloy for total joint replacement prosthesis applications. The biomedical alloy Ti-35%Nb-7%Zr-5%Ta was selected as the focus of the study, and the standards over which improvements were sought. ECAE processing and boron additions were selected as the primary means for producing property improvements in the reference alloy. To achieve the desired goal, the following research objectives were addressed.

1. The temperature and strain rate combination for successful ECAE processing of the TNZT alloy was determined by high-temperature compression testing over a range of temperatures and strain rates. The peak flow stress, extent of plastic flow without cracking, and the dominant deformation mechanisms under different processing conditions were determined.
2. The finite element code DEFORM-3D was used to simulate the ECAE process and predict the strain distribution in the extruded billet.
3. Multi-pass ECAE processing experiments were carried out based on the results from high-temperature compression testing and the DEFORM simulation to produce maximum property improvement.

4. The effectiveness of boron as a grain refining/stabilizing agent for the TNZT alloy was evaluated.
5. The microstructure and substructure changes resulting from ECAE processing were determined by optical and transmission electron microscope examinations of the processed specimens.
6. Tensile properties resulting from different ECAE schedules were determined. The resulting changes were used to select the optimum conditions for property improvement.
7. The effects of ECAE processing on the fatigue properties and sliding wear resistance of the TNZT alloy were determined.
8. The overall effectiveness of boron addition and ECAE processing for the mechanical property improvement of the TNZT alloy was evaluated.

Chapter 4

High-Temperature Deformation Characteristics of TNZT

4.1 Alloy selection

The alloy chosen for this study is the Ti-35%Nb-7%Zr-5%Ta biomedical titanium alloy. As mentioned earlier, there are many different alloys that have been historically used for structural joint replacements including CPTi, Ti-6Al-4V, stainless steel, Co-Cr, TMZF, 21SRx, etc. The TNZT alloy has been chosen for two main reasons: (1) it is composed of elements that have been shown to be totally inert and biocompatible within the human body, and (2) Because it stands as the material with the highest potential performance gain in the group due to its low modulus value.

In this study, three TNZT type alloys were used. The first was a 35wt%-Nb, 5wt%-Ta, 7wt%-Zr, balance-Ti, the second had the same chemical composition with 0.5wt% B added (hereafter referred to as high-boron), and the third had 0.15% B added (hereafter referred to as low-boron). The boron additions are meant to induce the formation of second phase particles that will pin the grain boundaries and restrict grain growth during processing stages that require high temperatures. The relatively small amounts of boron added were purposely chosen in order to prevent the formation of

unnecessarily coarse particles. Larger amounts of boron would lead to the creation of a larger volume fraction and larger size particles that would be detrimental to both the ductility and the modulus of the material since the particles possess a greater stiffness value than the surrounding matrix material. [17]

The materials for the preliminary examination were prepared by the TIMET facility in Henderson, Nevada in the form of 227g button ingots. The as-received microstructures are shown below in figure 4.1, figure 4.2, and figure 4.3. When comparing the two materials to each other the most obvious differentiating feature is the presence of boride particles in the low and high boron samples (indicated by arrows).

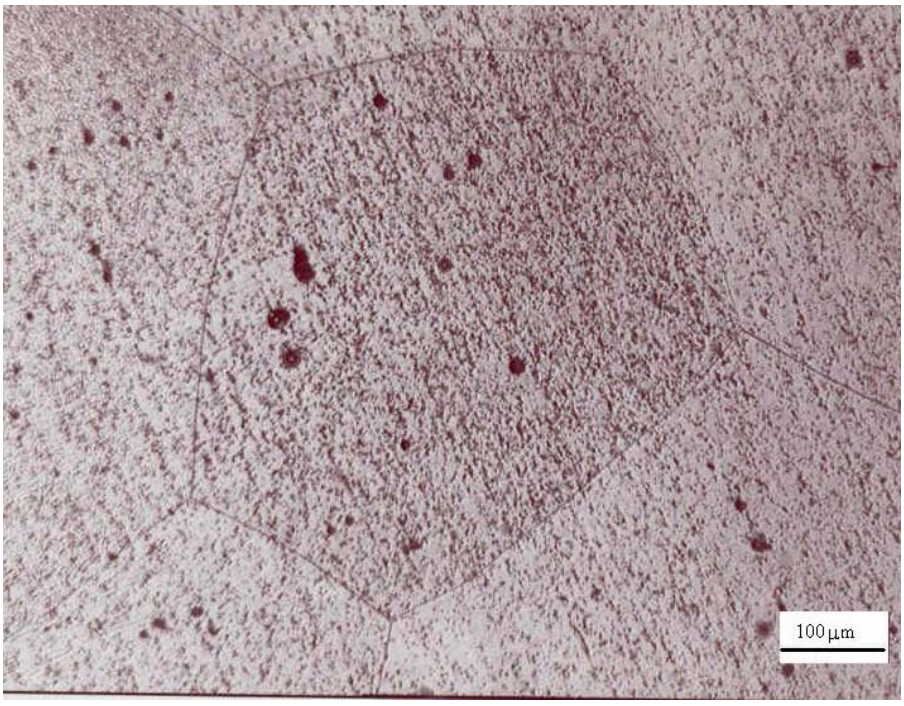

Figure 4.1 TNZT starting microstructure

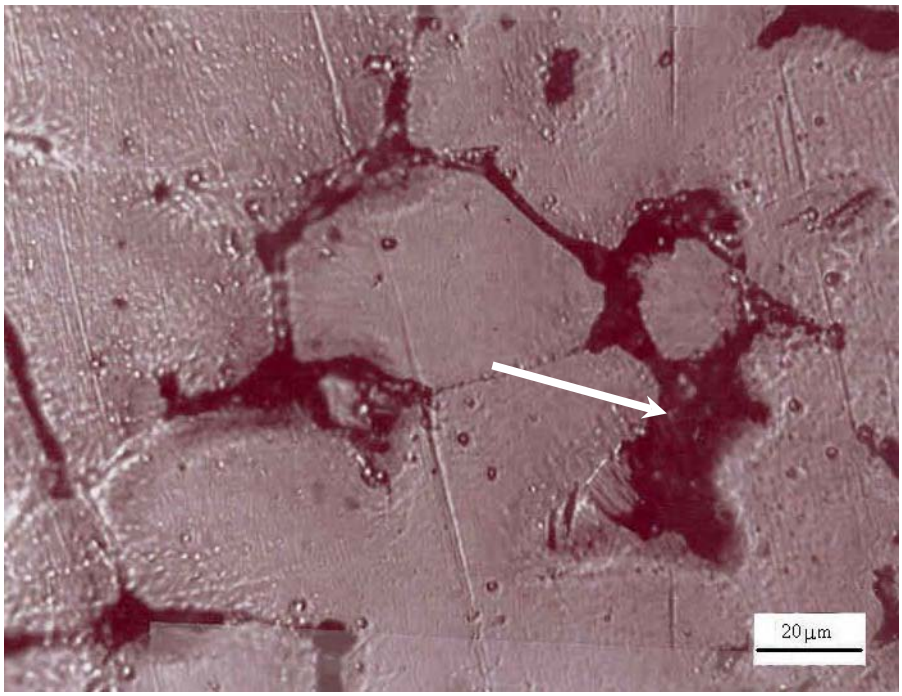

Figure 4.2 TNZT+0.15%B starting microstructure

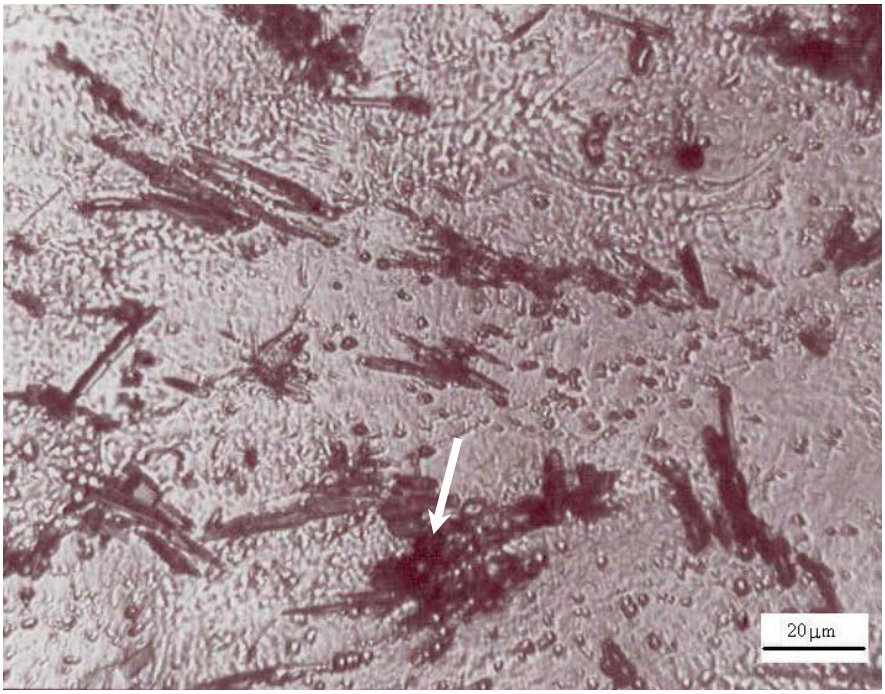

Figure 4.3 TNZT+0.5B starting microstructure

The second feature of note is the highly coarse nature of the structures. The TNZT micrograph, which was taken at lower magnification, shows that the grain size is very large; on the order of 600-1000μm.

4.2 High-temperature compression testing

4.2.1 Experimental methods

In order to evaluate the hot-workability and determine the deformation mechanisms of the TNZT alloys, isothermal high-temperature compression (HTC) tests were performed under various combinations of temperature and strain rate. The test conditions were constant strain rates of 10^{-3} and 10^{-1} per second at temperatures of 270°C, 470°C, 670°C, 795°C, and 840°C. Testing was conducted on a computer-controlled screw-driven UTM using a PID controller to maintain the constant strain rate during the tests. Temperature control was provided by a resistance-heating split furnace that surrounded the test region with a thermocouple inserted next to the specimen. The experimental set-up is shown below in figure 4.4.

Figure 4.4 Experimental set-up for isothermal high-temperature compression testing of TNZT alloys

Specimens were machined by EDM to 0.25in diameter by 0.375in tall cylinders and coated on the top and bottom with a molybdenum disulfide based lubricant to promote uniform deformation during compression. The alloys were then beta annealed at 850°C for 30 minutes and water quenched to eliminate the presence of any residual alpha phase in the structure. The samples were deformed to an engineering strain of 75% except for the 300°C and 500°C samples that reached 65% before exceeding the

load cell limit. After testing, the samples were sectioned parallel to the compression axis and prepared for metallographic examination by the standard techniques. Selected samples were subjected to a post-deformation annealing treatment at 850°C for 5 minutes to observe the microstructural evolution. Hardness testing was performed on a LECO Vicker's microhardness tester at a load of 500g.

4.2.2 Results and discussion

True stress-true strain plots from compression testing at both the high and low strain rate are shown in figures 4.5-4.10.

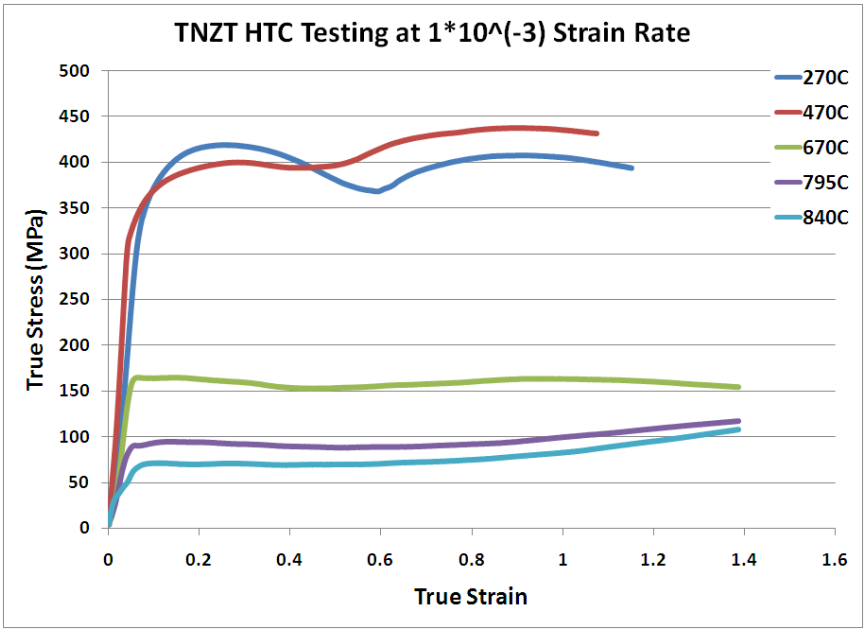

Figure 4.5 True stress-true strain curves for the TNZT alloy undergoing HTC testing at 270°C, 470°C, 670°C, 795°C, 840°C and 1×10^{-3}/s.

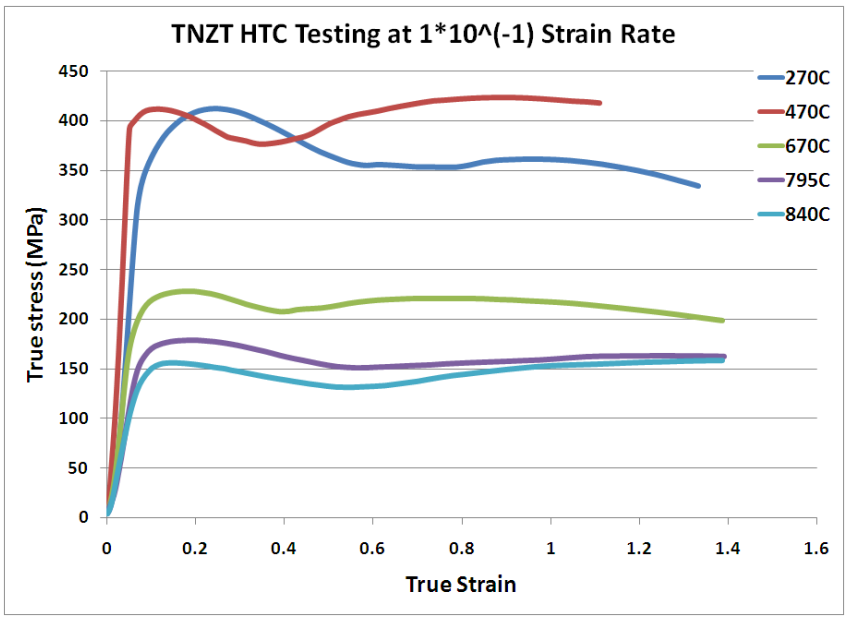

Figure 4.6 True stress-true strain curves for the TNZT alloy undergoing HTC testing at 270°C, 470°C, 670°C, 795°C, 840°C, and 1×10^{-1}/s.

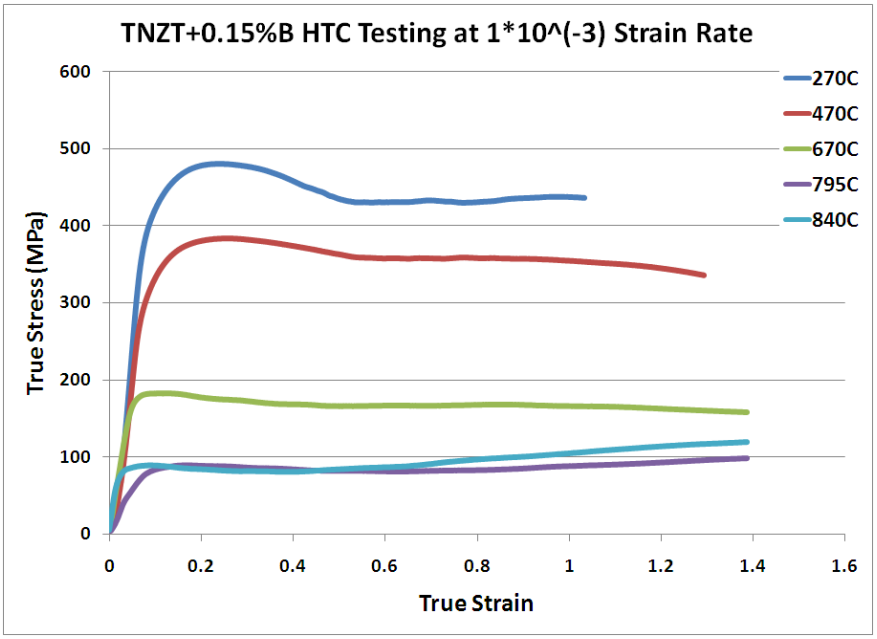

Figure 4.7 True stress-true strain curves for the TNZT+0.15%B alloy undergoing HTC testing at 270°C, 470°C, 670°C, 795°C, 840°C and 1×10^{-3}/s.

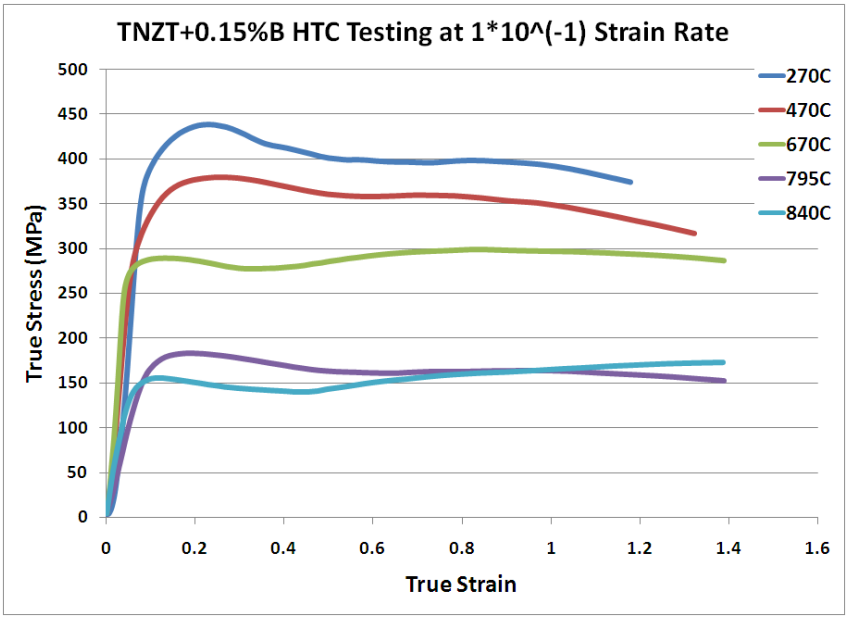

Figure 4.8 True stress-true strain curves for the TNZT+0.15%B alloy undergoing HTC testing at 270°C, 470°C, 670°C, 795°C, 840°C, and 1×10^{-1}/s.

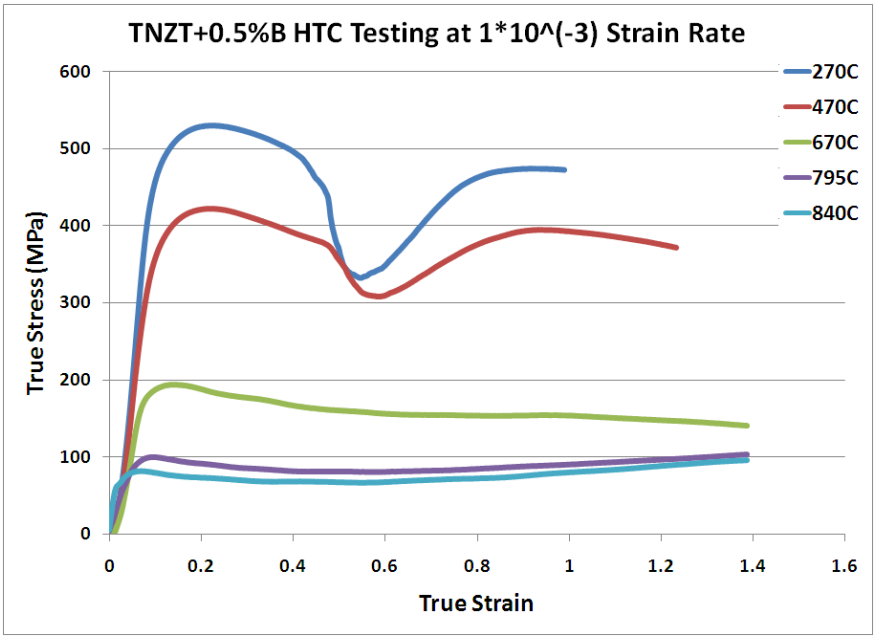

Figure 4.9 True stress-true strain curves for the TNZT+0.5%B alloy undergoing HTC testing at 270°C, 470°C, 670°C, 795°C, 840°C and 1×10^{-3}/s.

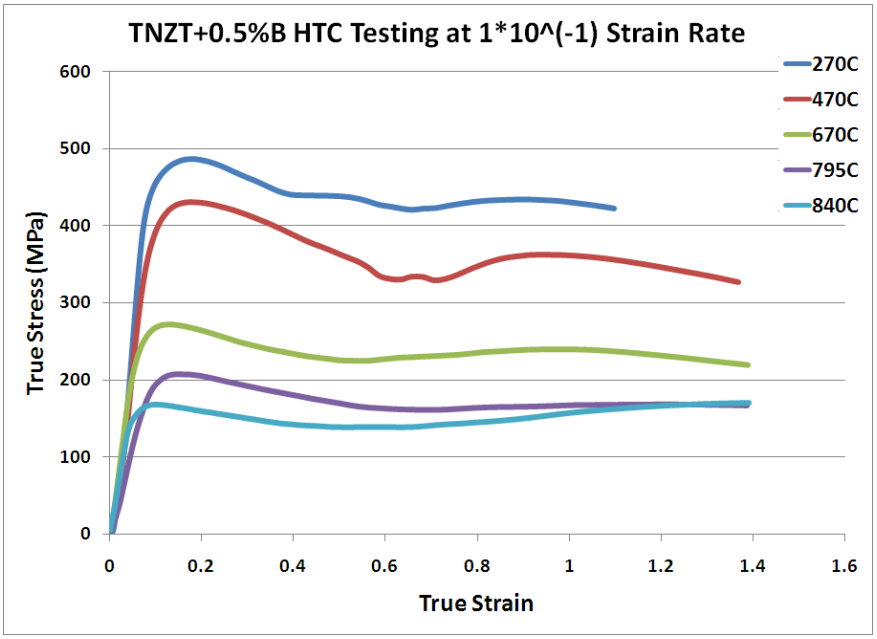

Figure 4.10 True stress-true strain curves for the TNZT+0.15%B alloy undergoing HTC testing at 270°C, 470°C, 670°C, 795°C, 840°C, and 1×10^{-1}/s.

The large stress drop seen in the curves at 270°C and 470°C and 1×10^{-3} 1/s in the high boron alloy is due to relatively severe shear cracking that occurred during testing. The curves from all three alloys display the same trend. First, there is a significant stress drop from 470°C to 670°C. This initial observation indicates a possible change in the operating deformation mechanism between the low temperatures (<470°C) and the high temperatures (>670°C). This notion is supported by an observed change in the strain rate sensitivity (m-value) which is calculated and shown below in table 4.1.

Table 4.1 Strain rate sensitivity values at different temperatures

Alloy	270°C	470°C	670°C	795°C	840°C
TNZT	0.003	0.005	0.071	0.139	0.170
Low Boron	0.001	0.002	0.1	0.156	0.12
High Boron	0.002	0.004	0.073	0.157	0.157

The strain rate sensitivity is very low for all the alloys deformed at 470°C and below. In the range of 670°C-840°C, the m-value increases to approximately 0.1-0.16 respectively for all three alloys. The lack of strain rate sensitivity at the lower temperatures indicates that the material is most likely still undergoing deformation considered characteristic to cold working. [17] The highest m-values correspond to a stress exponent slightly greater than 5 which would indicate power law creep and some type of dislocation controlled process governing deformation. The level shape of the flow curves during testing at high temperatures and slow strain rates normally indicate dynamic recovery, while the stress drop seen at high temperatures and high strain rates would signify the occurrence of dynamic recrystallization. [17]

Activation energy values were calculated by plotting the natural log of the peak flow stress at constant strain rates versus 1/T. These values can be matched with handbook values for rate-controlling mechanisms to give more insight into the nature of deformation. Table 4.2 below shows the summary of the results.

Table 4.2 Summary of activation energy values

Activation Energy Values (kJ/mol)								
	Strain rate = 0.001 /s				Strain rate = 0.1 /s			
Material	Temperature Range (Celsius)				Temperature Range (Celsius)			
	270-470	470-670	670-795	795-840	270-470	470-670	670-795	795-840
TNZT	0.72	25.7	35.4	62.6	0.03	17	15.4	30.7
TNZT+0.15%B	3.7	21.4	46.1	30.1	2.4	7.8	29.5	35.9
TNZT+0.5%B	3.8	22.3	42.1	46.7	2	13.1	17.6	46.1

The activation energy values for all the processing conditions are very low. Ordinary values for titanium and its alloys are much higher, for example self-diffusion in the β phase is approximately 130kJ/mol, self-diffusion in α is approximately 160kJ/mol, and superplastic flow by grain boundary sliding is even higher at 200kJ/mol and higher. [54] This lack of sensitivity to temperature changes, which is essentially what the activation energy is a measure of, indicates that diffusion based mechanisms are not likely controlling the deformation. Instead this tends to reinforce the idea that dislocation based mechanisms are the dominant deformation mode. The increase in activation energy values from the low temperature 270°C-470°C range to the high temperature 670°C range also reinforces the idea that there is a different dominant mechanism operating between low and high temperature.

Microstructural examination of all the as-deformed specimens showed no evidence of dynamic recrystallization in any of the alloys under any of the applied processing conditions. The as-deformed samples were then subjected to a post-deformation heat

treatment of 850°C for 5 minutes. Selected microstructures of these samples are shown below in figure 4.11 and figure 4.12.

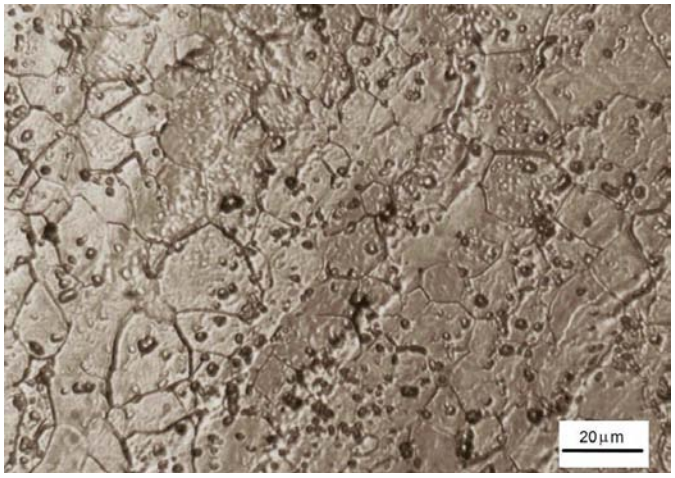

(a)

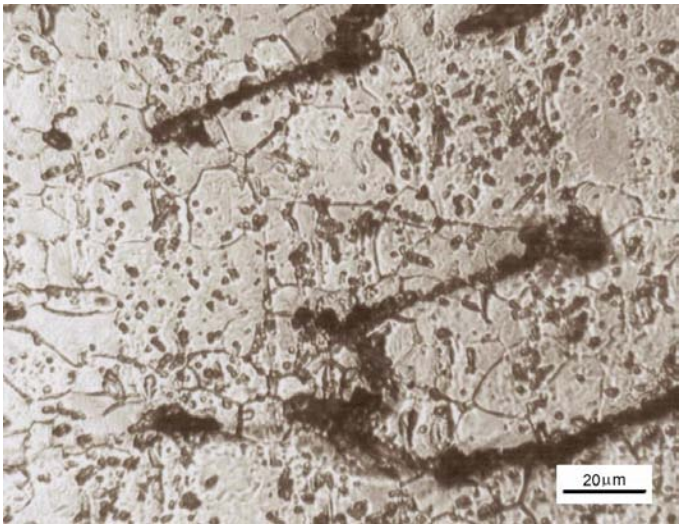

(b)

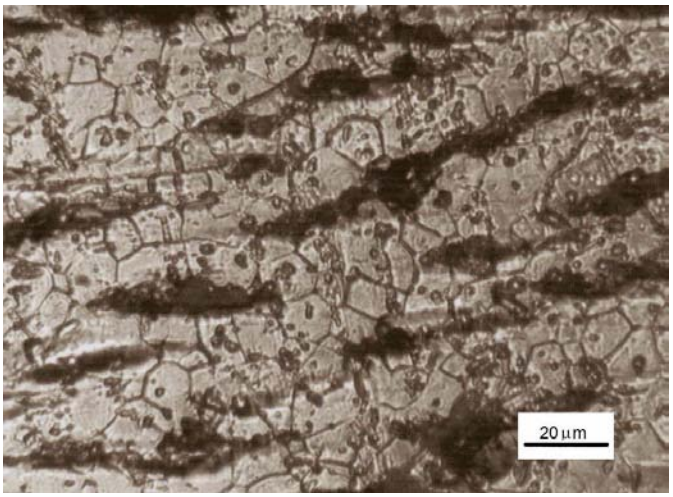

(c)

Figure 4.11 Micrographs of the TNZT alloys after HTC testing at 300°C 1×10^{-1}/s and annealing at 850°C for 5 minutes (a) TNZT (b) TNZT+0.15%B (c) TNZT+0.5%B

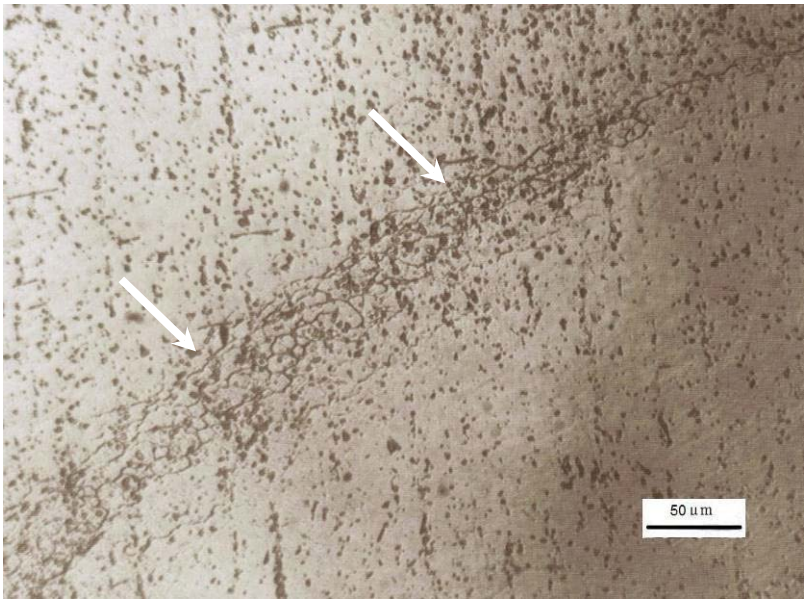

(a)

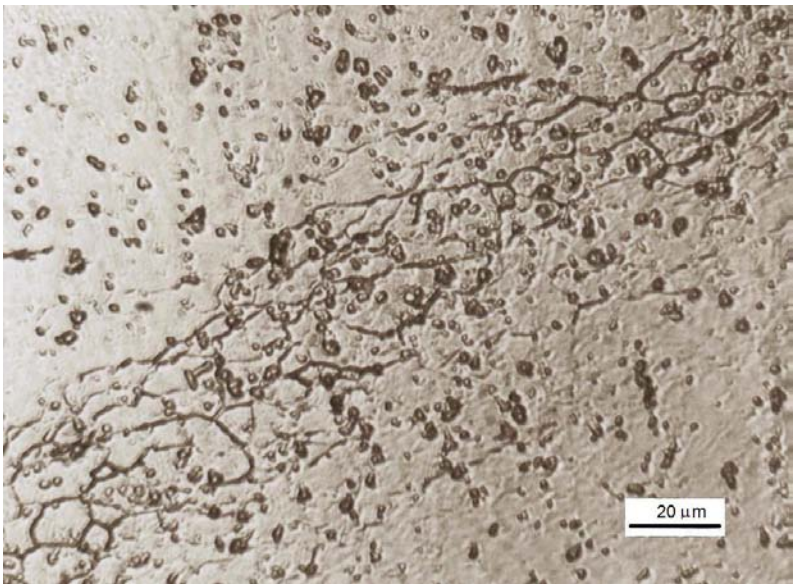

(b)

Figure 4.12 Micrograph of the TNZT alloy after HTC testing at 840°C 1×10^{-3}/s and annealing at 850°C for 5 minutes. (a) 200X (b) 500X

As seen in figure 4.11, all of the samples originally HTC tested at 270°C and 470°C have undergone static recrystallization after annealing. This finding further supports the idea that these temperatures still lie within the cold working regime for these alloys. It is worthwhile to note that the recrystallized grain size in the TNZT and TNZT+0.15%B samples are approximately the same (~18μm), while the recrystallized grain size in the TNZT+0.5%B sample is significantly smaller (~10μm). It is apparent that the higher boron content is acting to restrict grain growth during processing, however 10μm is not a small enough grain size to expect significant property improvements.

Figure 4.12 shows that the samples HTC tested at temperatures of 670°C and above with an annealing treatment are undergoing recrystallization only at the prior β grain boundaries (indicated by the arrows), sometimes called 'necklace recrystallization'. This behavior has been observed before in high-temperature deformation of metastable β-Ti alloys, and can be explained by the dynamic yield theory of Johnston and Gilman which is based on the rapid generation and multiplication of mobile dislocations from the grain boundaries. [55][56][57] Deformation is then highly localized near the grain boundaries while the grain interior remains relatively undeformed and may or may not undergo dynamic recovery. Upon application of the post-deformation heat treatment the strain energy stored near the boundaries gives rise to the nucleation of new recrystallized grains, which explains the appearance of necklace recrystallization. The theory has also been used to explain stress drops observed in flow curves at high temperatures and strain rates similar to those in the flow curves shown above. [55][56][57] The velocity of dislocations in a material is a function of stress and can be represented by the following equation.

$$v = \left(\frac{\sigma}{\sigma_0} \right)^n$$

In the equation, σ is the applied stress, σ_0 is a reference stress, and n is the stress exponent. The strain rate imposed on a material can be expressed by the relationship

$$\dot{\varepsilon} = \rho b v$$

where ρ is the mobile dislocation density, b is the Burgers vector, and v is the velocity of dislocations. Examination of the strain rate equation leads to the conclusion that in materials with an initially low dislocation density, the dislocation velocity must be high in order to match the applied strain rate. From the first equation then, these high velocities lead to higher flow stresses. As deformation proceeds and the mobile dislocation density increases, the velocity will drop which will cause the flow stress to drop along with it. Initial grain size can have an effect on the stress drop since the grain boundaries act as dislocation sources, the drop is proportional to grain boundary area which is inversely proportional to the grain size. Therefore as the initial grain size is increased, the magnitude of the flow stress drop will decrease. Recall that the initial grain sizes in the samples in this study were very large, on the order of 600-1000μm. This explains why the flow stress drops observed here are not as dramatic as those seen in literature. [55][56][57]

The dynamic yielding theory does not offer an explanation as to why the deformation is localized at the grain boundaries instead of proceeding uniformly through the entire granular volume. One possible explanation can be drawn from the fact that TNZT, and metastable β alloys in general, are very heavily solid solution-strengthened by the large amount of β stabilizers present. The theory is based upon the assumption that when deformation begins there is a low density of mobile dislocations. It is possible that the dislocations that are present in the grain interior are rendered relatively immobile due to a large number of dislocation-solute interactions with the stabilizing

elements. Because of this lack of dislocation mobility in the grain interior, a large number of dislocations are generated from grain boundary sources to accommodate the applied strains. This would lead to most of the deformation being confined to regions immediately adjacent to the boundaries while leaving the grain interiors comparatively unchanged.

Chapter 5

Finite Element Analysis of the ECAE Process Using DEFORM^{TM}3D

5.1 Experimental methods

Finite element simulations were preformed in order to analyze the uniformity of the strain distribution, and to get an idea of the required pressing force required during extrusion. The geometries of the ECAE die, push rod, and workpiece were all generated using CAD software and imported into the DEFORM workspace as .stl files. A mesh of tetragonal elements was then generated using 35,000 elements and a size ratio of 5 in order to try to capture accurate information at the very sharp inside corner of the channel intersection. Material properties were then assigned to the workpiece. Ordinarily, material information is imported from an internal library but there is no stored or default information for TNZT or similar alloys. The simulation was chosen to be performed on the TNZT alloy at 500°C, so the true stress-strain curves that were experimentally determined during HTC testing at that temperature were loaded into DEFORM and saved in the user library. Once this was completed, the parts were all positioned properly and the proper contact boundary conditions were applied. The friction coefficient for the molybdenum disulfide lubricant was previously determined over a range of temperatures. In this range it is equal to 0.17.

In order to cut down on processing and simulation time, only one longitudinal half of the workpiece was used along with a symmetric boundary condition. The pushrod was set to extrude at 0.01 in/s which was the same rate that was used for the true experiment. Once the problem was completely defined, the FEM solver was started, and the results of the solution were examined using DEFORM's post-processor.

5.2 Results and discussion

The initial accuracy check for ECAE simulations was to examine the final material shape and the strain distribution to determine if either one deviates significantly from expectation. Initial simulation results are shown below in figure 5.1.

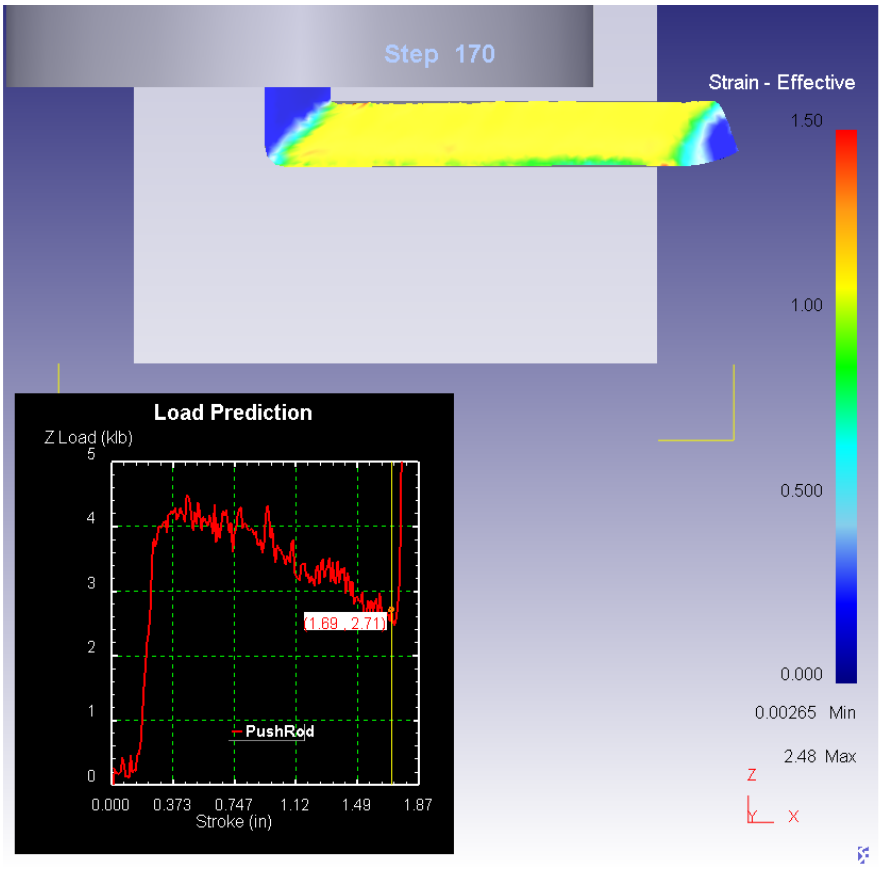

Figure 5.1 FE simulation of the strain distribution and extrusion force for a TNZT extrusion at 500°C

The final workpiece shape looks good. The strain level for one pass through a 90° channel angle dies is approximately equal to 1, which matches the simulation results. [23] The theoretical load-stroke curve in figure 5.1 was extracted and plotted with an experimental load-stroke curve in figure 5.2.

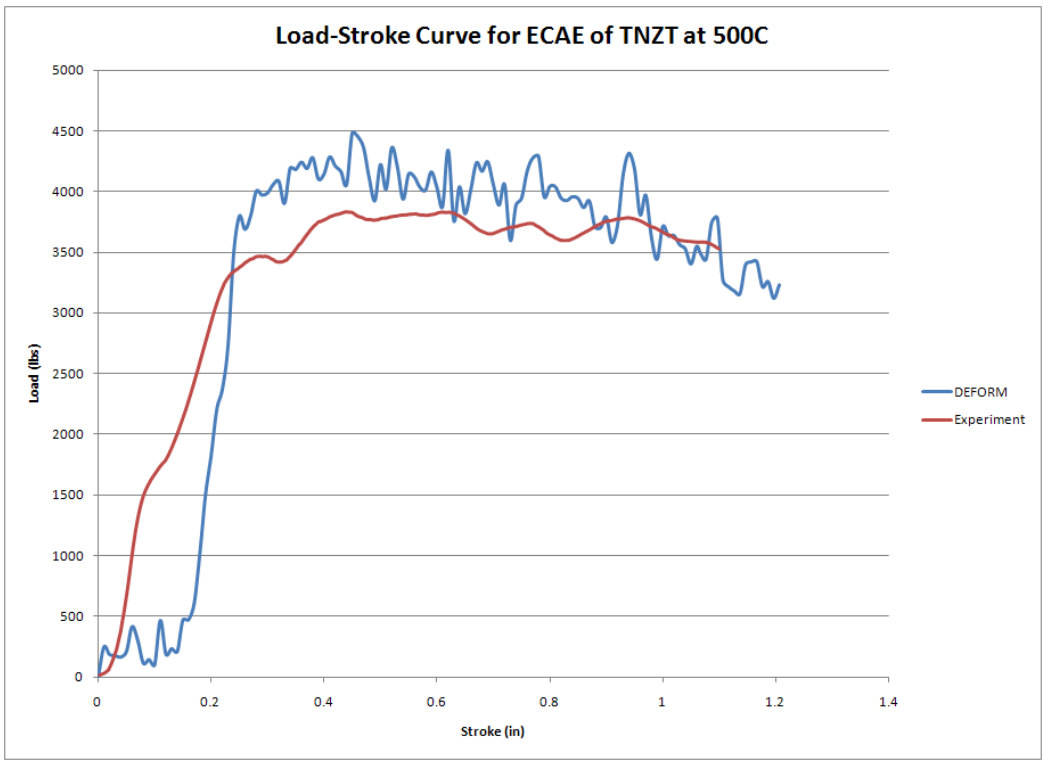

Figure 5.2 Theoretical and experimental load-stroke curves for ECAE of TNZT at 500°C

The theoretical and experimental load-stroke curves correlate reasonably well with an error of approximately 7-8%. This single plot would indicate that DEFORM overestimates the required pressing force compared to experiment, but this is not the case. If the curves for all of the experimental extrusions were plotted, the DEFORM curve would well within the experimental range.

As previously mentioned, the state variables in DEFORM's post-processor can be tracked at individual points to see if there is any variation over the cross-section of the workpiece. A point was placed at the bottom, center, and top edge of the sample billet

to determine if there was any significant variation. The results are shown below in figure 5.3 and figure 5.4

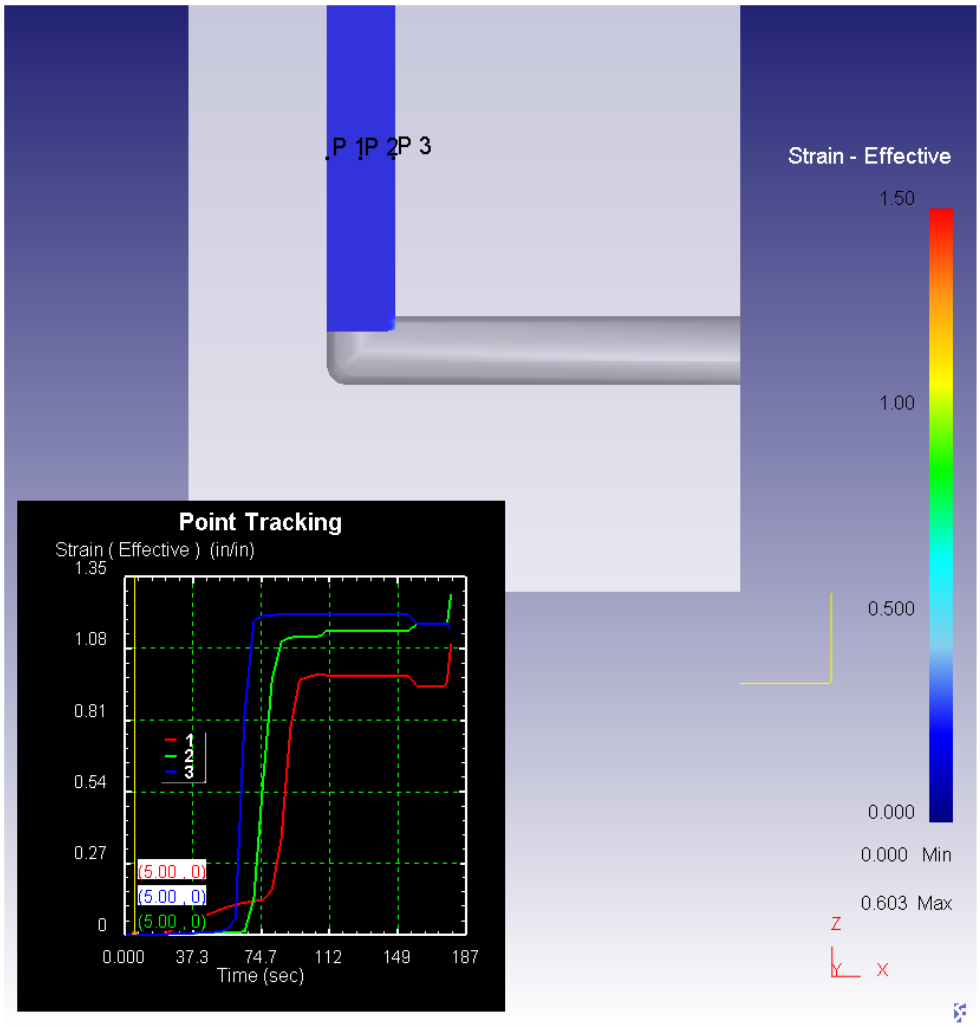

Figure 5.3 Start of the ECAE simulation showing the location of the three tracking points

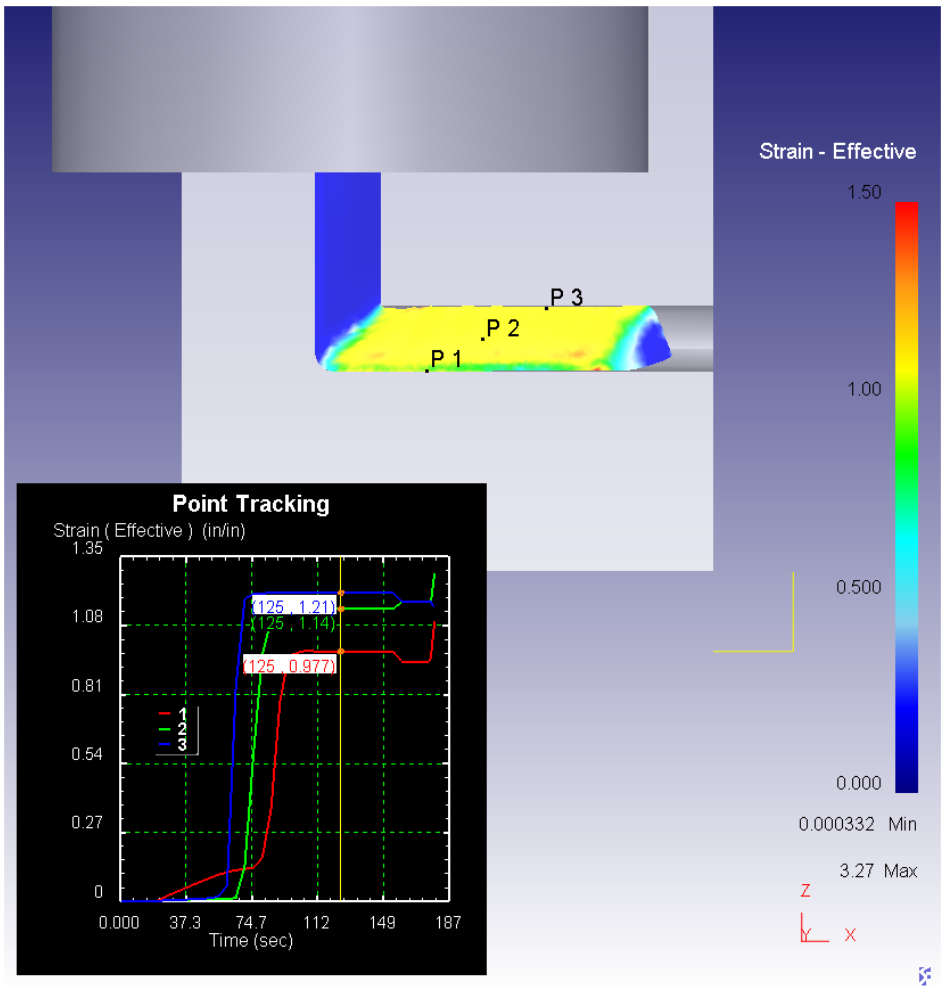

Figure 5.4 End of the point tracking simulation

There is always some expected variation in the strain distribution in ECAE processed billets for the reasons previously discussed. The material along the bottom edge has a tendency to be bent rather than sheared at the outer rounded corner due to the radius. [32] The maximum variation in strain levels is approximately 11% which is not significant enough to cause major property variations in the final billet piece.

The post-processor also has a feature called flow-net, where cubic elements of a user-defined size are drawn onto the workpiece in order to more easily visualize the flow patterns. The flow-net is shown in figure 5.5 and 5.6.

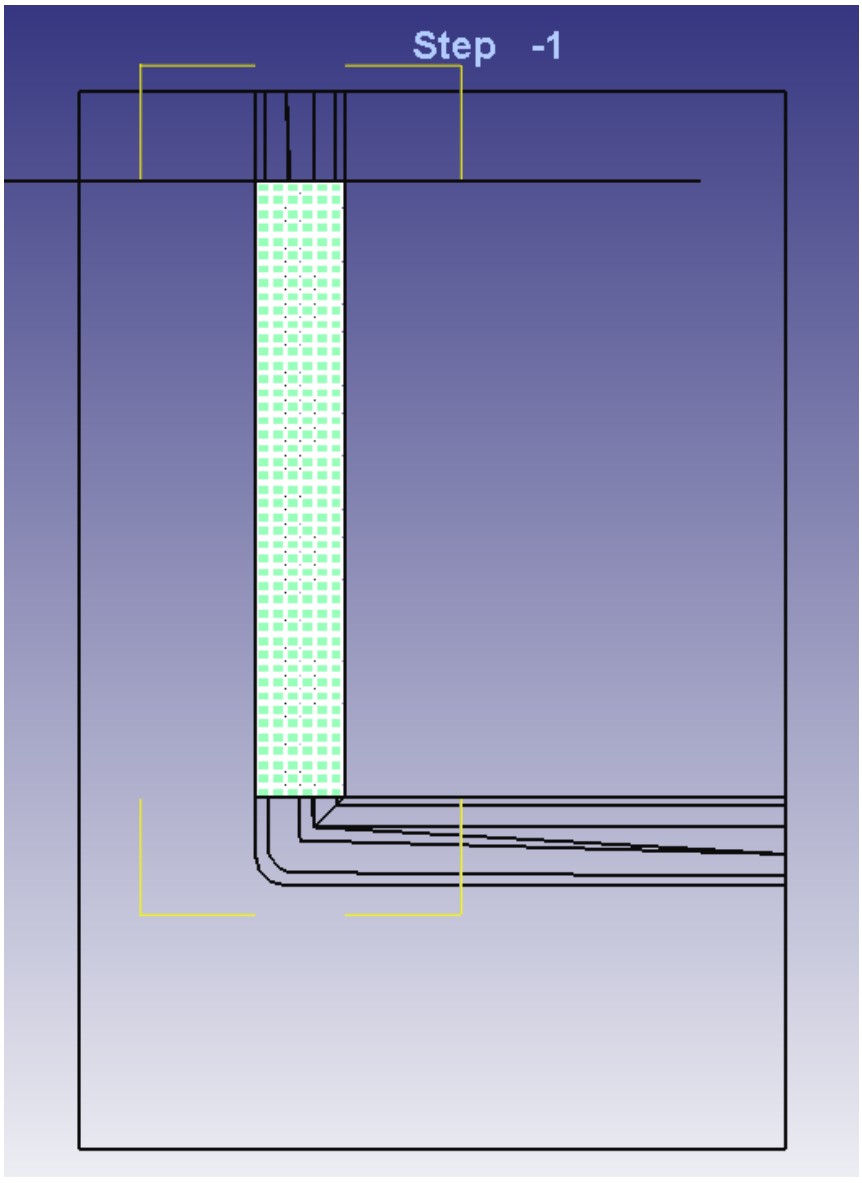

Figure 5.5 Flow-net at the start of the simulation

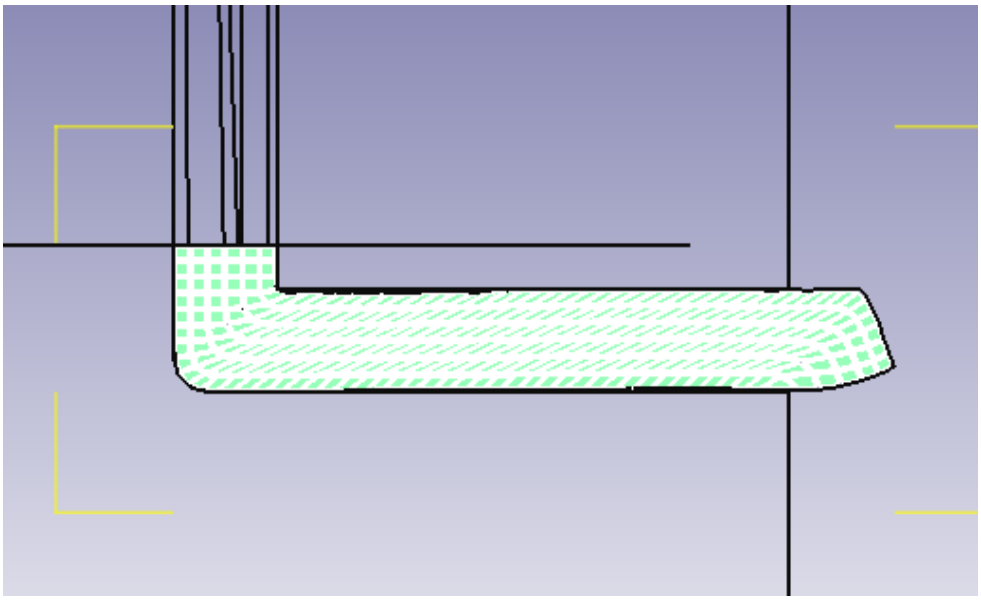

Figure 5.6 End of the flow-net simulation

The flow-net makes it much easier to view the flow pattern in the shear zone at the channel intersection. Careful inspection shows the deformation zone spread into a slight fan shape, and examination of the deformed cubic elements clearly shows that the ones along the bottom edge have not undergone that same amount of shear as others positioned higher in the billet. [32]

When all this was completed, the strain distribution in the billet was re-plotted with a smaller maximum value to increase the resolution and prevent small variations from being washed out. The results are shown below in figure 5.7 and 5.8.

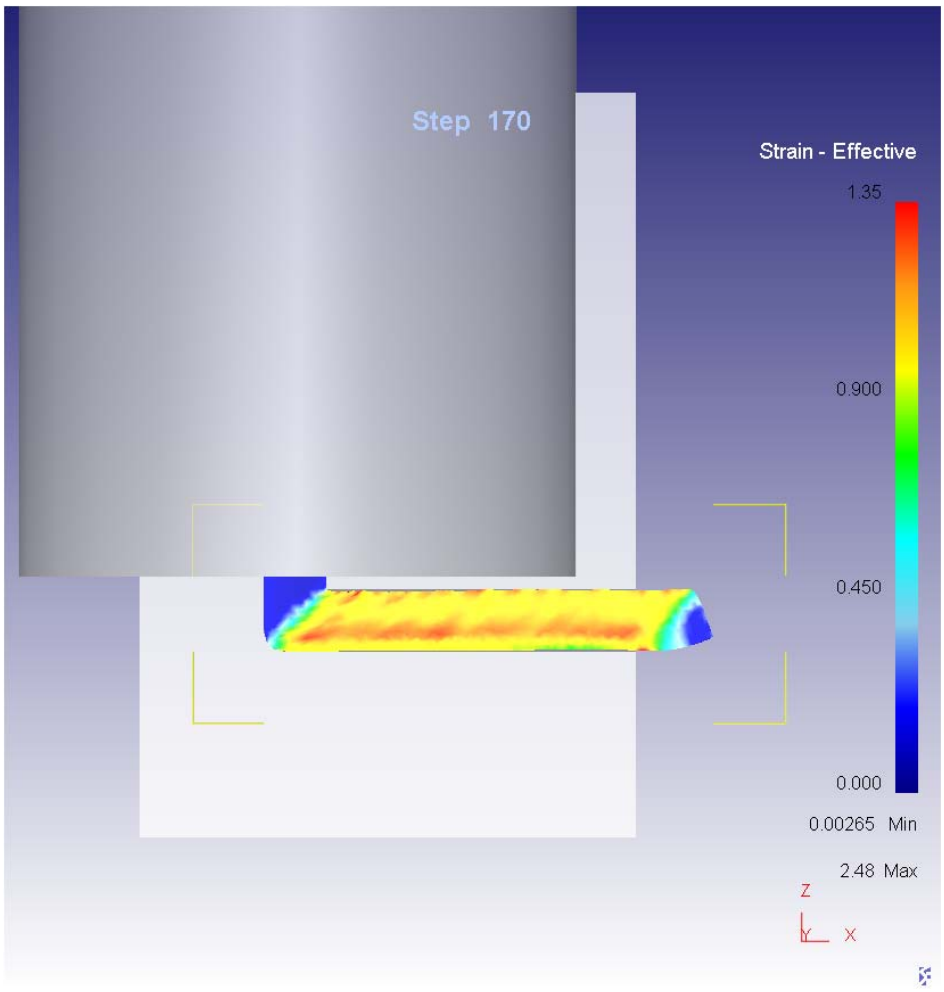

Figure 5.7 Theoretical strain distribution plotted using 1.35 as the maximum strain

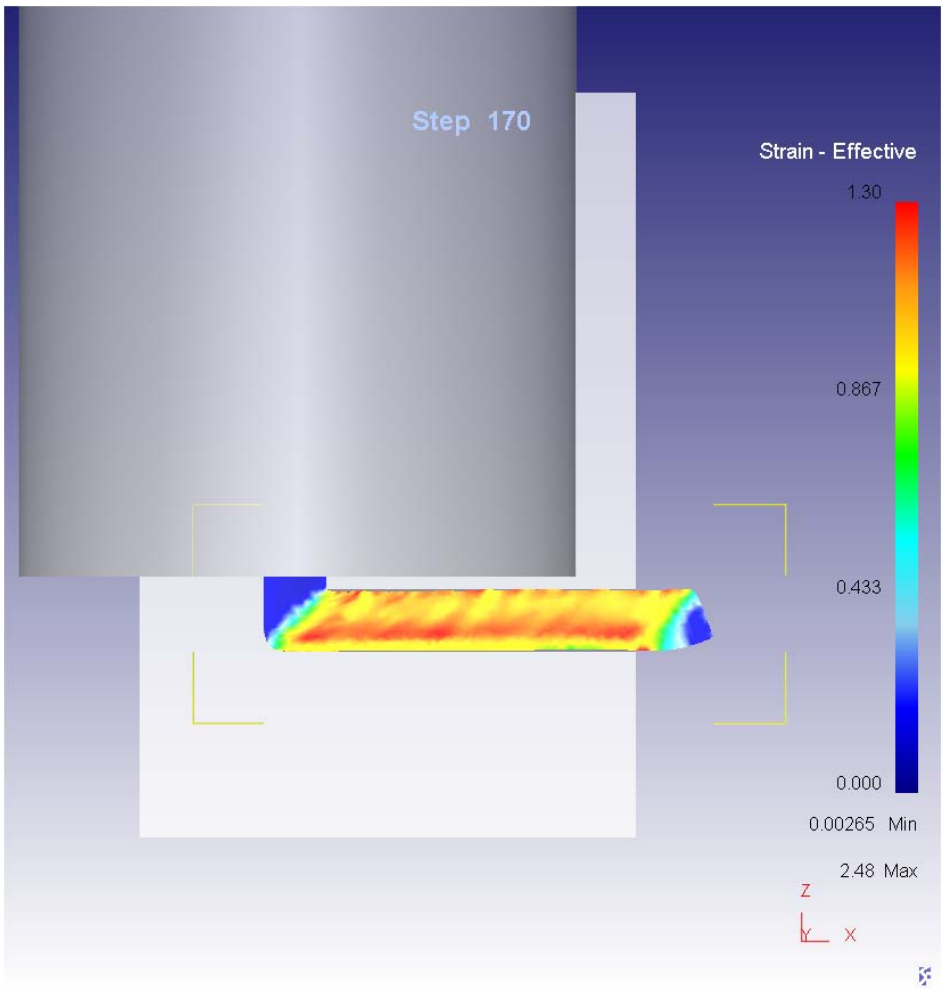

Figure 5.8 Theoretical strain distribution plotted using 1.3 as the maximum strain

The re-plotted strain distributions now show more variation that was previously indicated. The patterns are reminiscent of shear bands that sometimes occur in flow softening materials. [31] Shear bands are essentially localized regions of very high strains, and are normally an undesirable phenomenon in ECAE because they result in a non-homogeneous strain field.

Chapter 6

ECAE Processing the TNZT Alloys

6.1 Experimental methods

The results from compression testing indicate that uniform grain refinement is difficult to achieve in the TNZT alloys. Static recrystallization was able to produce relatively uniform structures but rapid grain growth, even in the best case high-boron alloy, limited grain size reduction to only 10μm which is not small enough to produce significant property improvements. Deformation at high temperatures produced a non-uniform mixed-grain microstructure with recrystallization occurring only at the grain boundaries while leaving the interior regions untransformed. In response to this, the ECAE processing conditions were chosen to try to maximize the strength improvements in the alloys rather than focus on producing only uniform grain refinement. The strategy was based upon the observed ductility of the samples and microhardness measurements that were taken on the HTC samples.

Hardness values for the as-deformed samples processed in the low temperature cold working range were the highest (≈200HV). The annealed samples that were processed at these temperatures had a 15% decrease in hardness (≈170HV), which is not unexpected due to the decrease in strain energy that occurs during static recrystallization. Hardness values for the as-deformed samples processed in the high

temperature dynamic yielding range were also higher prior to annealing, undergoing an approximate 5% decrease from ≈180HV to ≈170HV. A final processing temperature of 500°C for TNZT was chosen in order to ensure that the material had sufficient ductility to prevent shear cracking during ECAE processing. The boron containing alloys, especially high-boron, suffered from noticeable shear cracking when HTC tested in the low temperature range, and therefore would not likely survive the extreme strains induced by ECAE at those temperatures. Because of this, a final processing temperature of 825°C was chosen for the boron containing alloys. The as-deformed samples at 840°C had the highest hardness value for the samples that did not undergo cracking, but 840°C is very close to the operating temperature limit of the Inconel 718 ECAE die so the processing temperature was slightly decreased.

The die geometry used consisted of a ¼ inch channel diameter with a 90° channel angle and 20° corner angle for reasons stated earlier. [31] The die itself, which is shown below in figure 6.1, was made of two Inconel 718 halves that were bolted together using threaded studs and nuts also made of Inconel 718. The die and hardware material was chosen specifically for its high-temperature strength and durability.

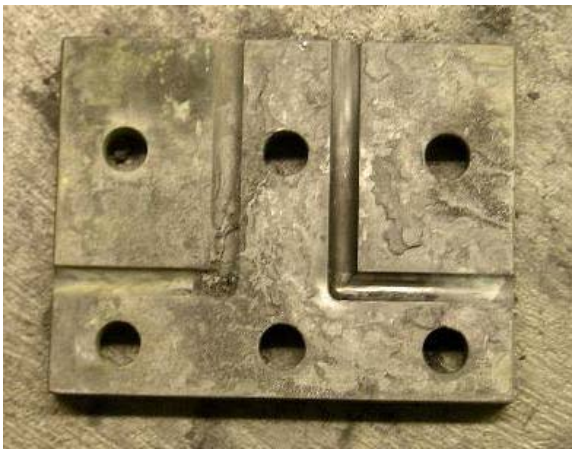

Figure 6.1 Inconel 718 die half used for ECAE processing

Samples billets were machined to ¼ inch diameter using EDM, cut to a length of 1.75 inches using wafering saw, and β annealed by the same procedure previously mentioned. The die hardware was coated with a high-temperature nickel anti-seize grease to ensure ease of opening of the die after the completion of one pass, and the die channel was painted with a molybdenum-disulfide based lubricant. The sample was inserted into the die channel which was then bolted tightly together. A tungsten carbide rod was then inserted on top of the sample to serve as the push rod. The extrusions were conducted using the same set-up that was used for HTC testing. As shown in figure 6.1, the die used was a double die but only one channel was used at a time. The exit channel that was not in use served as the location for the thermocouple probe from the temperature controller. The entire die assembly was inserted into the furnace and allowed to come up to temperature. When the proper processing temperature was reached, the sample was extruded using a crosshead speed of 0.01in/s for processing at 500°C and 0.1 in/s for processing at 825°C. After completion, the

die assembly was removed from the furnace, unbolted, the sample removed and immediately water quenched to try to prevent aging and second phase formation that would take place during normal air cooling. Samples were then either sectioned for metallographic examination, or machined into the proper shape for mechanical testing. TNZT samples were subjected to 1 pass and 4 pass, Route B_C schedules. The boron containing alloys were only subjected to 4 pass, Route B_C schedules since a single pass would likely produce a mixed-grain structure similar to the one seen in HTC testing. The x, y, and z shearing action in Route B_C may be able to induce a more homogeneous structure due to the crossing of the shear planes. [33]

6.2 Results and discussion

Microstructures for all the alloys subjected to ECAE processing are shown below in figure 6.2.

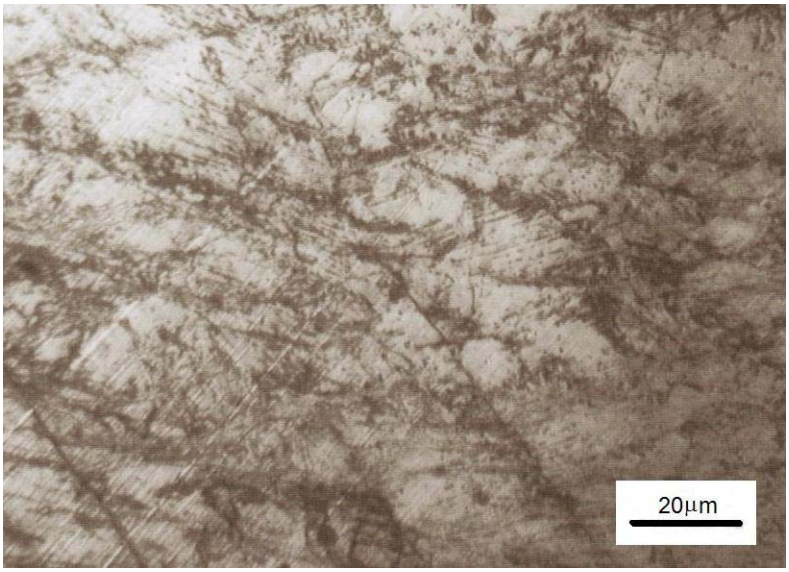

(a)

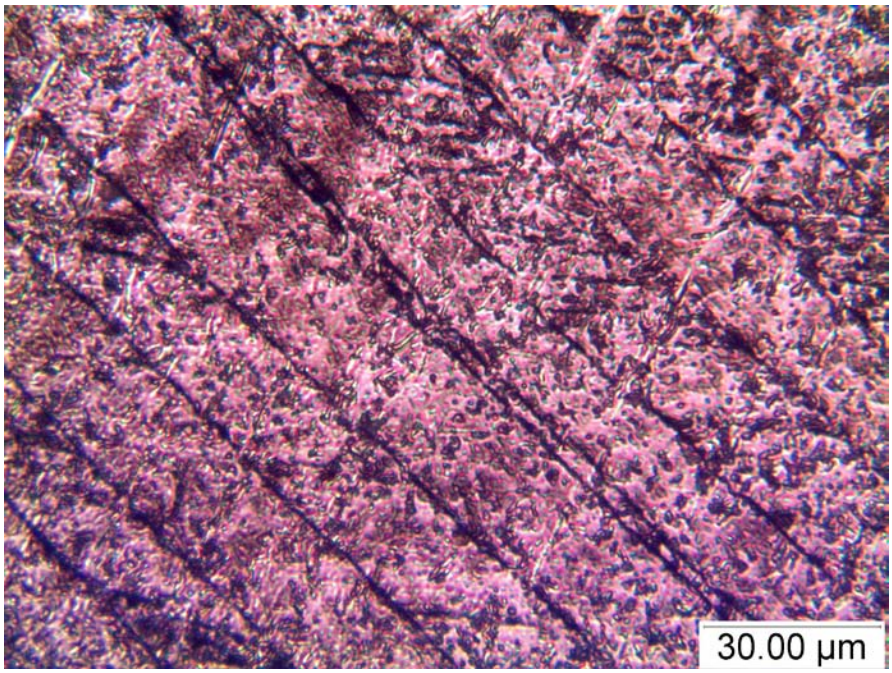

(b)

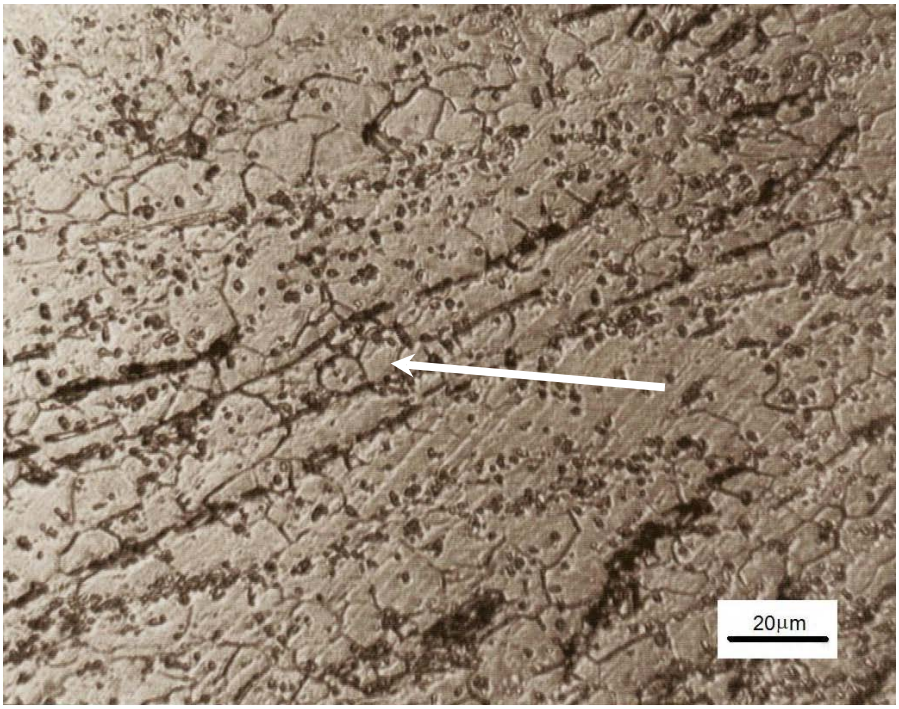

(c)

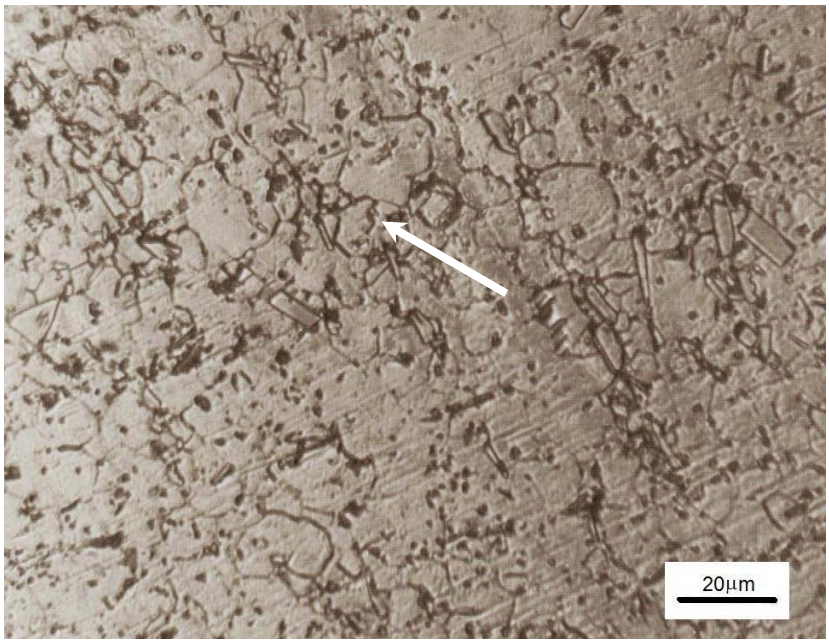

(d)

Figure 6.2 (a) TNZT alloy ECAE processed at 500°C for 4 passes (Route B_C) (b) TNZT alloy ECAE processed at 500°C for 1 pass (c) TNZT+0.15%B ECAE processed at 825°C for 4 passes (Route B_C) (d) TNZT+0.5%B ECAE processed at 825°C and 4 passes (Route B_C).

TNZT ECAE processed at 500°C for 4 passes through the die, shown in Figure 6.2a, shows a highly deformed substructure which is expected during extrusions at relatively low temperatures. The micrograph of the one pass sample shows the classic elongated grain structure that is typical of single pass extrusions. The picture is able to show a clearer picture of the shear deformation that takes place because the structure has only been elongated in one direction. The boron containing alloys underwent some dynamic recrystallization (indicated by arrows) during ECAE processing (Figure 6.2c and 6.2d), but there does not appear to be complete recrystallization throughout the sample. The grain size is non-uniform and still rather

large at ~10μm. It is worth noting that the morphology of the second phase borides is much finer compared to previous micrographs. Coarse particle breakdown due to the very high strains encountered in ECAE has been observed before, and could be beneficial to the mechanical properties of the high and low boron alloys.

Transmission electron microscopy was performed on TNZT in the β annealed, ECAE 1 pass, and ECAE 4 pass conditions. The micrographs are shown below in figure 6.3-6.5.

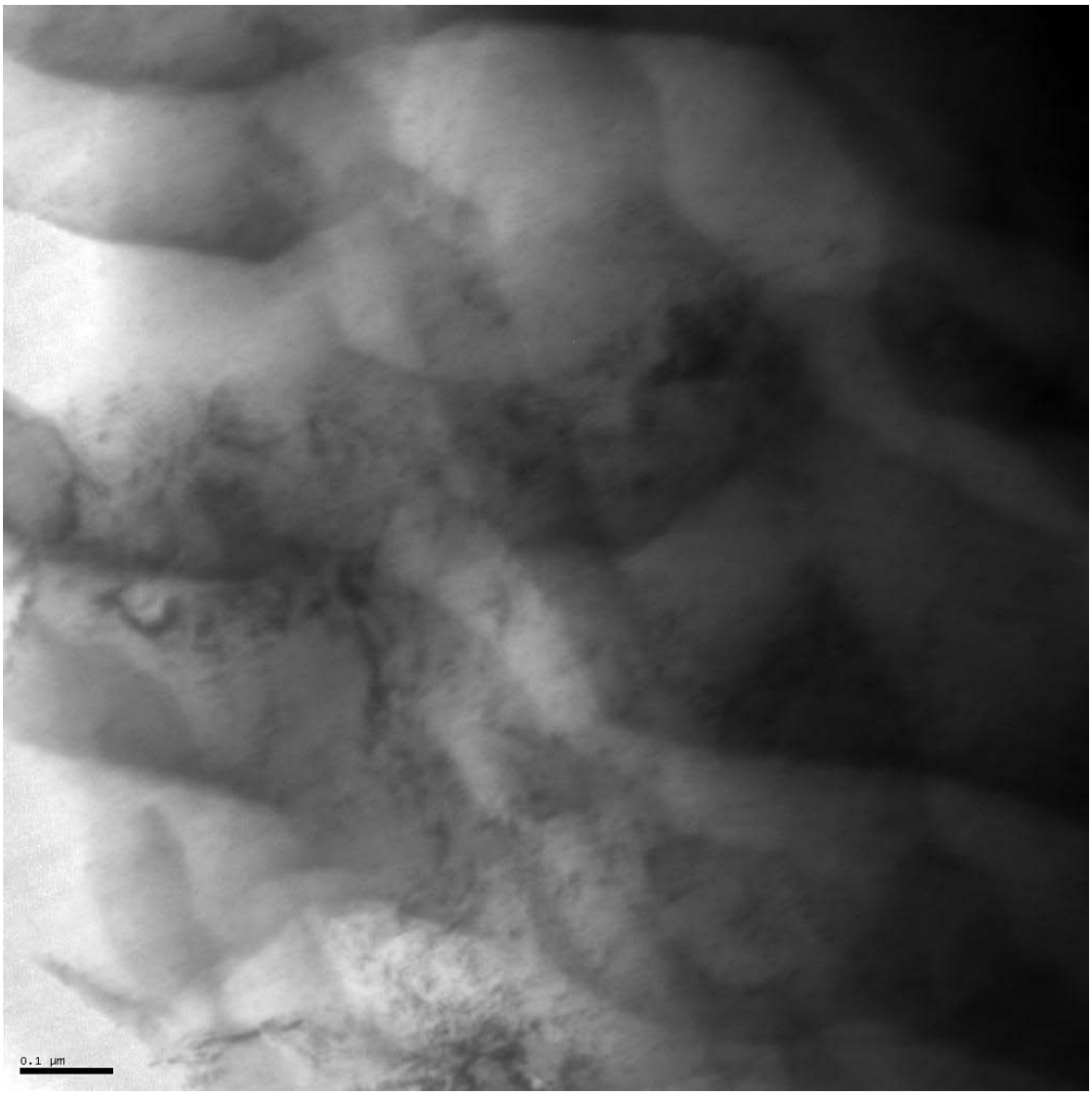

Figure 6.3(a) TEM micrographs of as-received, β annealed TNZT

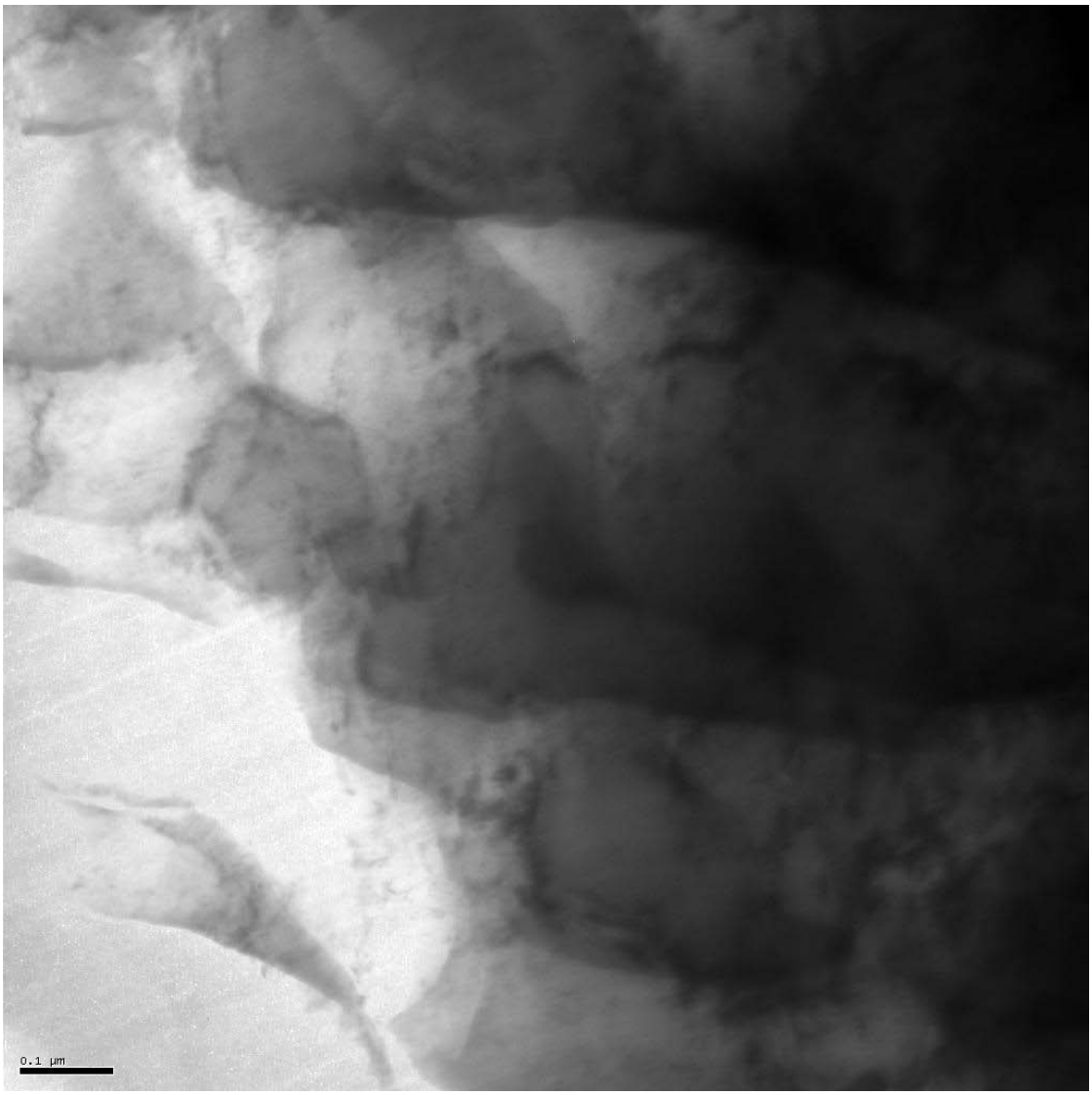

Figure 6.3(b) TEM micrographs of as-received, β annealed TNZT

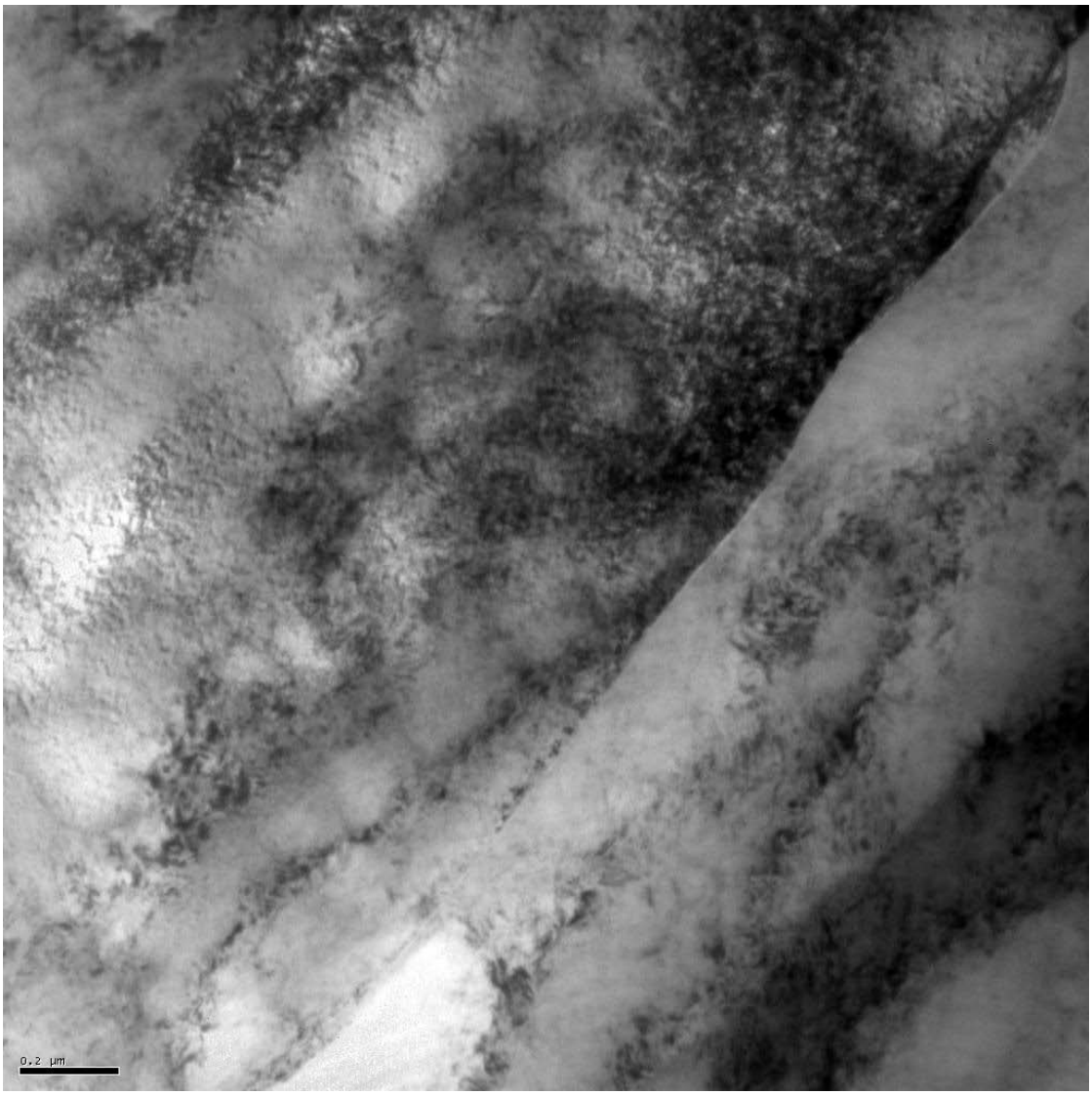

Figure 6.4(a) TEM micrographs of TNZT ECAE processed at 500°C 1 pass

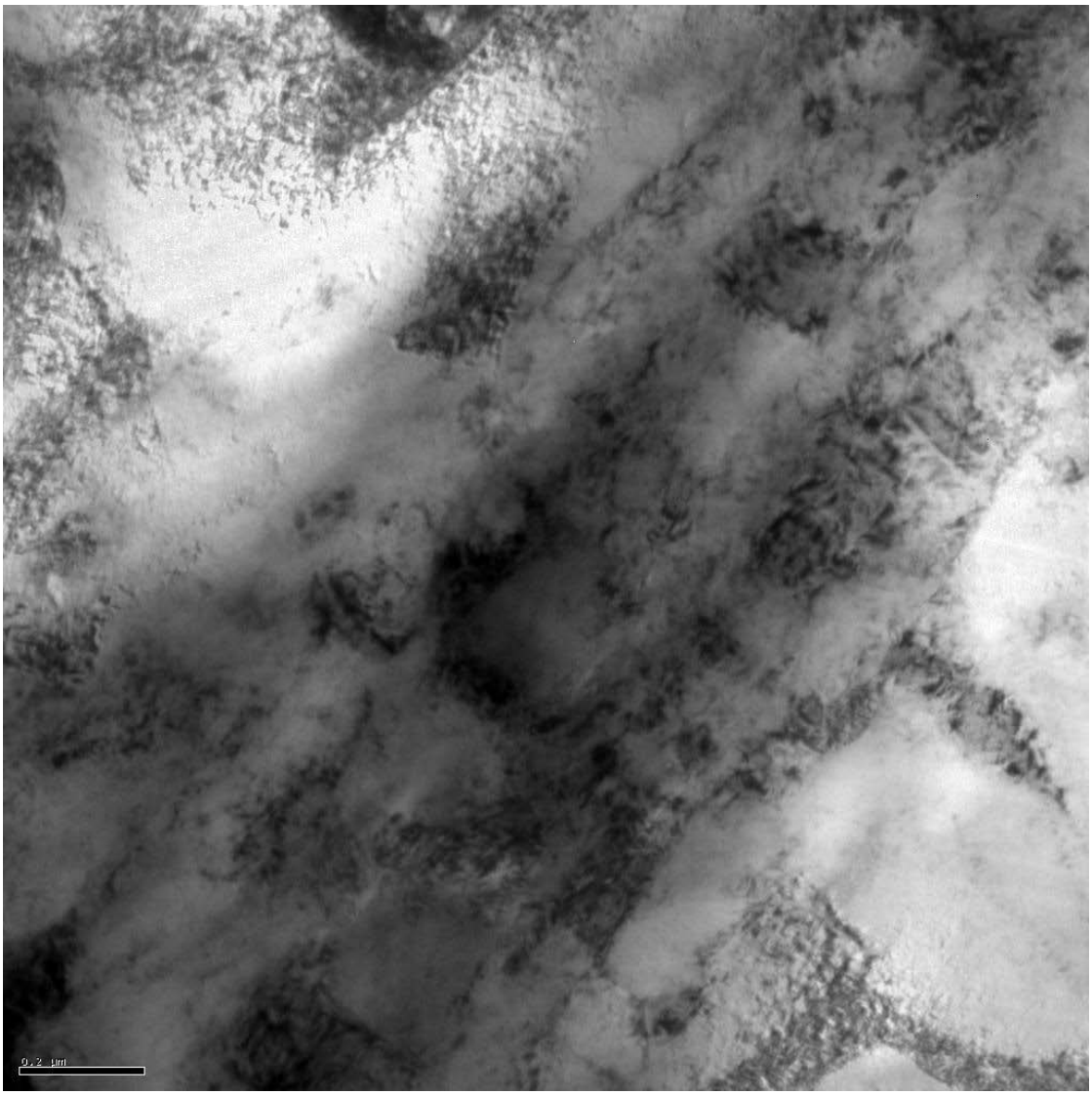

Figure 6.4(b) TEM micrographs of TNZT ECAE processed at 500°C 1 pass

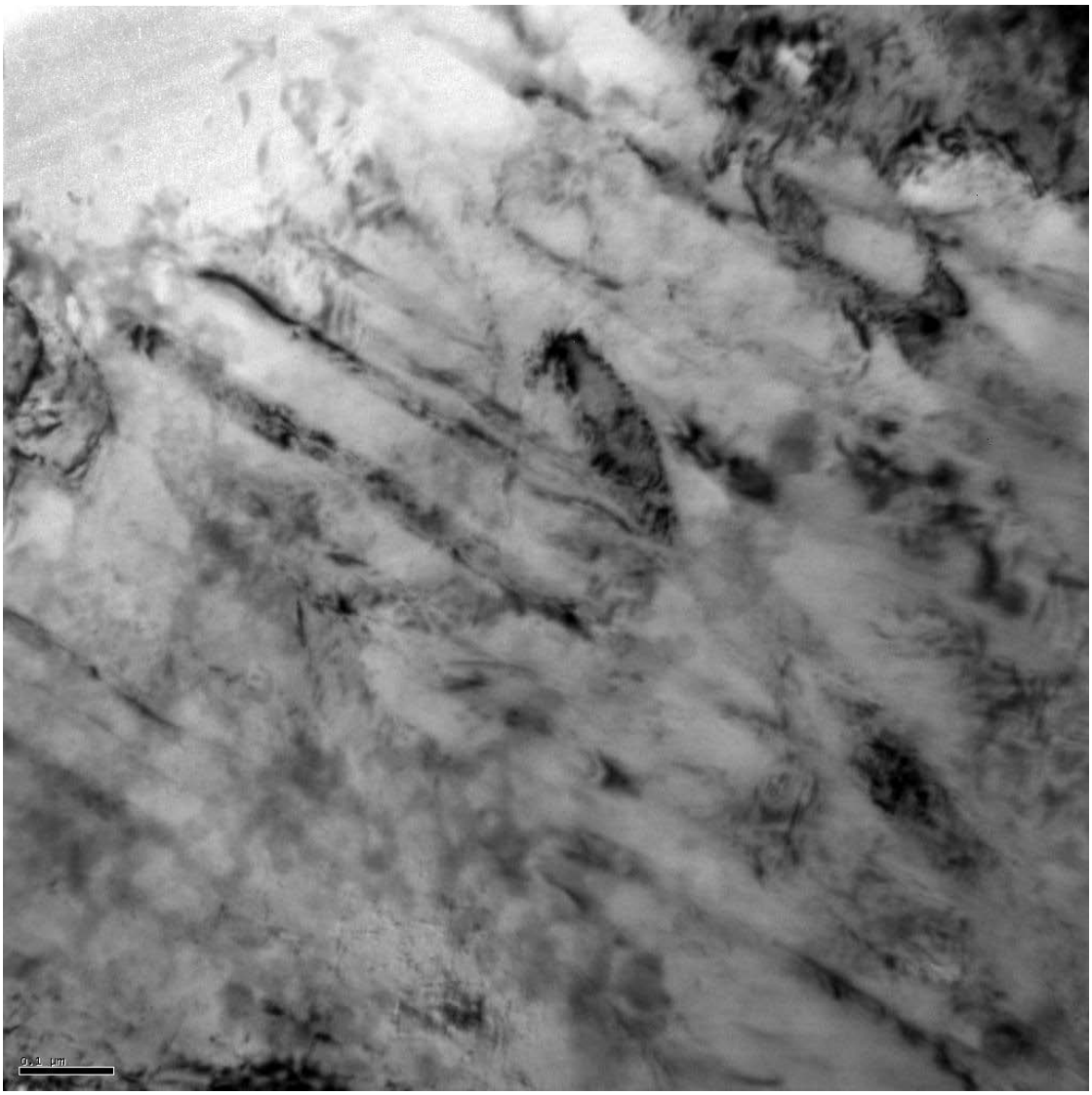

Figure 6.4(c) TEM micrographs of TNZT ECAE processed at 500°C 1 pass

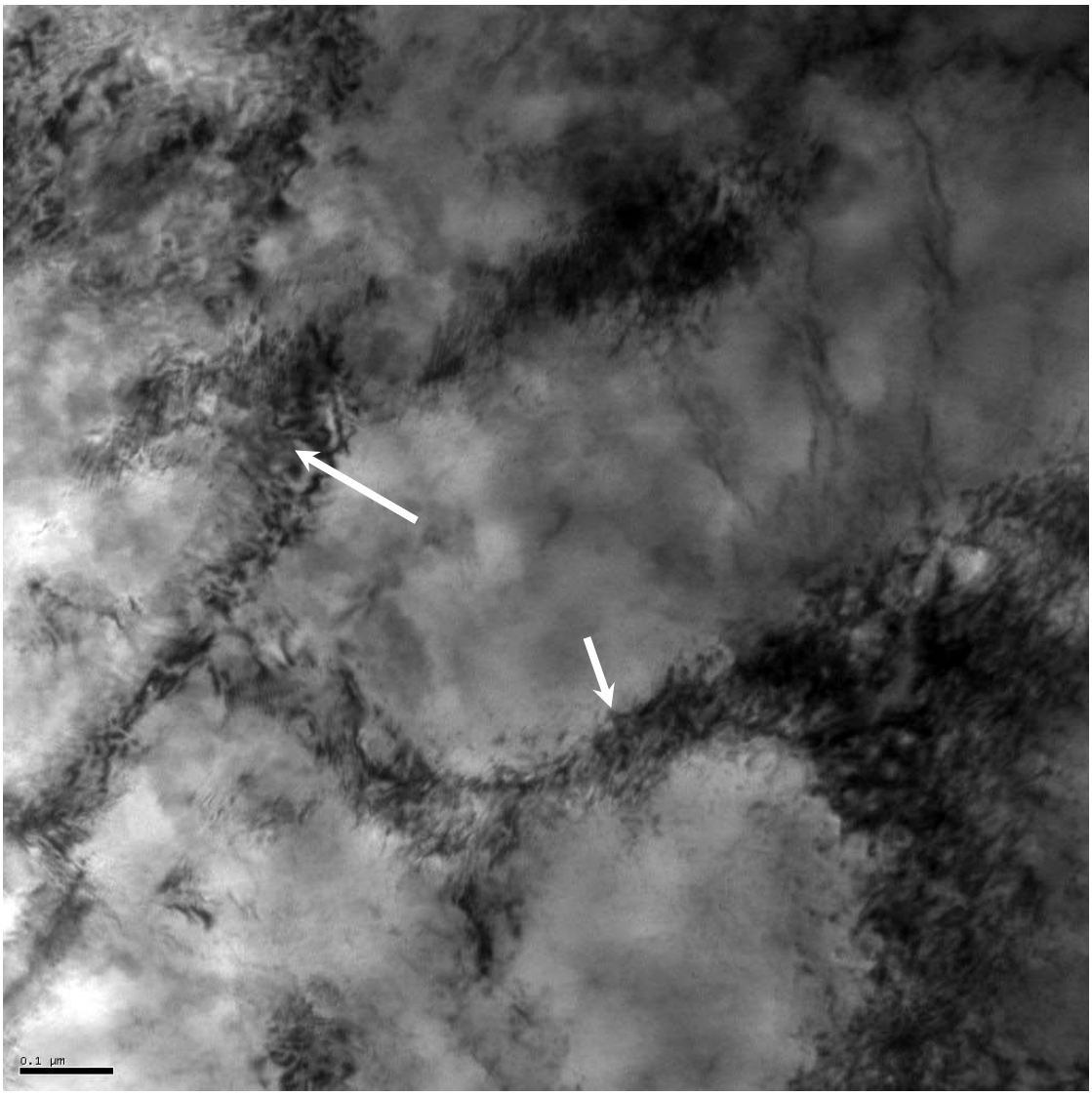

Figure 6.4(d) TEM micrographs of TNZT ECAE processed at 500°C 1 pass

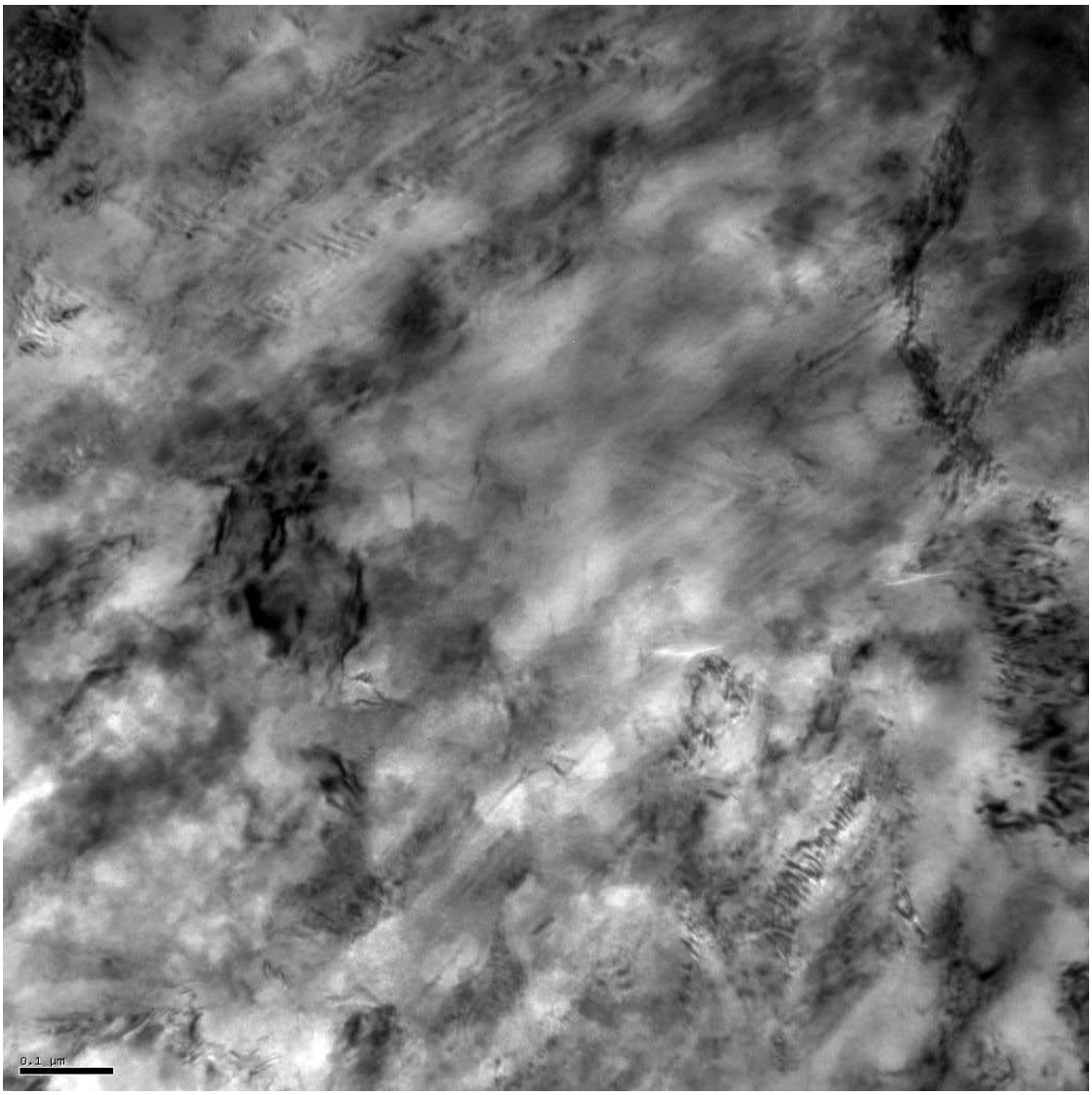

Figure 6.4(e) TEM micrographs of TNZT ECAE processed at 500°C 1 pass

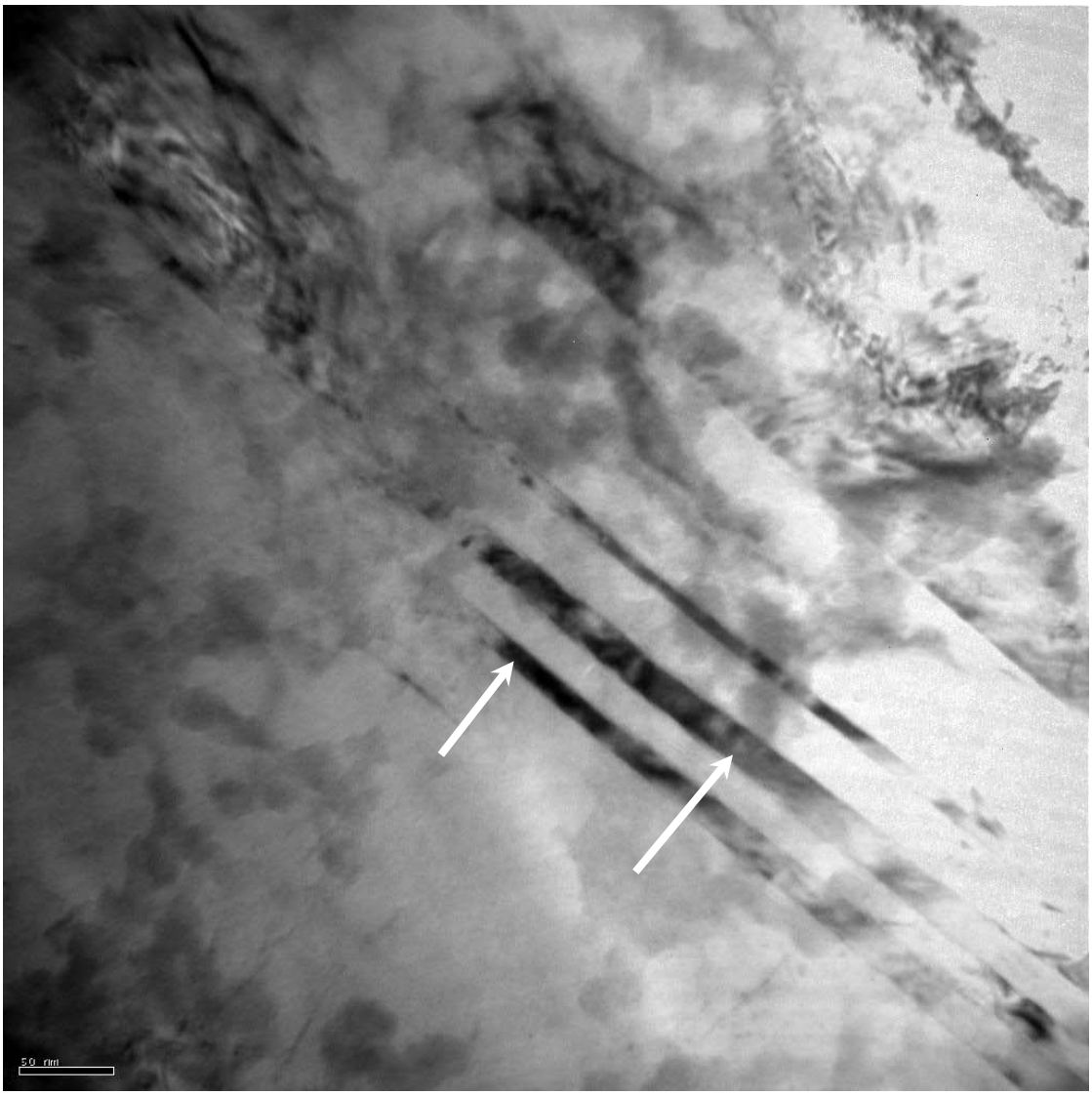

Figure 6.4(f) TEM micrographs of TNZT ECAE processed at 500°C 1 pass

.

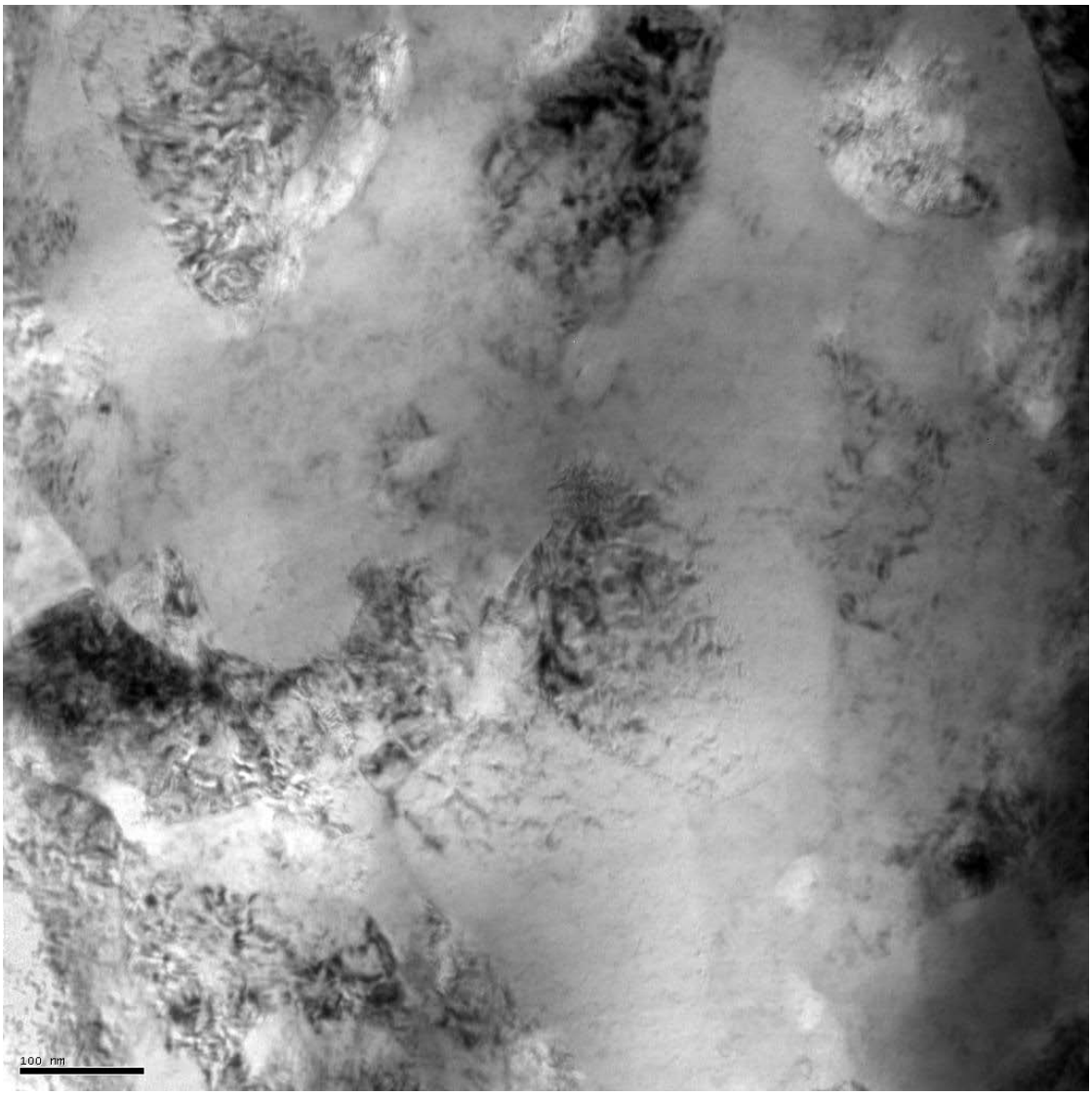

Figure 6.5(a) TEM micrographs of TNZT ECAE processed at 500°C 4 pass

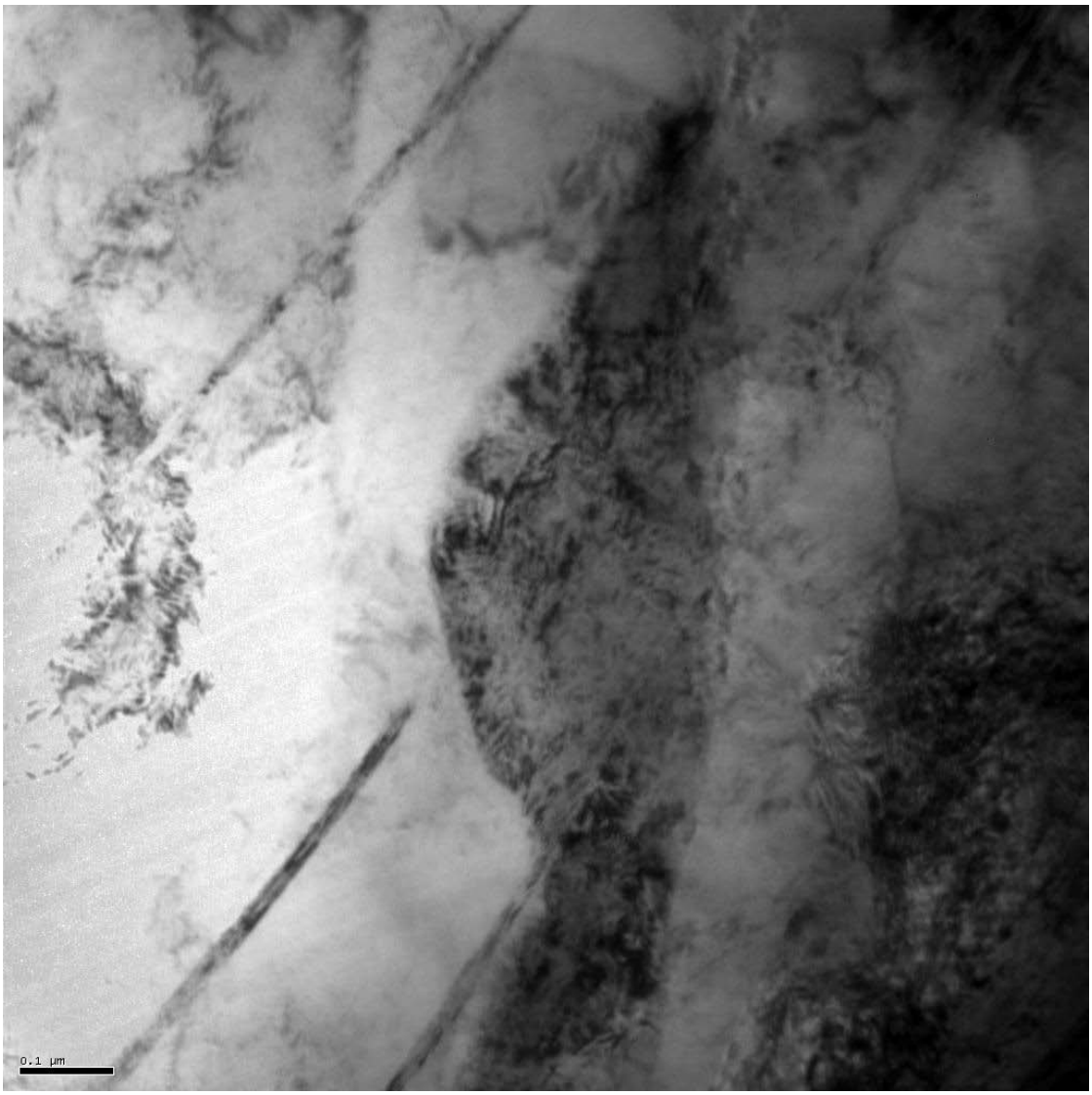

Figure 6.5(b) TEM micrographs of TNZT ECAE processed at 500°C 4 pass

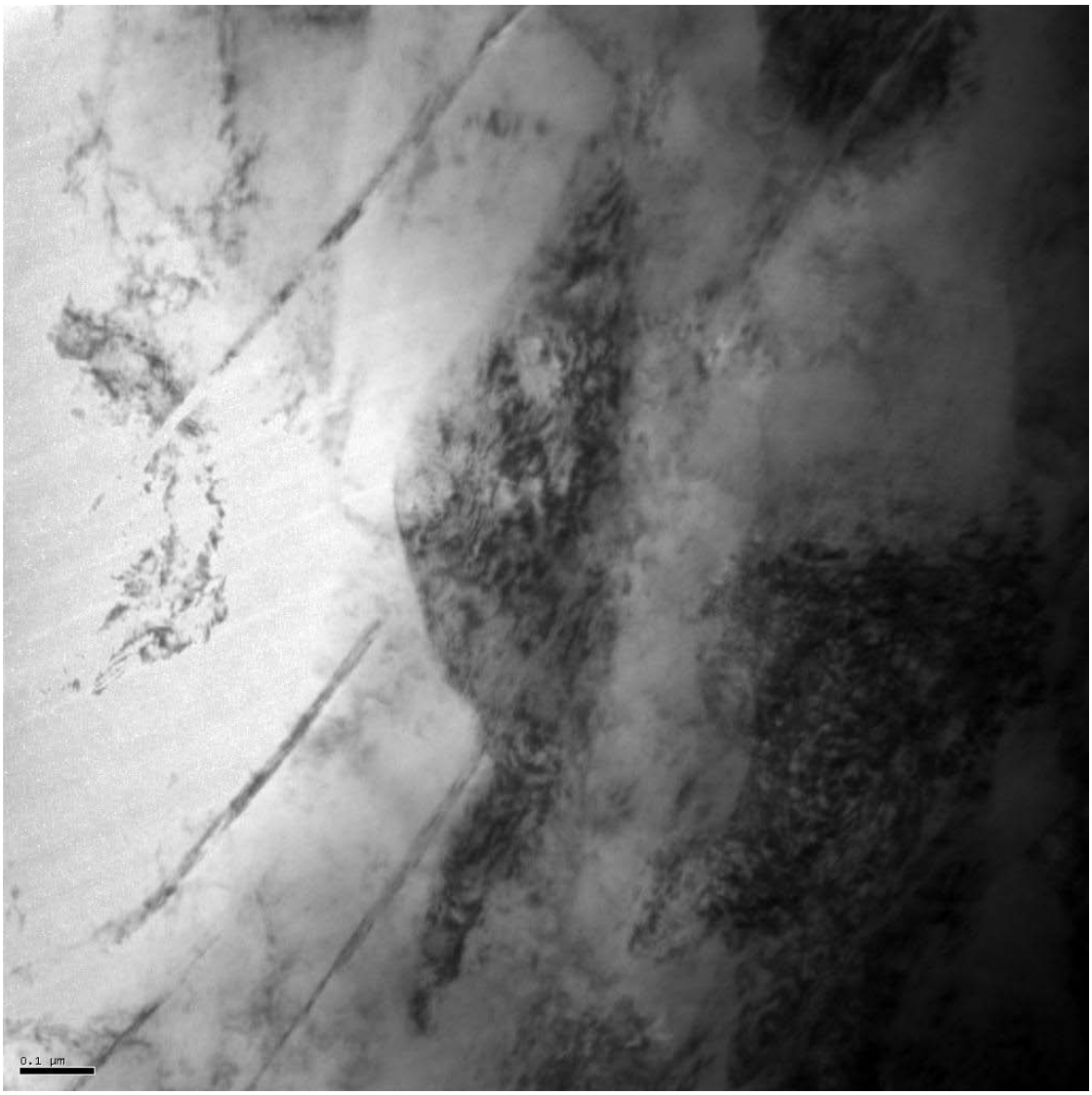

Figure 6.5(c) TEM micrographs of TNZT ECAE processed at 500°C 4 pass

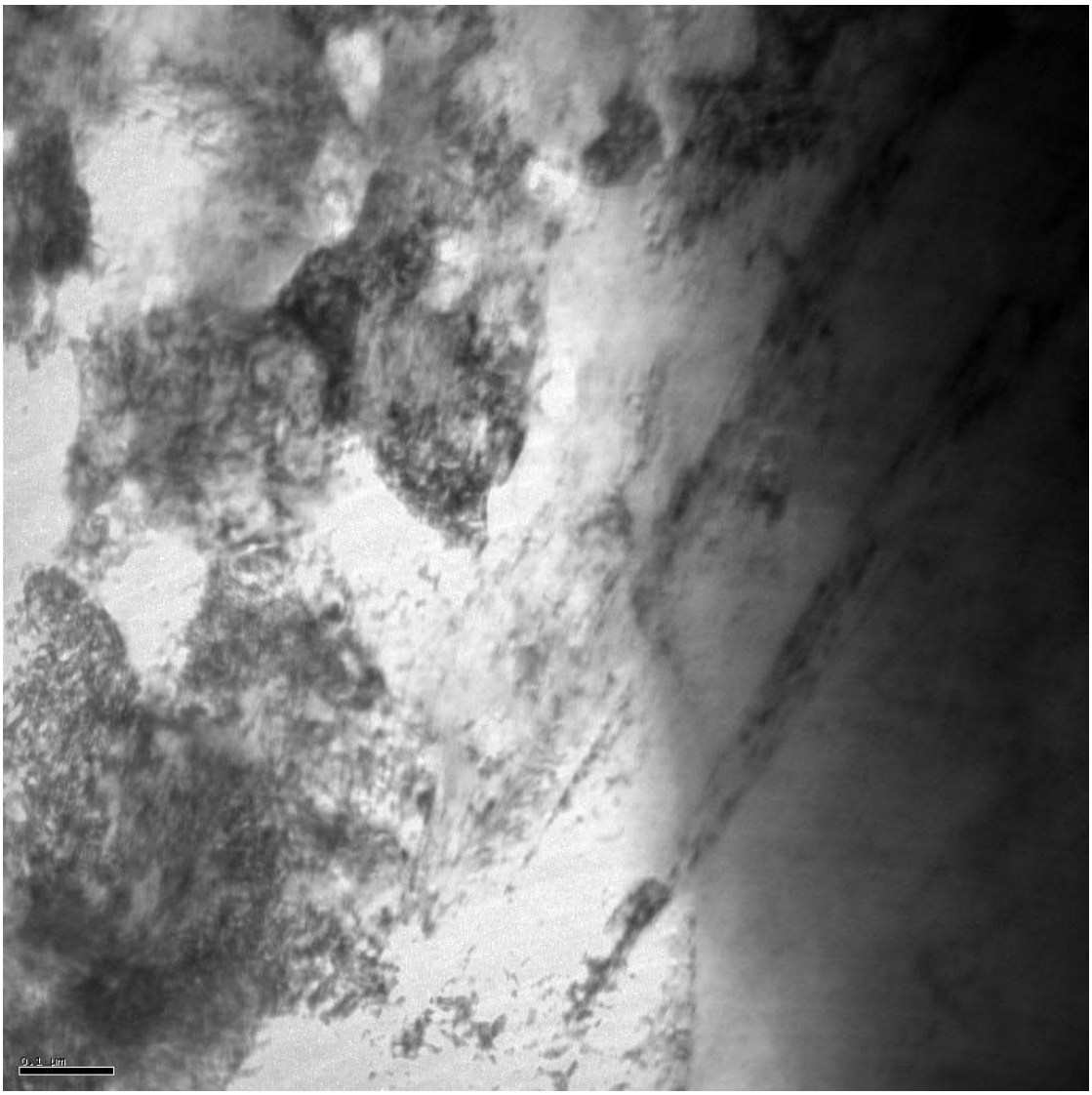

Figure 6.5(d) TEM micrographs of TNZT ECAE processed at 500°C 4 pass

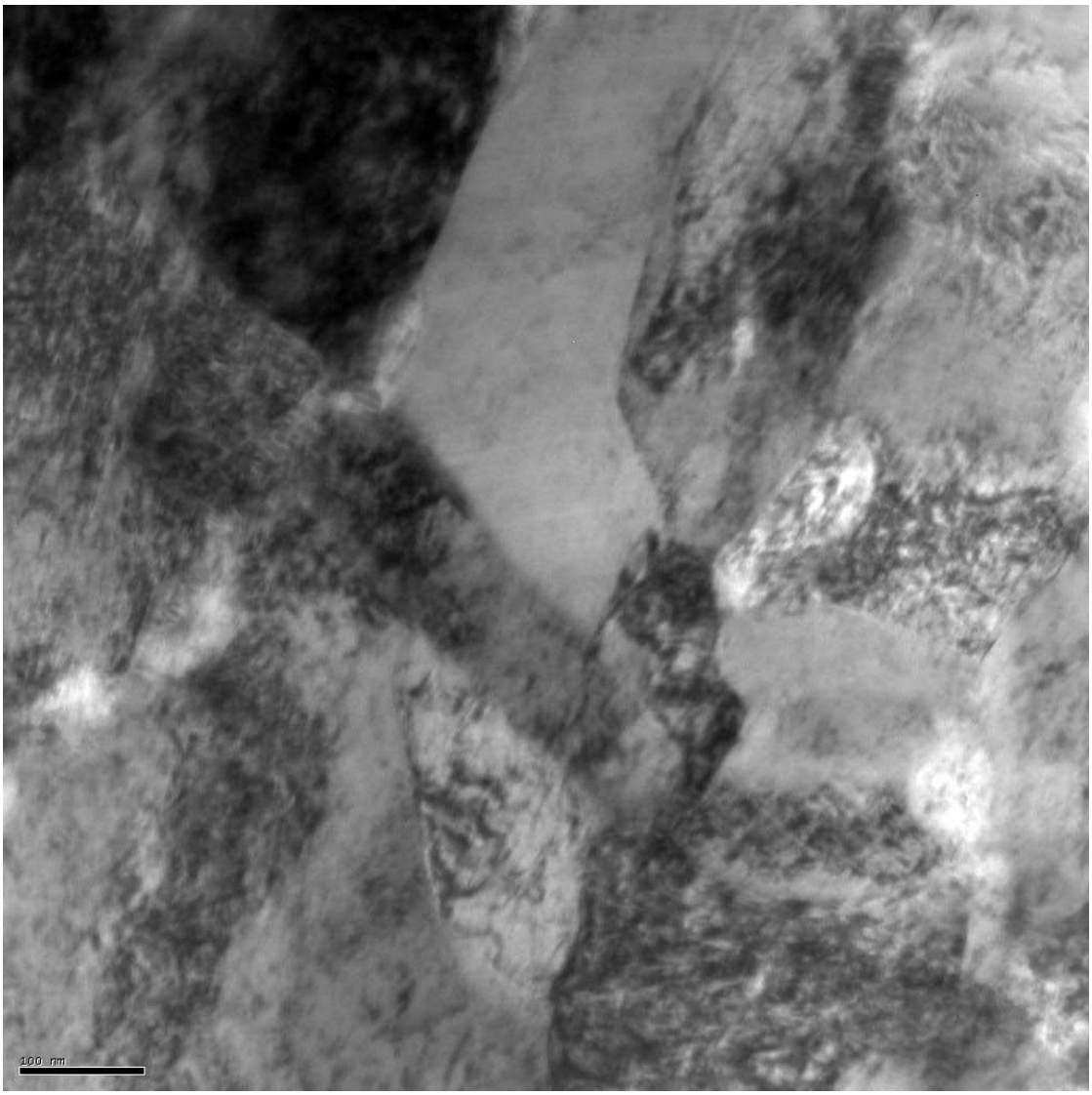

Figure 6.5(e) TEM micrographs of TNZT ECAE processed at 500°C 4 pass

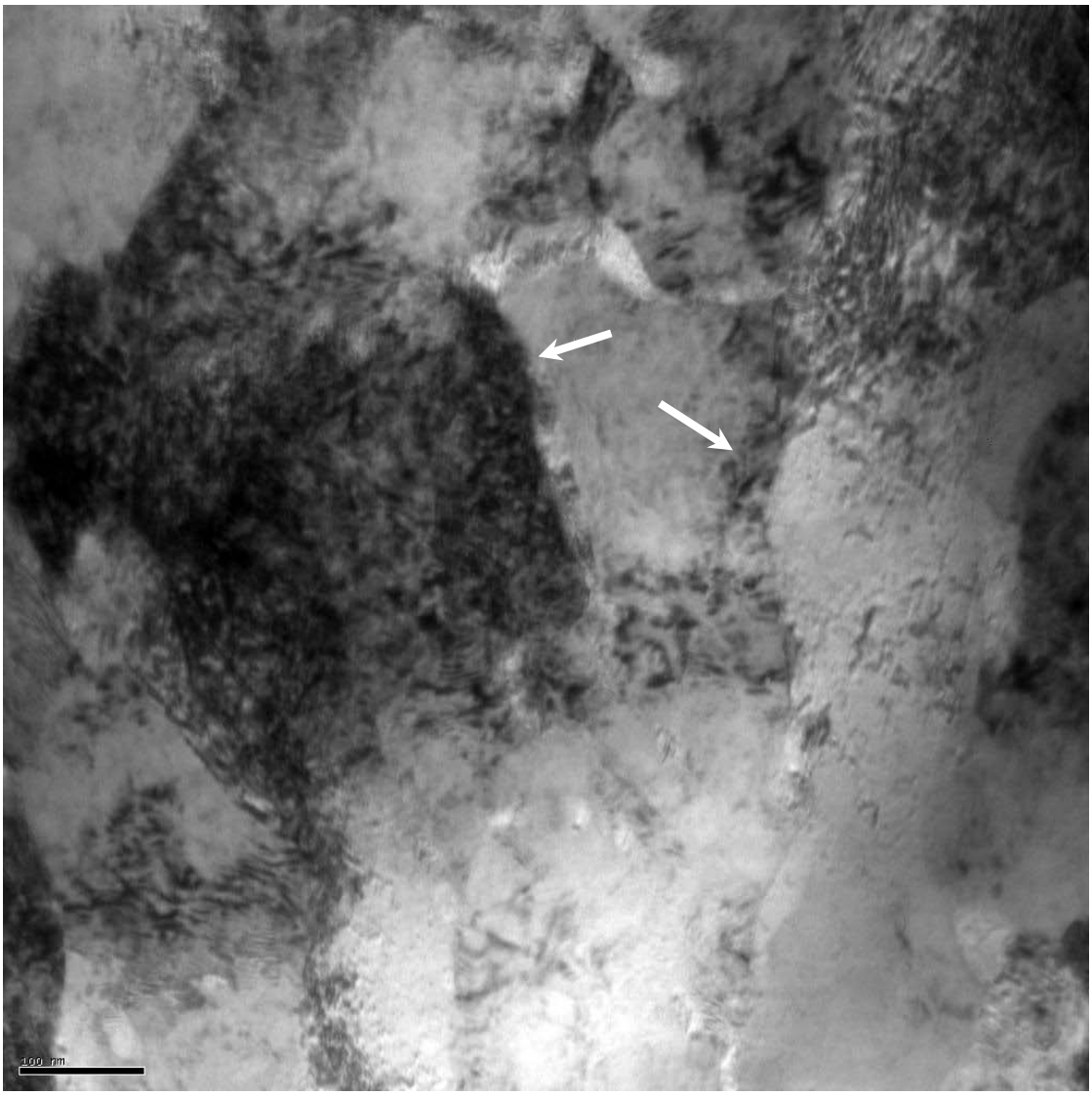

Figure 6.5(f) TEM micrographs of TNZT ECAE processed at 500°C 4 pass

The TEM micrographs of the β-annealed TNZT shows only single phase β structure as expected. The micrographs of the 1 pass sample shows dislocation tangles and dislocation cell structures (figure 6.4d), along with the presence of shear bands (figure 6.4f). This validates the simulation results from DEFORM which predicted the development of shear bands during processing. The micrographs of the 4 pass sample

show the same features as the 1 pass, but with a very high density of dislocations (figure 6.5f).

This study has used ¼ inch diameter rods as a means of convenience. The small size rods are easy to handle, machine, and fit perfectly with the sample geometry required for mechanical testing. However, the medical industry would find little use for rod of such small size even if the properties it displayed were exceptional. Fortunately, scale-up studies of the ECAE process have been performed that show good correlation between the grain refinement and property improvement achieved in small samples and large samples. [58] Facilities here at Washington University with the capacity to extrude sample billets up to two inches in diameter were developed and studied with that specific focus in mind. There is no required change in die geometry or other processing parameters to accommodate a larger size billet, therefore the difficulty in scaling up the ECAE process lies in engineering the processing equipment and procedures to deal with the increased weight and load requirements. To design the workstation, the extrusion pressures for a 2" diameter billet being pushed through a 90° die were estimated using DEFORM-3D. The results of the simulations are shown below. [58]

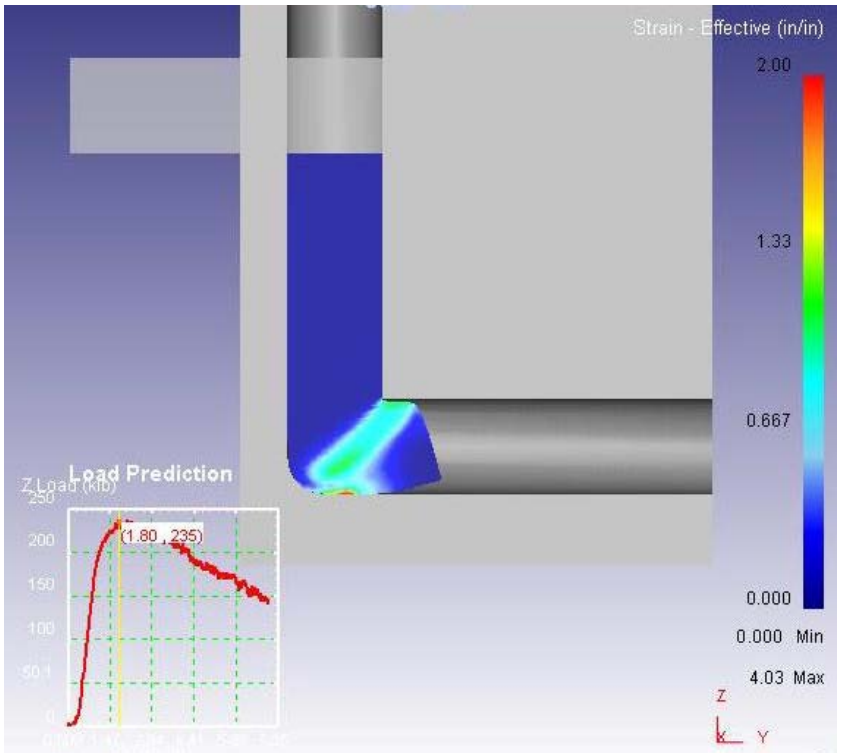

Figure 6.6 Two inch diameter ECAE simulation at maximum press force (117.5 tons)

After the required loads were found, it was determined that a 200 ton capacity H-frame press would be required along with a 300 ton cylinder for the application of side-clamping forces to prevent die separation. The H-frame press was not rated for side-clamping loads of this magnitude; therefore a design for reinforcing the H-frame is required. Concept sketches were produced, and eventually the finalized design resulted in the form of a relatively simple box frame (see figure below) with two reinforcing mechanisms; one being the six tie bars, and the second being the four reinforcing tabs. [58]

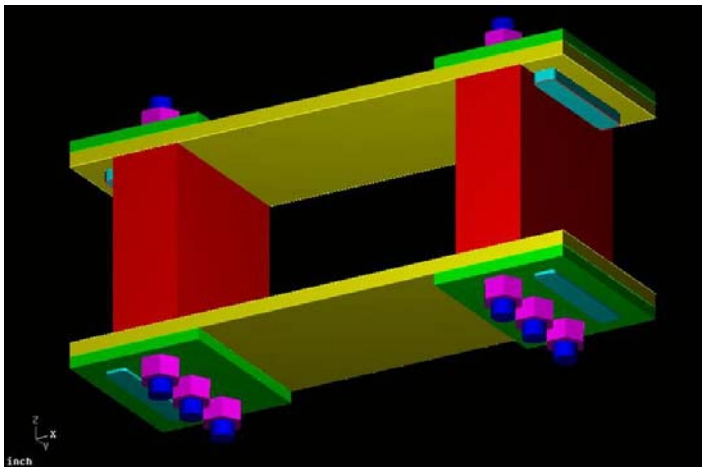

Figure 6.7 300 Ton Frame

The material chosen for the entire assembly was 4340 steel because of its high yield strength. The dies and the heating blocks which housed eight 750W cartridge heaters were both fabricated from Inconel 718 because of its high temperature strength. [58] The completed assembly and the dies and heating blocks are shown below.

Figure 6.8 Fully assembled ECAE scale-up workstation

Figure 6.9 ECAE die and heating block for scale-up assembly.

Copper and Ti-6Al-4V were successfully processed with this workstation. The copper billet was processed at room temperature, and upon extraction from the die showed no surface cracking or flashing due to die separation. Figure 6.10 shows a photograph of the copper billet taken after processing. The Ti-6Al-4V billet was processed at 700°C

with similar results to the copper extrusion. The completed Ti-6Al-4V extrusion is shown in Figure 6.11

Figure 6.10 Two inch diameter copper extrusion

Fig. 6.11 Two inch diameter Ti-6Al-4V extrusion

Evaluation of the large diameter billets by optical microscopy and microhardness testing showed no discernible difference in the uniformity of the strain distribution or the degree of grain refinement between large and small samples. [58] Scale-up work has not been performed on the TNZT alloy, but based on the previous work that has been completed it can be reasonably assumed that any result produced in small scale will have no issues being reproduced at larger scales.

Chapter 7

Mechanical Properties after ECAE Processing

7.1 Tensile testing

7.1.1 Experimental methods

Tensile testing was performed on all three alloys. TNZT samples were tested in the beta annealed, ECAE 500°C 1 pass, and ECAE 500°C 4 pass condition. TNZT+0.15%B and TNZT+0.5%B were tested in the beta annealed and ECAE 825°C 4 pass condition. Compact tensile test specimens were machined into dumbbell shapes with 0.125in diameter and 0.6in gage length. Testing was done on a screw-driven UTM at a strain rate of 5×10^{-4} /s. To get an accurate modulus value, an extensometer was attached until the sample reached 0.5% strain and then removed. After the extensometer was removed, the sample was tested until failure.

7.1.2 Results and discussion

The resulting stress-strain curves and a matrix summarizing the tensile properties are shown below in figure 7.1, 7.2, 7.3, and table 7.1

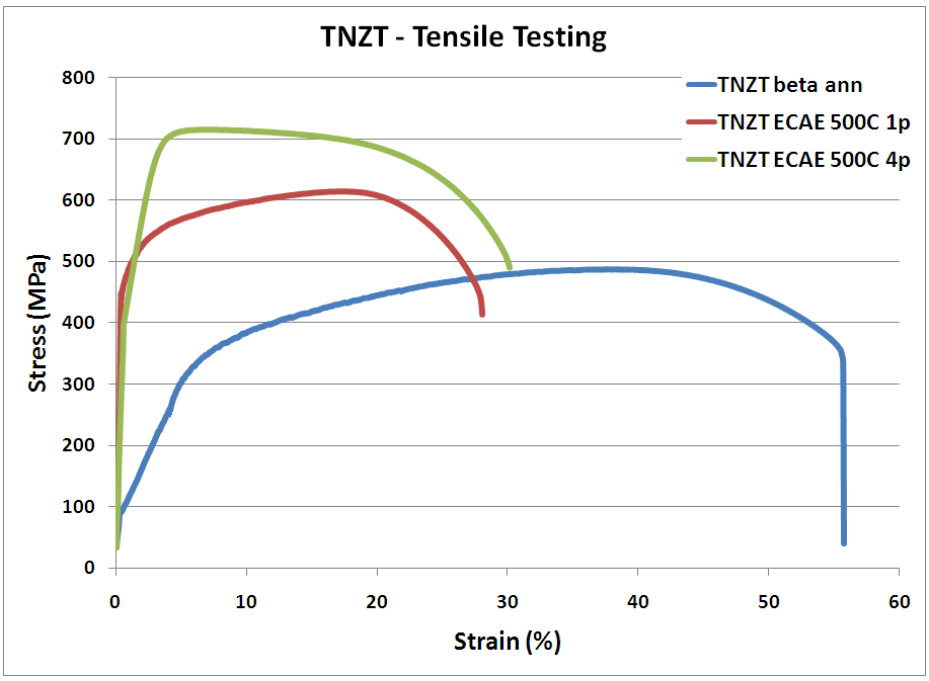

Figure 7.1 Stress-strain curves from tensile testing TNZT in various processing conditions

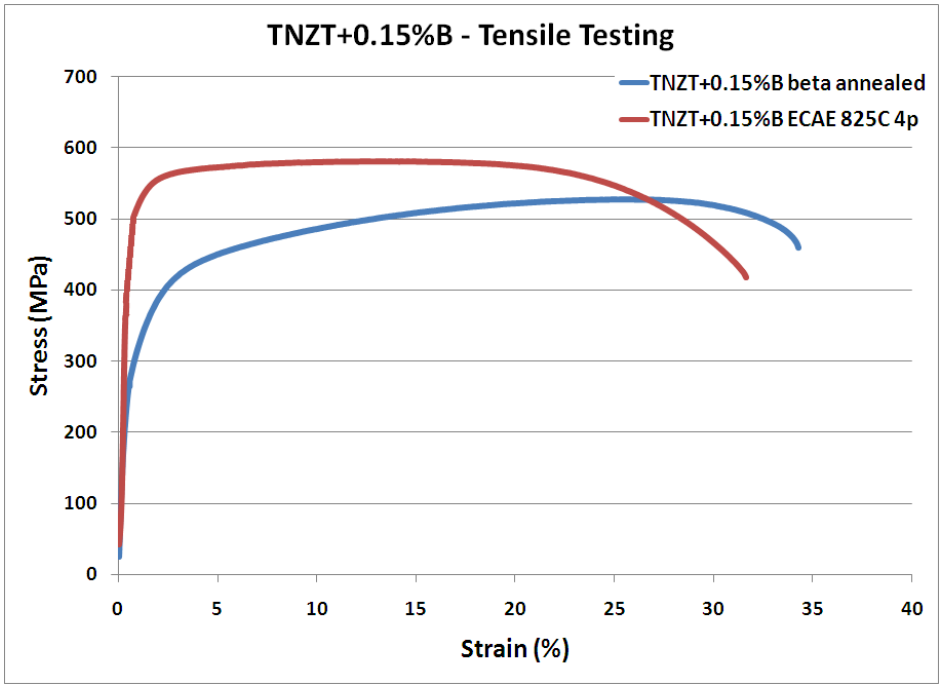

Figure 7.2 Stress-strain curves from tensile testing TNZT+0.15%B in various processing conditions

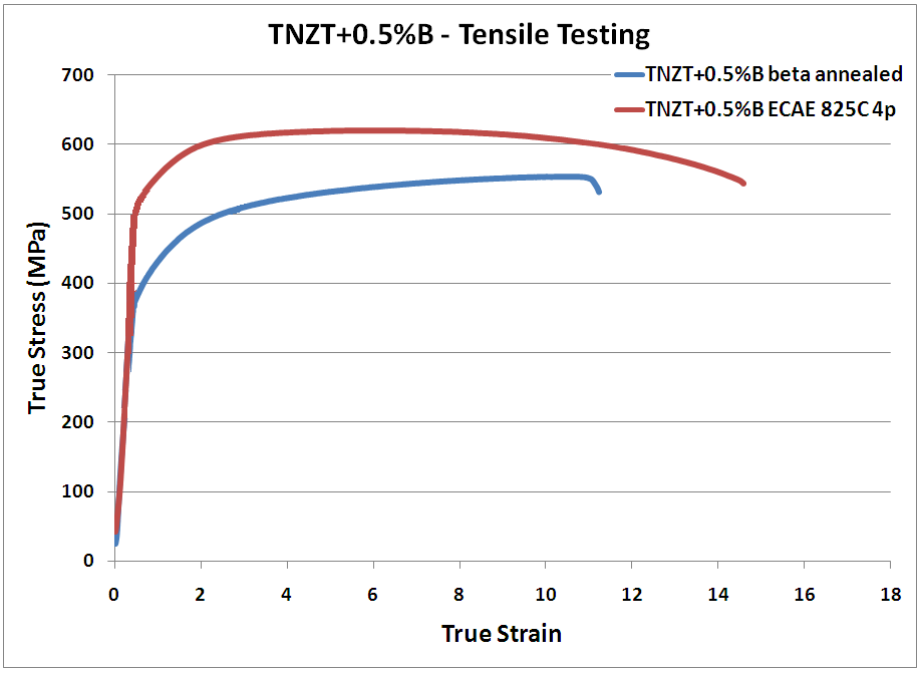

Figure 7.3 Stress-strain curves from tensile testing TNZT+0.5%B in various processing conditions

Table 7.1 Summary of the tensile properties of the TNZT alloys

Alloy	E(Gpa)	σ_y(Mpa)	σ_{uts}(Mpa)	%EL	%RA
TNZT β annealed	61	340	490	30	58
TNZT ECAE 500C 1 pass	80	540	615	12	63
TNZT ECAE 500C 4 pass	78	700	710	18	56
TNZT+0.15%B β annealed	76	380	535	20	30
TNZT+0.15%B ECAE 825C 4 pass	82	560	580	17	59
TNZT+0.5%B β annealed	105	435	550	8	8
TNZT+0.5%B ECAE 825C 4 pass	94	600	620	11	44

Examination of the results for the β annealed samples shows that the presence of boron has a negative impact on the modulus value of the alloy, increasing it from 61GPa to 105GPa from the no boron to the high boron alloy. In general, ECAE processing is beneficial to the strength of all of the alloys compared to their β annealed state. The strength levels in the β annealed state are rather low compared to

conventionally processed TNZT, but this can be explained by the very coarse nature of the as-received microstructures. TNZT subjected to 4 passes at 500°C stands out with the highest strength level while still maintaing reasonable ductility. The boron containing alloys show strength increases due to the small degree of grain refinement after processing, but they are not significant when compared to the strength values in conventionally processed TNZT. This is because the boron containing alloys have not undergone uniform refinement throughout the entire volume. A mixed structure consisting of recrystallized grains separated by untransformed regions will not efficiently restrict dislocation motion and will therefore not produce high strength levels. The improvement in ductility of the boron alloys is due to the refinement of the second phase boride particles discussed earlier. This type of mechanical behavior (strengthening due to development of a dense dislocation network) after ECAE is not unique, and has been observed in many other studies [59][60].

Unfortunately, the modulus value is not maintained in TNZT after processing, increasing by approximately 30%. Selected area electron diffraction (SAED) patterns taken from the TEM show additional spots which reveals the presence of second phase α particles in both the 1 pass and 4 pass sample. The α phase has a much higher stiffness value than the β phase, which explains the modulus increase. In addition, the higher dislocation density in the 4 pass sample gives it a higher strength value than the 1 pass sample.

7.2 Fatigue testing

7.2.1 Experimental methods

Fatigue response was investigated using a rotating-bending tester. TNZT rods subjected to four passes at 500°C were chosen for testing because these processing conditions gave the highest strength improvement. TNZT+0.15%B rods that were also subjected to four passes at 500°C were used. After viewing the tensile testing results, it was decided that pursuing processing at 825°C would not lead to a useful material due to the lack of any significant tensile strength improvements. The low boron rods were able to survive ECAE processing at the lower temperature, but the high boron rods did not survive intact and therefore were not tested. The ECAE processed billets were machined with a constant radius producing a stressed neck region 0.125in diameter and 0.25in length. Testing was performed in air at 60Hz at stress levels of 350MPa, 400MPa, 450MPa and 500MPa on the TNZT samples, and 400MPa and 450MPa on the TNZT+0.15%B samples. A picture of the tester is shown in figure 7.4.

Figure 7.4 Rotating-bending fatigue tester

The theory behind the test is relatively simple. As the sample is placed in bending, the top surface is in a state of tension while the bottom surface is in a state of compression. As the sample is rotated, the surfaces alternate their position which switches them between the tensile and compressive states. Single tests were stopped either at fracture of the sample or when 15 million cycles were reached.

7.2.2 Results and discussion

Fatigue test results were gathered and plotted on an S-N curve shown in figure 7.5. The curve has comparative data for Ti-6Al-4V, and for TNZT that has been processed by the traditional methods from another study [40].

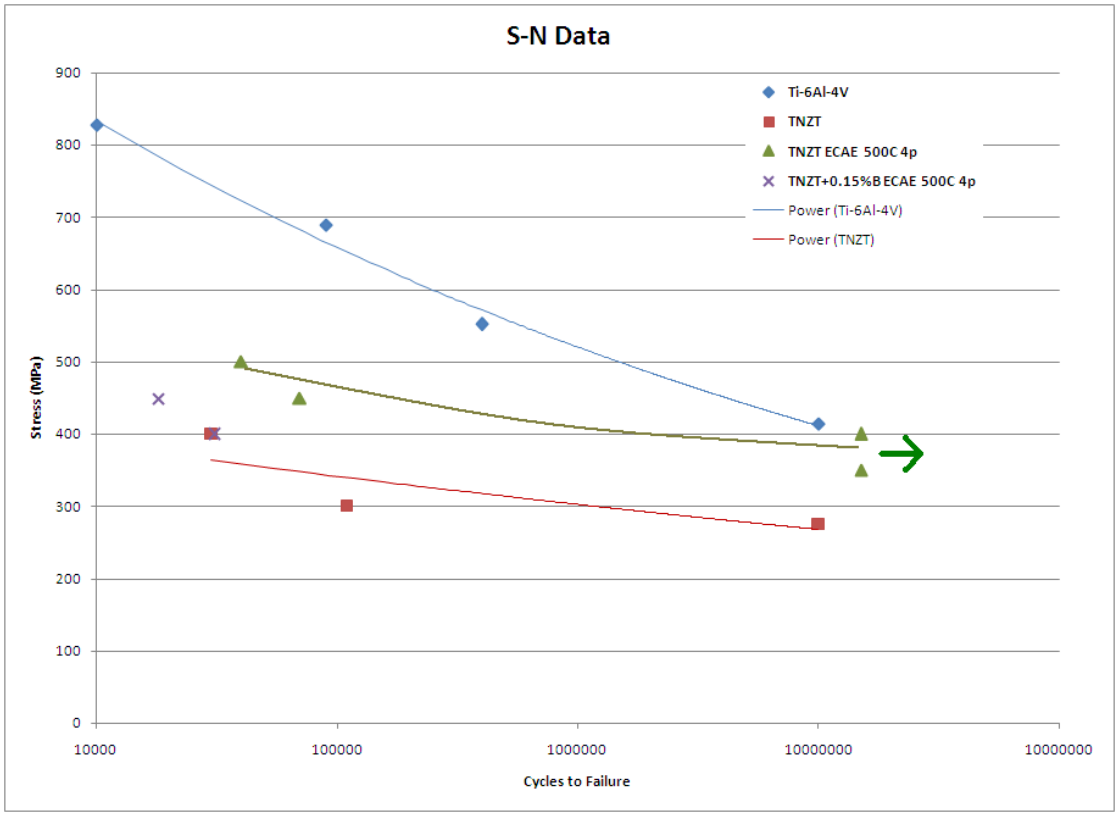

Figure 7.5 S-N curve of ECAE processed TNZT alloys vs. Ti-6Al-4V and conventionally processed TNZT [40]

The ECAE processed TNZT samples showed a significant increase in fatigue strength over the conventionally processed TNZT with the samples subjected to 350MPa and 400MPa stress levels undergoing run-out. The TNZT+0.15%B samples did not show any significant increase in fatigue strength, and in fact seem to have roughly the same fatigue strength as the conventionally processed TNZT. The fatigue strength increase in the TNZT alloy is due to the extremely dense dislocation network that is induced during processing. Strain localizations during cycling almost always appear as precursors to fatigue cracks, and these cracks most often nucleate at sites where plastic

flow is inhomogeneous. The severely hardened ECAE induced structure in TNZT suppresses dislocation activity by lowering the dislocation free-path length which reduces dislocation pile-ups and the resulting stress concentrations that can lead to non-uniform flow and slip band nucleation. [39] This dense network is also stable due to the fact that Ti-based alloys are planar-slip type in nature. This means that they have low stacking fault energies which inhibit cross-slip and easy dislocation motion. Most wavy-slip materials with this type of cold-worked substructure will undergo recovery and cyclic softening during fatigue due to the back and forth motion of dislocations. The easy cross-slip will allow dislocations of opposite signs to annihilate each other. [17] The TNZT+0.15%B did not show any fatigue improvement because of the second phase borides. The modulus mismatch between the borides and the matrix causes strain localizations and stress concentrations in the matrix that lead to fatigue cracks and ultimately shorten total life. [17]

7.3 Wear testing

7.3.1 Experimental methods

The friction and wear characteristics of the reference alloy and ECAE processed alloy were determined using a pin-on-disc type tester. TNZT was tested in the as-received β annealed condition and after ECAE processing at 500°C for four passes, Route B_C. The disc, or counter face materials chosen were hardened EN31 bearing steel and ultra-high molecular weight polyethylene (UHMWPE). The high hardness bearing steel was chosen in order to try to isolate the wear behavior of the TNZT alloy itself to

determine if ECAE processing provided any beneficial change. UHMWPE was used because it is the same bearing material that is commonly used between the acetabular cup and the ball in hip replacements. The testing was performed at DUCOM instruments using a TR-20LE pin-on-disc tribo-tester. This type of test places the pin in contact with the disc under a specified load, and rotates the disc at a constant speed. A schematic of the test set-up is shown below in figure 7.6.

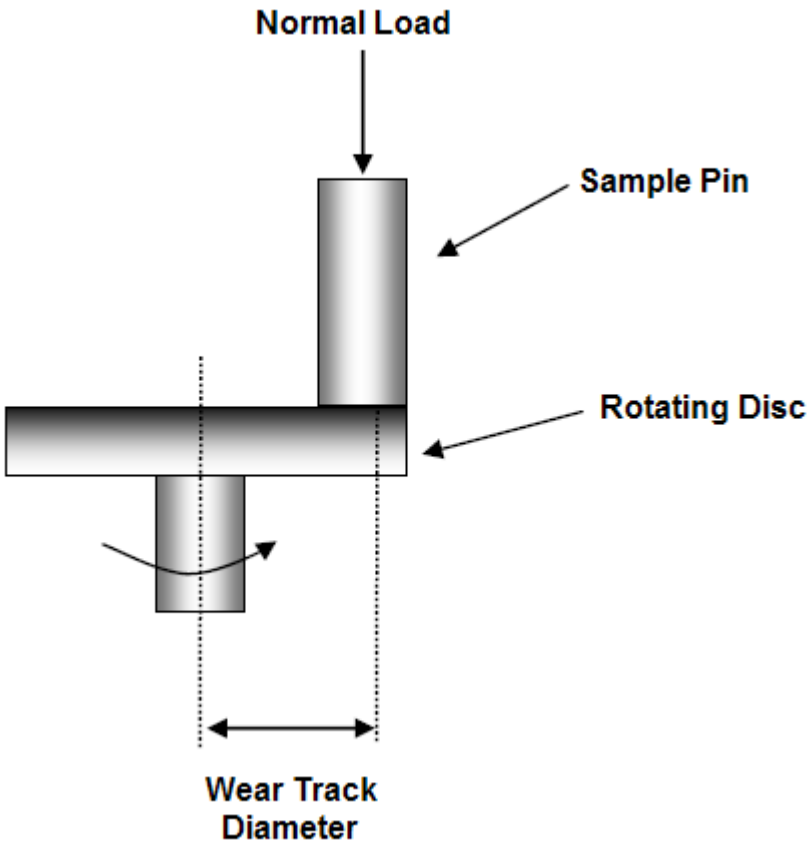

Figure 7.6 Schematic of pin-on-disc tester

Frictional forces and wear rates are monitored throughout the test. The TNZT samples are in the form of cylindrical pins with a diameter of ¼ inch and a length of approximately 1.2 inches. The counterface materials were machined into the form of a round, flat disc 120mm in diameter and 8mm thick. All of the contact surfaces were ground to an average surface roughness of 1.6μm. The stress level applied was 5MPa, the disc speed was 30RPM, the wear track diameter was 20mm, and the total test time was 5.5hrs for all the specimens. The 5MPa stress level was derived from a study which used an instrumented hip implant to measure the contact stresses over the entire surface of the ball of the implant. [61] The tests were run dry, with no lubrication at room temperature with a relative humidity of approximately 55%.

7.3.2 Results and discussion

Table 7.2 and table 7.3 show the sample descriptions and the summary of the test results respectively. Plots showing the variation of the friction coefficient and wear rate as a function of time for the individual test samples are shown below in figure 7.7 – figure 7.10

Table 7.2 Sample descriptions for wear test study

Specimen description	Counter face material
Sample 01:- TNZT (as received)	EN-31 steel ,hardened & ground to 1.6Ra surface roughness
Sample 02:- TNZT (as received)	UHMWPE(Ultra high molecular weight polypropylene, machined to 1.6Ra surface finish
Sample 03:- TNZT ECAE processed	EN-31 steel ,hardened & ground to 1.6Ra surface roughness
Sample 04:- TNZT ECAE processed	UHMWPE(Ultra high molecular weight polypropylene, machined to 1.6Ra surface finish

Table 7.3 Summary of wear test results

Test Sample	*Wear in microns*	*Frictional force in N*	*Co-efficient of friction = F/L*	*Computer path*	*Specimen*		
					Initial wt in gm	*Fiual wt in gm*	*Wt loss in gm*
Sample 01	825	55	0.343	*CSW 222 -1&1A*	4.615	4.457	0.158
Sample 02	56	17.8	0.108	*CSW 222 – 2,2A&2B*	4.672	4.672	0
Sample 03	623	75	0.443	*CSW 222 -3*	3.813	3.712	0.101
Sample 04	149	15.18	0.092	*CSW 222 -4*	3.726	3.724	0.002

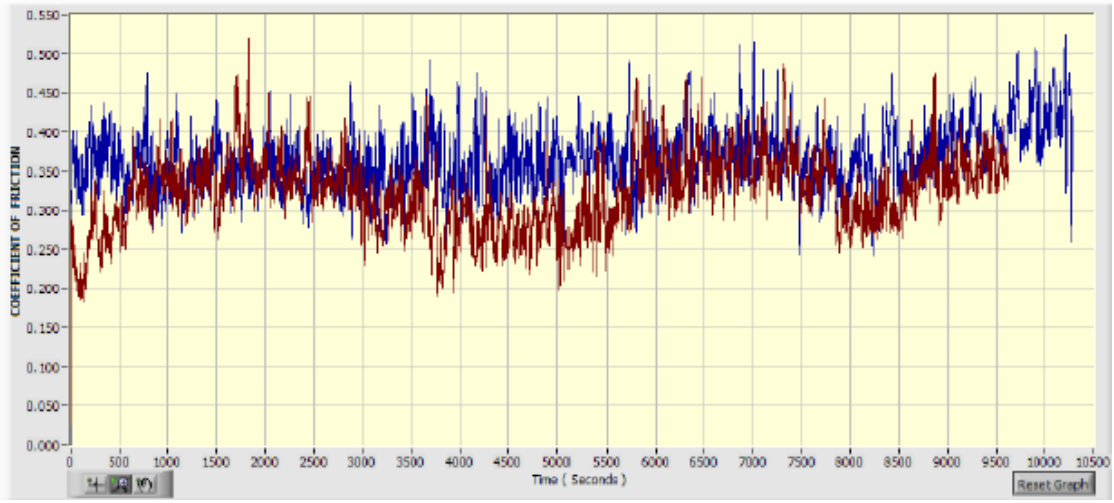

(a)

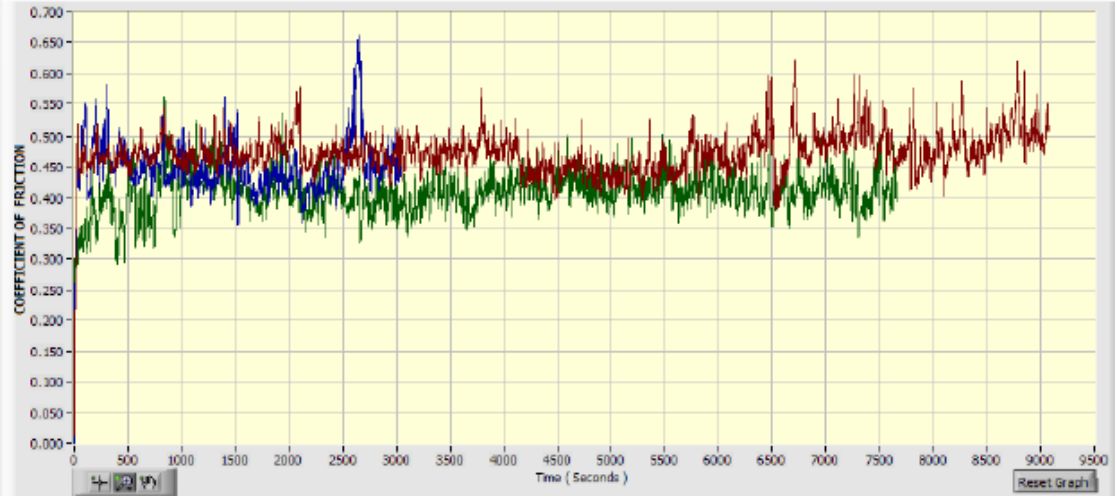

(b)

Figure 7.7 Coefficient of friction for (a) as-received TNZT on EN31 steel and (b) ECAE processed TNZT on EN31 steel

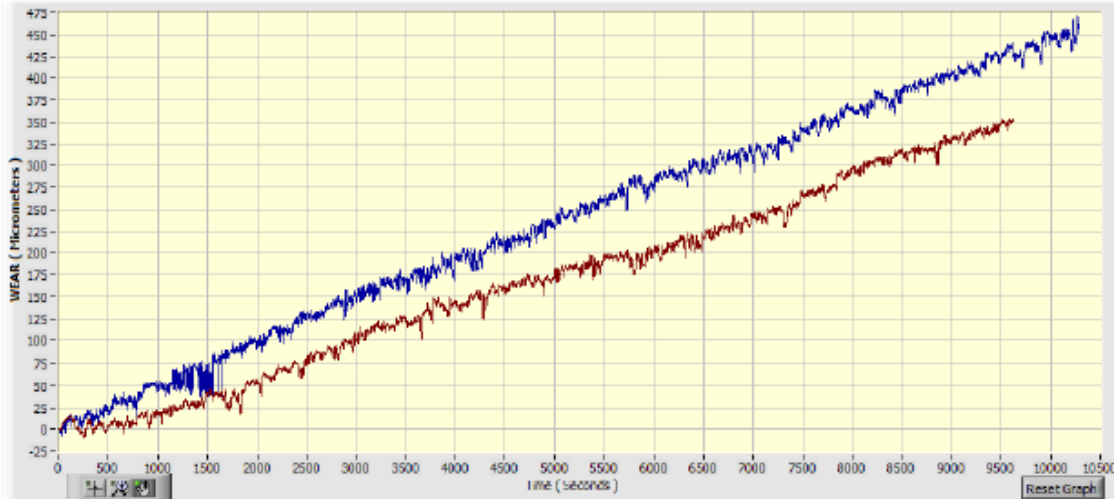

(a)

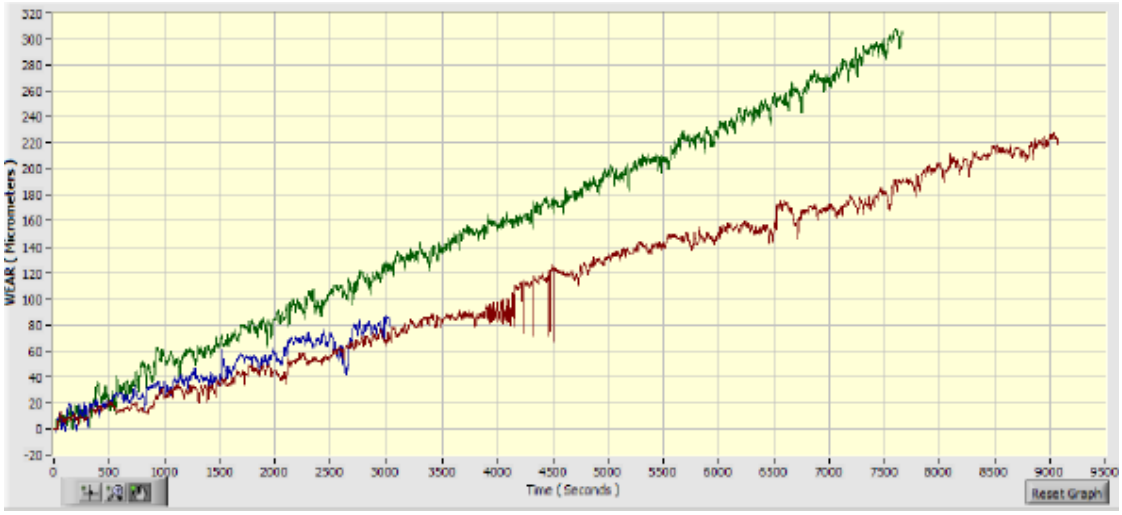

(b)

Figure 7.8 Wear vs. time for (a) as-received TNZT on EN31 steel and (b) ECAE processed TNZT on EN31 steel

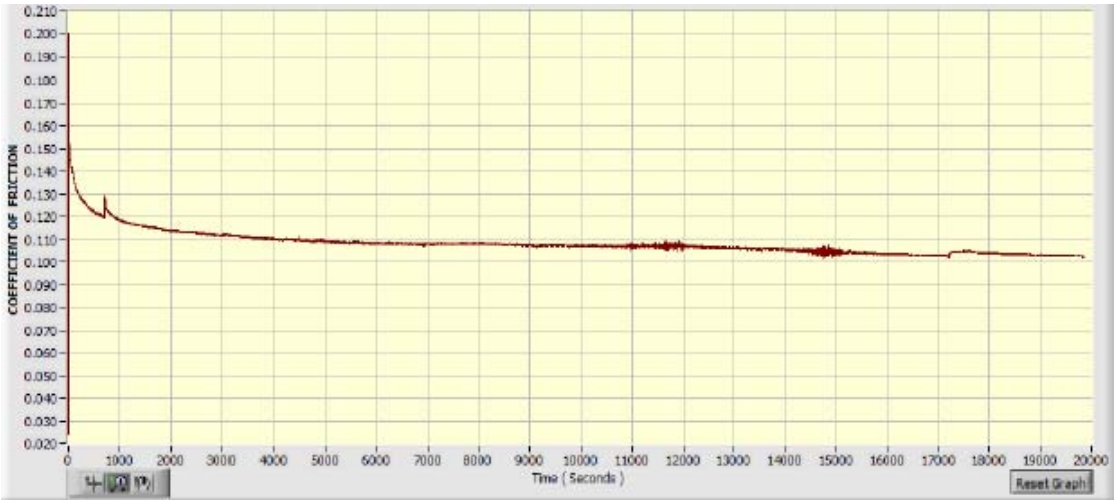

(a)

(b)

Figure 7.9 Coefficient of friction for (a) as-received TNZT on UHMWPE and (b) ECAE processed TNZT on UHMWPE

(a)

(b)

Figure 7.10 Wear vs. time for (a) as-received TNZT on UHMWPE and (b) ECAE processed TNZT on UHMWPE

The plots with multiple colors show experiments that were completed in different stages. A red line and a blue line were completed in two stages, while a red, blue, and green line was completed in three. Examination of the results from testing on the EN31 disc shows that ECAE processing increases the friction coefficient by approximately 30% while decreasing the total wear and weight loss by 24% and 36% respectively. It is very unlikely that ECAE processing has altered the adhesive friction component because substructure changes should not have any effect on surface bonding interactions or oxide development. [17] The change in friction coefficient is therefore due to a change in the deformation component. The deformation component arises from the resistance encountered when asperities from the harder material attempt to plow through asperities of the softer material. [41] The asperities in the ECAE processed sample posses higher strength and hardness and are therefore much

more difficult for the steel asperities to get through, causing an increase in the friction coefficient. The total wear is decreased because the improved properties in the ECAE processed sample compared to the as-received, tested at the same stress level, will prevent a large amount of damage and asperity fracture from occurring.

Examination of the results from testing on UHMWPE shows a minimal change in the friction coefficient and an increase in the total wear due to ECAE processing. The friction coefficient does not undergo a significant change because the property change due to ECAE is insignificant in this type of coupling. The polymer asperities are not strong or stiff enough to hold a significant load when they come into contact with the metal asperities. The polymer surface is so soft in relation to the metal surface that the entire surface of the polymer conforms to the irregular shape of the metal surface and can be considered to be in complete contact with it. Sliding resistance is then offered by adhesion forces between the surfaces, and essentially rigid metal asperities plowing through the polymer material. [41] Because of this contact condition, the friction behavior is determined almost exclusively by the mechanical properties of the polymer and not the contact metal. The total wear is increased by the ECAE processed pin because of its harder and stronger asperities. The property improvement allows them to penetrate deeper into the polymer surface and remove a larger amount of material with each sliding pass.

Chapter 8

Summary and Conclusions

A biomedical Ti-Nb-Zr-Ta alloy was modified by the use of equal channel angular extrusion and the addition of small amounts of boron in an attempt to improve the mechanical properties of the base alloy and broaden its potential application. The following conclusions and recommendations are drawn from this study.

(1) Results from high-temperature compression testing determined that temperatures of 500°C and below are still in the cold working regime for all iterations of the TNZT alloy. Deformation at temperatures of 700°C and higher occurs by non-uniform dynamic yielding and the rapid generation of dislocations at the grain boundaries. A small degree of grain refinement can be induced by static recrystallization after processing in the low temperature range, but deformation in the high temperature range results in the development a non-uniform mixed grain structure caused by recrystallization occurring preferentially at the grain boundaries (necklace recrystallization).

(2) DEFORM-3D accurately predicted the deformed material shape and required pressing force to ECAE process the TNZT alloy. The simulation also successfully predicted the presence of shear bands in the extruded sample which was confirmed by transmission electron microscopy.

(3) Multi-pass ECAE processing was successfully carried out on all three TNZT alloys. TNZT processed at 500°C showed evidence of shear banding and the development of a very dense dislocation substructure in the form of tangle and cells. The boron containing alloys processed at 825°C showed some evidence of dynamic

recrystallization, but the grain size reduction in the transformed regions was not significant.

(4) The boride particles in TNZT+0.5%B were able to restrict grain growth enough in the statically recrystallized samples to cause a 44% reduction in grain size (18μm → 10μm) compared to the samples with no boron and low boron. However, a 10μm grain size is not enough to cause significant property improvement, and the boride particles themselves were detrimental to the tensile modulus and fatigue response.

(5) ECAE processing at 500°C was able to improve the tensile and fatigue properties to more useful levels in the TNZT alloy through the introduction of a dense dislocation network, but the unintentional introduction of the α phase during processing increased the modulus value.

(6) High temperature processing of the boron alloys showed strength improvements compared to the unprocessed state, but the lack of uniform grain refinement produced final strength values that were not significantly higher than a conventionally processed TNZT alloy. Fatigue testing of the low boron alloy showed no property improvement with low temperature ECAE processing.

(7) ECAE processing improved the wear response of the TNZT alloy by increasing the strength of the surface asperities which were better able to resist plowing forces from the harder steel asperities. This same cause also increased the wear rate when in contact with the UHMWPE disc.

Recommendations for further study

(1) To improve upon the uniformity of the strain distribution, perform ECAE on the TNZT alloy with backpressure which has been shown to improve the strain distribution and shape retention in materials that have a tendency to undergo shear banding.

(2) Subject the boron containing alloys to a higher number of ECAE passes (8-12). Four passes produced incomplete dynamic recrystallization, it is possible that a higher number of passes would allow for complete transformation to a finer equiaxed microstructure and provide a larger strength increase.

(3) Determine the root cause of the deformation localization at the grain boundaries that is causing incomplete dynamic recrystallization. This can be accomplished by examining solute distribution from the grain interior to the boundary, determining dislocation density and distribution prior to and after deformation, and the use of strain interrupt tests and post-deformation annealing to determine the effect on the peak flow stress levels and the stress drop.

(4) Use a powder metallurgy approach to fabricate the alloys. This will allow for the use of much finer size boride particles, and potentially the production of finer grain sizes. Evaluate the mechanical properties of these alloys and determine if boride refinement has a beneficial impact on the fatigue and wear properties.

(5) Investigate and determine the cause of the low activation energy levels through the use of compression testing and electron microscopy.

References

[1] M. LONG, H.J. RACK: *'Titanium alloys in total joint replacement—a materials science perspective'*, Biomaterials, 19 1621-1639, (1998)

[2] S. NAG, R. BANERJEE, H.L. FRASER: *'Microstructural evolution and strengthening mechanisms in Ti-Nb-Zr-Ta, Ti-Mo-Zr-Fe and Ti-15Mo biocompatible alloys'*, Materials Science and Engineering, C25 357-362, (2005)

[3] H.J. RACK, J.I. QAZI: *'Titanium alloys for biomedical applications'*, Materials Science and Engineering, C26 1269-1277, (2006)

[4] F. GUILLEMOT: *'Recent advances in the design of titanium alloys for orthopedic applications'*, Expert Review of Medical Devices, 2(6) 741-748, (2005)

[5] K. WANG: *'The use of titanium for medical applications in the USA'*, Materials Science and Engineering, A213 134-137, (1996)

[6] D. KURODA, M. NIINOMI, M. MORINAGA, Y. KATO, T. YASHIRO: *'Design and mechanical properties of new β type titanium alloys for implant materials'*, Materials Science and Engineering, A243 244-249, (1998)

[7] M. NIINOMI: *'Mechanical properties of biomedical titanium alloys'*, Materials Science and Engineering, A243 231-236, (1998)

[8] V.M. SEGAL: *'Materials processing by simple shear'*, Materials Science and Engineering, A197 157-164, (1995)

[9] A. VINOGRADOV, V.V. STOLYAROV, S. HASHIMOTO, R.Z. VALIEV: *'Cyclic behavior of ultrafine-grain titanium produced by severe plastic deformation'*, Materials Science and Engineering, A318 163-173, (2001)

[10] S.G. STEINEMANN: *'Titanium – the material of choice?'*, Periodontology 2000, Vol. 17 7-21, (1998)

[11] S.G. STEINEMANN: *'Metal implants and surface reactions'*, Injury, Vol. 27 Suppl. 3, (1996)

[12] J. WOLFF: *'The law of bone remodeling'*, Springer, (1986)

[13] Y.L. ZHOU, M. NIINOMI, T. AKAHORI, M. NAKAI, H. FUKUI: *'Comparison of various properties between titanium-tantalum alloy and pure titanium for biomedical applications'*, Materials Transactions, Vol. 48 No. 3 380-384, (2007)

[14] U.S. PATENT 5,871,595. 1999 Feb 16.

[15] E. EISENBARTH, D. VELTEN, M. MÜLLER, R. THULL, J. BREME: *'Biocompatibility of β-stabilizing elements of titanium alloys'*, Biomaterials, 25 5705-5713, (2004)

[16] M. NIINOMI, T. HATTORI, K. MORIKAWA, T. KASUGA, A. SUZUKI, H. FUKUI, S. NIWA: *'Development of low rigidity β-type titanium alloy for biomedical applications'*, Materials Transactions, Vol. 43, No. 12, 2970-2977, (2002)

[17] T. COURTNEY: *Mechanical Behavior of Materials*, (2000)

[18] A. VINOGRADOV, S. HASHIMOTO: *'Multiscale phenomena in fatigue of ultra-fine grain materials—an overview'*, Materials Transactions, Vol. 42 No. 1 74-84, (2001)

[19] ASM INTERNATIONAL: *ASM Handbook, Phase Diagrams*, (1992)

[20] M. ANABTAWI, P. BECK, J. LEMONS: *'Biocompatibility testing of simulated total joint arthoplasty articulation debris'*, Journal of Biomedical Materials Research Part B: Applied Biomaterials, (2007)

[21] V.M. SEGAL, K.T. HARTWIG, R.E. GOFORTH: *'In situ composites processed by simple shear'*, Materials Science and Engineering, A224 107-115, (1997)

[22] D. YAMAGUCHI, Z. HORITA, T FUJINAMI, M. NEMOTO, T.G. LANGDON: *'Factors Affecting Grain Refinement in Equal-Channel Angular Pressing'*, Materials Science Forum, V331-337 607-612, (2000)

[23] K. NAKASHIMA, Z. HORITA, M. NEMOTO, T.G. LANGDON: *'Influence of channel angle on the development of ultrafine grains in equal channel angular pressing'*, Acta Materialia, V46 No.5 1589-1599, (1998)

[24] Y. IWAHASHI, Z. HORITA, M. NEMOTO, T.G. LANGDON: *'The process of grain refinement in equal channel angular pressing'*, Acta Materialia, V46 No.9 3317-3331, (1998)

[25] Y.C. CHEN, Y.Y. HUANG, C.P. CHANG, P.W. KAO: *'The effect of extrusion temperature on the development of deformation microstructures in 5052 aluminium alloy processed by equal channel angular extrusion'*, Acta Materialia, V51 2005-2015, (2003)

[26] A. YAMASHITA, D. YAMAGUCHI, Z. HORITA, T.G. LANGDON: *'Influence of pressing temperature on microstructural development in equal-channel angular pressing'*, Materials Science and Engineering, A287 100- 106, (2000)

[27] Y.T. ZHU, T.C. LOWE: *'Observations and issues on mechanisms of grain refinement during ECAP process'*, Materials Science and Engineering, A291 46-53, (2000)

[28] W.D. CALLISTER: *Materials Science and Engineering an Introduction*, (2000)

[29] P. COTTERILL, P.R. MOULD: *Recrystallization and grain growth in metals*, (1976)

[30] Y. IWAHASHI, Z. HORITA, M. NEMOTO, AND T.G. LANGDON: *'An investigation of microstructural evolution during equal channel angular pressing'*, Acta Materialia, V45 No16 4733-4741, (1997)

[31] B. POND: *'Analysis of strain distribution in equal channel angular extrusion by finite element method simulation and experimental validation'*, Washington University Doctoral Dissertation, (2006)

[32] J.R. BOWEN, A. GHOLINIA, S.M. ROBERTS, P.B. PRANGNELL: *'Analysis of the billet deformation behaviour in equal channel angular extrusion'*, Materials Science and Engineering, A287 87-99, (2000)

[33] M. FURUKAWA, Y. IWAHASHI, Z. HORITA, M. NEMOTO, T.G. LANGDON: *'The shearing characteristics associated with equal channel angular pressing'*, Materials Science and Engineering, A257 328-332, (1998)

[34] K. OH-ISHI, Z. HORITA, M. FURUKAWA, M. NEMOTO, T.G. LANGDON: *'Optimizing the rotation conditions for grain refinement in equal channel angular pressing'*, Metallurgical and Materials Transactions, V29A, (1998)

[35] V.V. STOLYAROV, Y.T. ZHU, I.V. ALEXANDROV, T.C. LOWE, R.Z. VALIEV: *'Influence of ECAP routes on the microstructure and properties of pure Ti'*, Materials Science and Engineering, A299 59-67, (2001)

[36] V. PROTASOV: *'Superplastic forming of ECAE processed Titanium Alloys'*, Washington University Masters Thesis, (2006)

[37] P.B. BERBON, M. FURUKAWA, Z. HORITA, M. NEMOTO, T.G. LANGDON: *'Influence of pressing speed on microstructural development in equal channel angular pressing'*, Metallurgical and Materials Transactions, V30A, (1999)

[38] A. VINOGRADOV, S. HASHIMOTO: *'Fatigue of severely deformed metals'*, Advanced Engineering Materials, 5 No. 5, (2003)

[39] A. VINOGRADOV: *'Fatigue limit and crack growth in ultra-fine grain metals produced by severe plastic deformation'*, Journal of Materials Science, 42 1797-1808, (2007)

[40] M. LONG, R. CROOKS, H.J. RACK: *'High-cycle fatigue performance of solution-treated metastable-β titanium alloys'*, Acta Materialia, Vol. 47 No. 2 661-669, (1999)

[41] I.M. HUTCHINGS: *Tribology: friction and wear of engineering materials*, (1992)

[42] M. LONG, H.J. RACK: *'Friction and surface behavior of selected titanium alloys during reciprocating-sliding motion'*, Wear, 249 158-168, (2001)

[43] S.J. LI, R. YANG, S. LI, Y.L. HAO, Y.Y. CUI, M. NIINOMI, Z.X. GUO: *'Wear characteristics of Ti-Nb-Ta-Zr and Ti-6Al-4V alloys for biomedical applications'*, Wear, 257 869-876, (2004)

[44] V.V. STOLYAROV, L. SHUSTER, M. MIGRANOV, R.Z. VALIEV, Y.T. ZHU: *'Reduction of friction coefficient of ultrafine-grained CP titanium'*, Materials Science and Engineering, A371 313-317, (2004)

[45] B. JUNG: *'Microstructural refinement of α-brass and Ti-6Al-4V by equal channel angular extrusion processing – modeling and experimental validation'*, Washington University Doctoral Dissertation, (2006)

[46] P. DHULIPALA: *'Microstructural evolution during equal channel angular extrusion: simulation and experimental validation'*, Washington University Masters Thesis, (2006)

[47] AMERICAN SOCIETY FOR TESTING AND MATERIALS: *Annual book of ASTM standards: Medical devices and services*, (1997)

[48] A.L. YETTRAM, K.W.J. WRIGHT: *'Dependence of stem stress in total hip replacement on prosthesis and cement stiffness'*, Journal of Biomedical Engineering, Vol. 2, (1980)

[49] K.J. MATHIAS, J.C. LEAHY, A. HEATON, W.F. DEANS, D.W.L. HUKINS: *'Hip joint prosthesis design: effect of stem introducers'*, Medical Engineering & Physics, 20 620-624, (1998)

[50] S.J. HAMPTON, T.P. ANDRIACCHI, J.O. GALANTE: *'Three dimensional stress analysis of the femoral stem of a total hip prosthesis'*, Journal of Biomechanics, Vol. 13 443-448, (1980)

[51] P.S. CHRISTEL, A. MEUNIER, D. BLANQUAERT, J. WITVOET, L. SEDEL : *'Role of stem design and material on stress distributions in cemented total hip replacement'*, Journal of Biomedical Engineering, Vol. 10, (1988)

[52] G. BERGMANN, G. DEURETZBACKER, M. HELLER, F. GRAICHEN, A. ROHLMANN, J. STRAUSS, G.N. DUDA: *'Hip contact forces and gain patterns from routine activities'*, Journal of Biomechanics, 34 859-871, (2001)

[53] G. BERGMANN, F. GRAICHEN, A ROHLMANN: *'Hip joint contact forces during stumbling'*, Langenbecks Archives of Surgery, 389 53-59, (2004)

[54] AMERICAN SOCIETY FOR METALS: *Material properties handbook: titanium alloys'*, (1994)

[55] I.WEISS, S.L. SEMIATIN: *'Thermomechanical processing of beta titanium - an overview'*, Materials Science and Engineering, A243 46-65, (1998)

[56] M. LONG, H.J. RACK: *'High temperature discontinuous yielding in β-phase Ti_3Al-(Nb,V,Mo) alloys'*, Titanium '95: Science and Technology, (1996)

[57] M.N. VIJAYSHANKAR, S. ANKEM: *'High temperature tensile deformation behavior of β-Ti alloys'*, Materials Science and Engineering, A129 229-237, (1990)

[58] G. COLOMBO: *'Equal channel angular extrusion (ECAE) scale-up and forgeability improvements in ECAE processed billets'*, Washington University Masters Thesis, (2007)

[59] I.P. SEMENOVA, G.I. RAAB, L.R. SAITOVA, R.Z. VALIEV : *'The effect of equal channel angular pressing on the structure and mechanical behavior of Ti-6Al-4V alloy'*, Materials Science and Engineering, A387-389 805-808, (2004)

[60] R.Z. VALIEV: *'Structure and mechanical properties of ultrafine-grained metals'*, Materials Science and Engineering, A234-236 59-66, (1997)

[61] W.A. HODGE, K.L. CARLSON, R.S. FIJAN, R.G. BURGESS, P.O. RILEY, W.H. HARRIS, R.W. MANN: *'Contact pressures from an instrumented hip endoprosthesis'*, Journal of Bone & Joint Surgery, 71 1378-1386, (1989)